POLITECNICO DI TORINO

Corso di laurea magistrale in Ingegneria Energetica e Nucleare

Tesi di Laurea Magistrale

Manufacturing methods of the electrolyte for Proton Conducting Cells

THE UNIVERSITY OF CALIFORNIA IRVINE

Relatori:
Prof. Massimo Santarelli
Prof. Jack Brouwer

Candidata:
Martina Bigucci

Marzo 2023

Anno accademico 2022-2023

Acknowledgements

I would like to thank my supervisors Massimo Santarelli and Jack Brouwer for giving me the opportunity to work at my thesis at the University of California, Irvine. It has been an unforgettable academic and life experience that I will always keep in my heart.

Thanks to Christian Rose, who has first introduced me to the research work field, shared with me long hours of work and without whom this thesis would not have been possible.

Thanks to Luca Mastropasqua, who has been a brilliant guide in this project, helping me finding solutions and enriching my knowledge in this field.

Thanks to the Spanish team, true friends and perfect travel companions who were there with me during happy and difficult moments, and never failed to cheer me up.

Thanks to my partner and my friends, who showed me that distance and time matter nothing when the bond is strong and real.

Finally, I'm grateful to my parents and family who have always supported me throughout my entire life and in the realization of my dream to conclude my studies abroad, making this experience possible.

Abstract

Protonic ceramic cells have attracted tremendous attention in the past decades due to their unique advantages, such as lower operating temperature and easier reversible operation. Moreover, in recent years, the hydrogen economy has been strongly favored by governmental and industrial bodies worldwide. To improve the development of proton conductor-based cells, rational design of high-performance electrolyte materials with novel compositions and proper manufacturing techniques are needed to scale-up the cells and make this technology ready for commercialization. In this work, the manufacturing methods of the electrolyte for protonic conducting solid oxide cells and their challenges are described, as part of a joint project of Politecnico Di Torino, Politecnico di Milano, University of California Irvine and SNAM, in the attempt to obtain low thickness electrolytes, along with the description of the imaging and analysis techniques employed. At first, a Yttria Stabilized Zirconia (YSZ) slurry is produced in order to better understand how its composition must be to obtain a suitable value of viscosity to perform tape casting, a scalable and industrially established manufacturing process, which has been completed for values of layer thickness of 400, 300, 200 and 100 μm. Consequently, trials of tape casting on a Ceria and Yttria doped Barium Zirconate (BZCY) slurry are reported, highlighting the need to obtain both a proper value of viscosity, which has to be relatively low and checked performing rheology, while still keeping a quantity of binder that allows to peel off the dried slurry and, ultimately, perform sintering. Tape casting on the BZCY slurry has been successfully completed obtaining the following values of layer thickness: 400, 300, 200, 100, 20, 15, 10 and 5 μm. The BZCY slurry has been produced with the addition of a Manganese Oxide sintering aid, which has shown the capability to change the surface structure of BZCY using the scanning electron microscope (SEM). Also, various sintering protocols have been performed, proving that heating up the sample to 1350 °C, dwelling at the same temperature for two hours and cooling back to room temperature at a rate of 100 °C/h constitutes an effective strategy. It is expected that the technical readiness level of PCCs might advance more quickly, toward field demonstrations and commercialization for a clean and sustainable energy era.

Contents

List of figures

List of tables

List of equations

1.Introduction

Solid oxide electrochemical cells, as promising electrical-chemical conversion devices, have been actively studied because of their high energy conversion efficiencies and potential applications in electrochemical reactors. However, the high operating temperature (700–900°C) of conventional oxygen-ion-conducting solid oxide electrochemical cells is an obstacle to commercialization, due to exacerbated degradation, uneconomical manufacturing and maintenance costs. For this reason, tremendous efforts have been devoted to lowering the operating temperature of solid oxide electrochemical cells. In the 1980s, solid oxide electrochemical cells using protonic ceramic materials (i.e. PCECs), were developed and soon considered promising candidates for ceramic electrochemical devices in the intermediate temperature range (400–700°C) due to their high ionic conductivity and low activation energy of proton transport. Recent advancements in composition refinement on classic doped barium zirconate/cerate electrolytes and prospective proton conductors have been made. Moreover, significant achievements in air electrode catalytic activity and stability through advanced structural and compositional innovation could be reached; and microstructural engineering on Ni-based electrodes and strategies to increase their tolerance and performance have been tested. To make SOFC technology economically feasible and competitive with established energy conversion systems, its operating temperature must be further reduced from high to intermediate temperatures. Reduced operating temperatures would minimize long-term degradation, reduce chromium poisoning, enable the use of less expensive materials, and open the possibility of a rapid start-up. In this regard, protonic ceramic materials were proposed as a solution for intermediate temperature SOFC with an operating temperature under 700°C owing to the low activation energy (0.3–0.5 eV) of proton transport, which is approximately half of the typical value for oxygen ion transport. Also, the solid oxide electrolysis cell (SOEC) is an economically attractive and sustainable technology to efficiently convert electricity from abundant renewable energy sources to hydrogen fuel with zero carbon emissions. Hydrogen could serve as an attractive energy carrier, as a feedstock for synthetic gas, as well as a potential clean fuel for heating, electricity, and vehicle applications.

Despite the advantages of using proton ceramic materials, the commercialization of protonic devices for fuel cell and electrolysis cells is yet to be realized due to several barriers: low chemical stability of proton-conducting oxides in a high p(H2O) environment, poor sinterability of Zr-rich electrolytes, electronic leakage and low Faradaic efficiency at thermodynamically favorable temperature (600–700°C) and impaired electrode performance at lower temperatures (<600°C). Most of the available materials and strategies in the reported sources cannot solve all of these problems simultaneously, because the manufacturing-ready components must meet several strict requirements. For example, besides the essential requirement of high conductivity, the electrode and electrolyte should have a comparable thermal expansion to ensure high thermo-mechanical compatibility, negligible chemical reactions with other cell components to ensure sufficient chemical compatibility, and high chemical stability with reactants to ensure long-term operational stability.

The most important challenges for the application of proton conductor-based SOECs are electronic leakage and low Faradaic efficiency and some important players that determine it are gas composition and operating temperatures. Long-term reliability is another great concern, as the air electrode materials need to be chemically stable under moist air during operation. From the chemical point of view, coke deposition and sulfur poisoning are the phenomena that affect the electrodes the most. Lower temperature operation (from 500 to 650° C) can accelerate the coke deposition on the fuel electrode in direct methane fueled SOFCs and accelerate sulfur poisoning. Lower operating temperature also favors shifting the water–gas shift towards CO2 in steam reforming of methane in PCECs, leading to a low CO/CO2 ratio to reduce boundary reaction and mitigate coking. However, the biggest challenge resulting from low operating temperature is the insufficient activity for fuel catalysis. [1]

In this work, part of a project involving Politecnico di Torino, Politecnico di Milano, University of California is developed. The main challenges presented for solid oxide proton conducting cells are analyzed, focusing on the manufacturing processes of the electrolyte, the anode and the cathode, and their composing materials, finding the most suitable modus-operandi and highlighting the critical steps with the aim of obtaining a scalable-up cell that will potentially be commercialized. Also, detailed descriptions of imaging and spectroscopy techniques, and the relative software used are included in this study.

2.Overview of the project

The framework of the joint project of Politecnico Di Torino, Politecnico di Milano, University of California Irvine and SNAM rete gas is here described, planning to dedicate three years to the development of two types of electrolyte-supported button cells, namely asymmetric proton conductive electrolysis cells (PCECs) and symmetric cells for hydrogen separation/compression. In PCECs, BZCY is chosen for the electrolyte, Ni-BZCY cermet as the cathode, BLC as the anode. The symmetric configuration will mount the Ni-BZCY cermet on both sides. These cells will be prepared by screen-printing and will be taken as reference. This reference performance will be improved by infiltration of the Ni electrode and addition of dopant elements. These novel electrodes by infiltration of the BCZY scaffold will be produced, followed by incorporation of metal precursors solutions and in situ formation of the electrochemically active phase. Aim of the activity is providing the partner units a preferential electrode composition for scale-up to pre-commercial 5 cm x 5 cm size. Metal supported planar button cells (2 cm of diameter) for hydrogen generation (PCEC) will be developed, as well as separation and compression, based on the following chemistry Ni-BSCY|BZCY|BLC. The metal support will be designed using additive manufacturing methods performed by NASA jet propulsion laboratory to achieve a mechanically resistant and high surface area structure useful for high pressure operation. The goal is the manufacturing of at least 5 promising planar metal supported button cells, which will be ready to scale up to large sized cells and stacks. A scale-up to 5x5cm cells of the most promising cell designs will be done (either the infiltrated electrode or the metal supported cell or both) and their characterization for both final applications considered. A benchmarking activity with other pre-commercial cells will be developed, focusing on asymmetric cells for PCEC operation (BZCY electrolyte, Ni-BZCY or Ni-SZCY supports, BLC as steam electrode) and symmetric cells for separator operation (BCZY electrolyte surrounded by two cermet electrodes (BCZY-Ni)). The benchmarking activity provides the inputs for the development of a Single Repeating Unit (SRU) for 5 cm x 5 cm proton conductive cells. Step regarding design, processing and preliminary testing of glass-based sealing, interconnects and ceramic coatings that are needed for the development of the SRU, and will perform the SRU manufacturing, assembly, and testing. Finally, in the last part of the project the SRU will be extended to a short-stack configuration, considering the most performing structure of the previously developed SRU (with symmetric cells for separator mode, or with asymmetric cells for electrolysis mode): the Consortium will select the best cell configuration, a suitable number of 5 cm x 5 cm size cells will be produced, and the final 5-cells short-stack will be tested. A multi-scale modeling activity, from the single-cell scale to the SRU and short-stack scale, and reaching the system analysis scale, will be performed as a collaborative activity by the whole partnership.

In this work, a focus on the development of optimal electrode-electrolyte assembly chemistries for electrolysis and hydrogen membrane and pump end-use has been done. The initial material selection is expected to use an Yttrium- and Cerium-doped Barium Zirconate (BZCY721) as electrolyte, a Lanthanum Barium Cobaltite (BLC) as steam electrode, and a 40%wt BZCY721+60%wt NiO cermet (after in-situ reduction) as hydrogen electrode. Based upon the initial literature search and given the feedback from other team members' chemistries the compositions for each final end-use will be adapted. The initial cell design will be planar metal supported to target a temperature operating range of 400-550°C. The support will be designed to provide thermo-mechanical structural strength to the cell and to provide sufficient active area. Structures produced via additive manufacturing for the nanoengineering of the porosity will be used as metal support structures. The design and manufacture of such metal structures will be performed by NASA JPL. The study of the interface and bonding between the electrode and the metal support is fundamental. Coating solutions and sintering methods will be compared against brazing solutions to ensure the appropriate contact and to facilitate ionic and electronic conduction in the two phases. Sintering at the appropriate temperatures to allow for low intra-grain ionic resistance will be evaluated in relation to the metal support composition and thermo-mechanical properties. Coefficient of thermal expansion (CTE), metal support wettability, and thermo- chemical stability of the electrode-metal bonding will be characterized at different sintering temperatures. Button cells of 20 mm diameter (12.5 mm electrode diameter) will be used to study the performance of the catalyst material, the chemistry of electrode/electrolyte materials, as well as to optimize the manufacturing process of the metal support/electrode bonding interface. The goal of this work package is the manufacturing of at least 5 promising planar metal supported button cells, which will be ready to scale up to large sized cells and stacks in the subsequent work packages. It's also planned to provide material characterization expertise, cell design concepts and metal support concepts and manufacturing techniques together with NASA JPL, and cell performance characterization in hydrogen electrolysis and separation and steam reforming applications to the working group. Input and discussion with the working group would be needed to define mechanical requirements of the cell design to facilitate the subsequent stack design (e.g., seals, loading, fixture, manifolds).

Electrochemical tests on electrodes and cells will also be carried out. The main targets are: screening of the electrochemical performance of electrodes at various compositions; individuating the best performing materials. A Probostat unit equipped with galvanostat/potentiostat and frequency response analyzer will be used for the experiments. The protonic conduction properties of the BCZY pellets will be verified with EIS to validate the preparation method. The optimal electrode materials will be selected by comparing the performance of the reference screen-printed cells with the performance of the infiltrated cells. Polarization (I/V curves) and EIS tests will be carried out under atmospheric pressure at varying temperature and composition, with N2/H2O/H2 mixtures for PCEC experiments, and with H2/N2 mixtures for hydrogen separation experiments. Relevant feed compositions at different reactants ratios will be also evaluated. The results will provide feedback regarding the effects of the infiltrate composition and amount, which will be tuned to achieve the optimal performance, according to the target (electrolysis or hydrogen sepIn this work package, the cells produced in WP1 will be tested using the two Probostat® solid oxide fuel cell and electrolysis cell holders for measurements of electrical properties, transport parameters, and kinetics of materials, solid/gas interfaces and electrodes at high temperatures under controlled atmospheres that are available at UCI. We will test the cell primary electrochemical performance characteristics via the measurement of polarization curves, electrochemical impedance spectroscopy (EIS), and cyclic voltammetry (CV) at different operating temperatures (400-600°C) and with different molar inlet composition. In particular, the hydrogen separation and compression design will be tested first with forming gas mixtures (N2/H2) and then with simulated natural gas blends with hydrogen. Moreover, a maximum pressure differential between the hydrogen and steam electrodes of 5 bar is going to be tested to verify the mechanical stability of metal supported cells. In both applications, a sensitivity analysis will be performed on the composition and flow of the sweep gas and upon the inlet mixture composition and operating temperature. Finally, the thermochemical stability of the electrode design will be assessed post-mortem with SEM-EDX, X-ray Fluorescence Spectroscopy, and Glow Discharge Spectrometry.

The most promising button cell designs (for both infiltrated electrode and metal supported electrode designs) will be scaled up to planar cells of 5x5 cm of active area. Tape casting and screen printing will be used as coating deposition methods using the facilities currently available at UCI. Hydrogen generation and compression designs will be demonstrated up to 5 bar of hydrogen delivery pressure (i.e., 5/1 pressure differential cell) for a period of at least 500h. The electrochemical performance of the cell will be assessed via classical electrochemical characterization techniques (VI, EIS) and the range of operating conditions will be selected based upon the system modeling operating conditions already identified and from the other team members. During the 500h testing period, condition monitoring methodologies will be used to detect cell degradation. At the end of the test period, post-mortem analysis via scanning electron microscopy imaging methods will be used to determine the principal degradation causes.

The UCI team will collaborate with the working group to design a short stack for hydrogen separation and compression, and hydrogen generation. First, UCI will model a 5x5cm cell via electrochemical and thermodynamic 2D cell simulations along the cell channel primary fuel and oxidant flow directions. The electrochemistry model will use zero-D assumptions. The cell model will aid the design of the larger cells and stack to identify the temperature and flow rate operating regimes that the unit cells will operate at. In particular, the stack thermal management for the steam electrolysis application will be evaluated as a function of current density.

3.Electrochemical cells

In general, the efficiency of an electrochemical process is higher than a thermodynamic one, as the electrochemical process is a one-step transformation, avoiding combustion, many intermediate steps and has no Carnot limit.

Electrochemical cells are organized in three layers:

1. Electrolyte central layer, which is a very good conductor of ions or protons and has low to no molecular diffusion.
2. Anode layer, in which an oxidation reaction occurs delivering electrons. At this point, two possible scenarios are present. If the electrolyte conducts positive ions, a positive ion is released and conducted, while if the electrolyte conducts negative ions, the electron released transforms into another molecule.
3. In the Cathode layer, the reduction reaction happens, so a recombination of electrons with the nucleus takes place. If this electrode conducts negative ions, the molecule generates a negative ion, if it conducts positive ions, the molecule will form another molecule.

It has to be noted that positive ions migrate from anode to cathode and vice versa.

An external circuit is added to conduct electrons, since oxidation and reduction generate a charge separation, and so, a voltage gradient through the cell.

Considering a reaction with $\Delta g<0$ and a positive electrical work, organizing a redox reaction, separating oxidation and reduction generating a coherent flow of electrons, it's possible to obtain electrical work, since the Gibbs free energy is not in equilibrium. Other pathways for a positive electrical work can be obtained changing the material of the electrolyte. Considering a ceramic material (such as YSZ or other ceramic materials) the global reaction is the same, but not the half reactions.

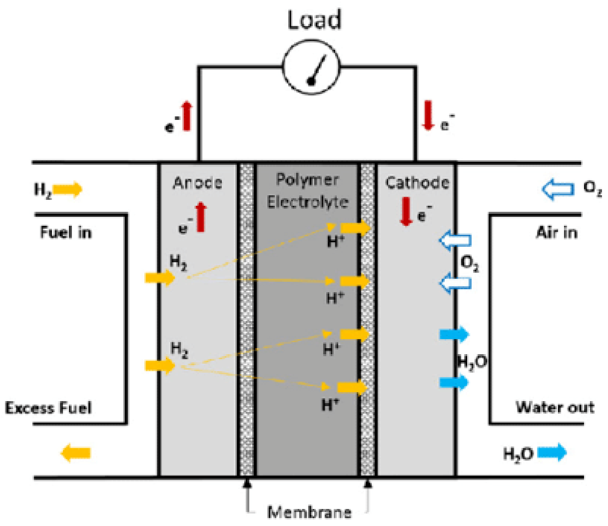

Figure 1. Electrochemical cell in fuel cell mode

Considering a reaction with Δg>0 and a negative electrical work, the electrochemical cell works in a reversed mode, needing energy to drive a non-spontaneous reaction, such as water splitting.

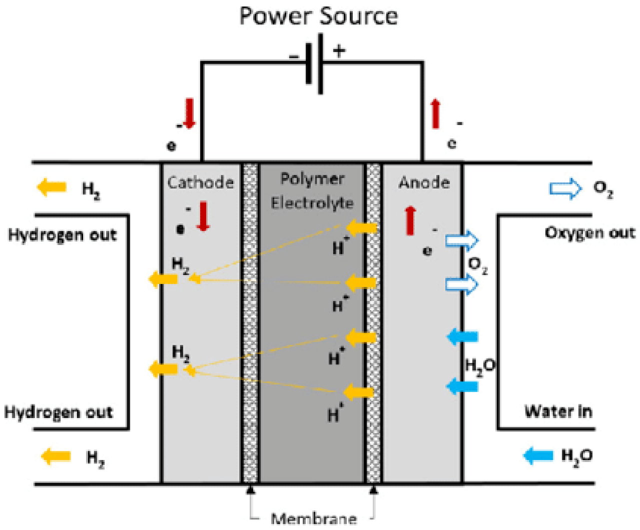

Figure 2. Electrochemical cell in electrolyzer mode.

The Faraday law connects the number of moles of a chemical species "*i*" participating to the reaction with the current

$$n_i^0 = \frac{I}{z_i \cdot F}$$

Equation 1. Faraday Law

where F=96487 C/mol is the Faraday constant and *zi* the charge number.

The ionic conductivity in the electrolyte material is expressed as

$$\sigma_i = F^2 \cdot z_i^2 \cdot c_i \cdot U_i$$

Equation 2. Ionic conductivity of the electrolyte

Where ci is the concentration of the chemical species and *Ui* the ionic mobility. As the temperature increases, the conductivity increases as well and vice versa.

3.1 Thermodynamic analysis of an electrochemical cell

Describing a thermodynamic analysis of an electrochemical cell, the modification of chemistry between reactants and products is not totally transformed in work, as part is transformed into heat, considering a cell that delivers positive electrical work. This is described by the Nernst Law, which general expression is

$$E = \mp \frac{\Delta \bar{g}_{\mathrm{REACT}}\left(T,P_0\right)}{Z_F \cdot F} \pm \frac{\ln \prod^R \left(\frac{P_i}{P_0}\right)^{\nu_i}}{\ln \prod^p \left(\frac{P_i}{P_0}\right)^{\nu_i}}$$

Equation 3. General expression of Nernst law

E is also called Nernst potential or OCV (open circuit voltage), measured at equilibrium, at open circuit, with no entropy generation obtained at zero current. If there is a temperature increase, both The Nernst potential and the Gibbs free energy decrease, having a negative effect on energy production.

3.2 Polarization plane and transport phenomena

As soon as the circuit of the electrochemical cell is closed, transport phenomena start, so it’s useful to draw an operational map of the machine to visualize the voltage drops (losses) caused by transport phenomena.

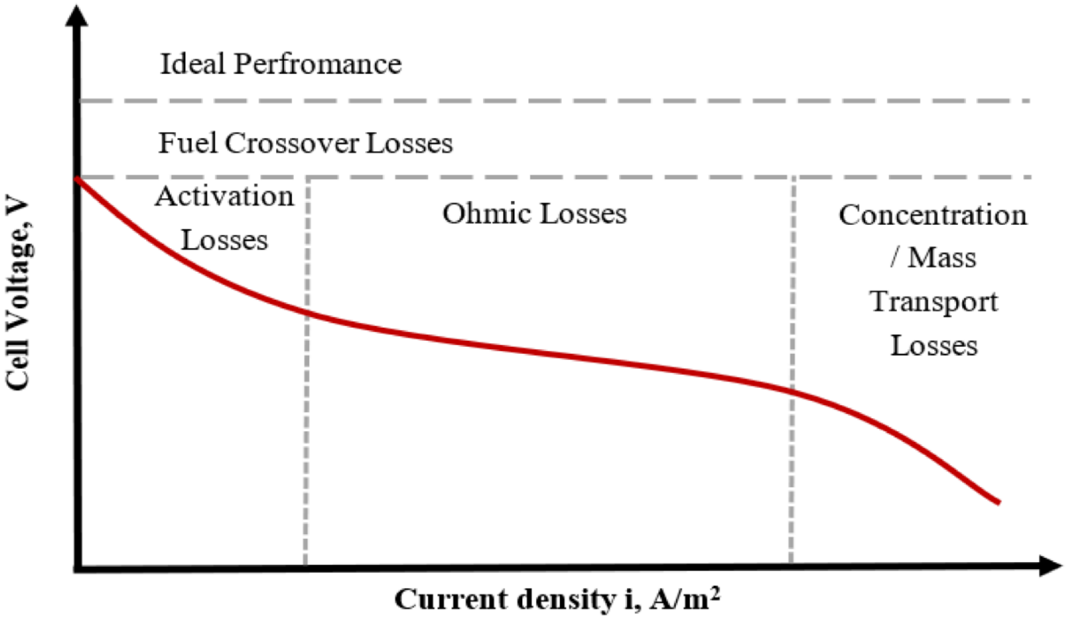

1. Charge transfer, activation voltage. It’s related to the kinetic of the electrochemical reaction, it’s the fastest phenomena with a nonlinear voltage drop.
2. Charge migration, ohmic overvoltage. This is the simplest phenomena due to migration of ions or protons in the electrolyte and part of the electrode and related also to the passage of electrons through the external circuit. This phenomenon is characterized by a linear voltage drop and it’s slower in respect to charge transfer.
3. Mass transport, concentration overvoltage. The molecular diffusion becomes the limiting factor if the supply of reactant isn’t fast enough, this phenomenon is characterized by a nonlinear voltage drop.

The main overvoltage effects can be considered by the following formula

$$V_c = E \mp \sum_{k=1}^{3} \eta_k(I)$$

Equation 4. Overvoltage effects

The negative sign is adopted for a spontaneous reaction, while the positive sign for a non-spontaneous reaction.

3.2.1 Activation overvoltage

Considering what's happening at nanoscale, there is a molecule in contact with the catalyst subject to adsorption processes and the delivery of electrons and protons. This constitutes an electrochemical reaction with a related kinetic law. So, the rate law of charge transfer, considering forward and backward rates, is expressed by the Butler-Volmer law.

$$K_R = K \exp\left(\frac{nRDS \cdot \beta \cdot F}{RT}\eta\right) - K \exp\left(-\frac{nRDS \cdot (1 \cdot \beta) \cdot F_1}{RT}\eta\right)$$

Equation 5. Butler-Volmer law

Where Kr is the reaction rate, K is the rate constant and η the overvoltage.

1. Rate constant K. If there is no overvoltage, K=Kr=I0 which is the exchange current, current measured when the circuit is open, function of temperature, type of reaction, catalyst, electrodes. Moreover, it depends on the length of the three-phase boundary (lTPB) sites, meaning the electrode needs a pore phase, connecting the catalyst to the ambient, an electronic phase to move the electrons delivered by the catalyst and an ionic phase to conduct the produced ions. As the exchange current increases, both the kinetics and the capability to start a reaction improve.
2. nRDS is the number of electrons exchanged in the rate determining step of reaction, which is the slowest step.

3. Parameter β. An electrochemical reaction is enhanced by the presence of an electrical field. β is a value that ranges between 0 and 1. If β is equal to 1, the electrical field is given to the energy level of the reactant, if β equals zero there is a decrease of the level of enthalpy of the product. Usually, β is assumed to be 0,5.

3.2.2 Ohmic overvoltage

It’s generated due to the migration of the charged species, electrons and mostly ions.

$$\Delta V = \eta_{\mathrm{OHM}} = RI \tilde{=} (pL)_{\mathrm{IONS}}$$

Equation 6. Ohmic overvoltage

Where rho is the thermal resistivity of the electrolyte and L is the length of the pathway of the charged species. The goal is to lower the thermal resistivity as much as possible, minimizing the conductor thickness and its cost, but if the electrolyte is too thin the electrons can pass through it causing a short circuit.

3.2.3 Concentration or diffusion overvoltage

Since the molecule enters the electrode by diffusion mechanism, it can be limiting at high current values, because at a certain point the concentration can drop in absence of reactant, being the flow of hydrogen molecules needed to increase. In order to model this overvoltage, the concentration at the catalyst Cr is needed, but the only way to retrieve it is from models from molecular diffusion starting from the concentration at the bulk, which is easier to measure. There are three models able to describe this overvoltage:

1. Fick’s model, the simplest one, just applicable to a mixture of two species
2. Stefan-Maxwell model, suitable for a mixture of more than two chemical species
3. Dusty-Gas model, also called Stefan-Maxwell model corrected by Knusden diffusion. Diffusion happens in a porous matrix experiencing impact with the walls.

With these models the concentration at the catalyst is calculated correctly, being in no need to correct the Nernst voltage with eta concentration.

Using the simplified approach of Fick’s model, it’s possible to define η concentration.

$$\frac{n_i^{\circ}}{s} = D_i^{EFF} \nabla C_i$$

Equation 7. Simplified approach of Fick's law

Where Di eff is the effective diffusion coefficient of species “*i*”.

It’s possible to find a very important parameter called limiting current density, the maximum current that an electrode can elaborate when the concentration at the catalyst tends to zero.

$$i = Z_i \cdot F \cdot D_i{}^{EFF} \cdot \frac{C_{\text{BULK,}}}{t} = i_L$$

Equation 8. Limiting current density

Simplifying to just the most limiting molecule to the diffusion process it’s possible to obtain the following expression for the overvoltage:

$$\eta_{\text{conc}} = \left| \frac{RT\nu}{ZF} \ln\left(1 - \frac{i}{iL}\right) \right|$$

Equation 9. Concentration overvoltage

4.Solid Oxide Cells

In solid oxide fuel cells or electrolyzers the electrolyte is made of ceramics, oxides of transition metals or rare earth. The most used ceramic materials are YSZ and BZCY and they are ion conductive and proton conductive, respectively. Temperature must be high enough to get sufficient ion or proton conductivity.

Advantages in employing solid oxide cells include fuel flexibility, as there is a vast range of fuels that can be fed to these electrochemical devices, there is no need of precious catalysts, such as platinum, it shows enhanced transport processes, heat can be recovered at high temperatures, hybridization with other system such as gas turbines can be performed and overall, there are good values of electrical efficiency.

Disadvantages regarding costs, which are still an issue these days, long start-up times of the system, very fast rates of degradation and generally slow dynamics.

4.1 Structures of the cell

The cell can be anode, electrode or cathode supported, meaning that one of these parts is bigger than the others:

1. Anode supported: this constitutes the best and most efficient solution in most cases
2. Cathode supported: in this configuration, big cathode diffusion issues arise
3. Electrolyte supported: high values for Ohmic voltage drops. Also, the electrolyte should be as thin as possible as previously mentioned.

4.3 Materials

In this section an overview on the main classes of materials for SOC is presented.

4.3.1 Ceramics

Ceramics are inorganic, nonmetallic materials, crystalline compounds between metallic and nonmetallic elements with ionic or covalent very strong bonds, having high values of Young’s modulus, hardness, melting points, low values for thermal expansion coefficient and good chemical resistance. Once these bonds are broken, they can’t form in another position, so no plastic deformation happens at room temperature, where the behavior is completely brittle. It’s easy to think of pottery and its poor properties, but only engineered ceramics with high mechanical properties are considered in this study. Engineered ceramics are known for their peculiar preparation and manufacturing processes.

4.3.1.1 Defects and mechanical behavior

As in glasses, the curvature radius in ceramic is small and sharp and can’t be modified. Going above the tensile strength means immediate failure due to crack propagation. The smaller the defects, the higher the load that can be applied. ceramics must be loaded and tested in compression mode, so there is no stress generation factor. Zirconia has a peculiar behavior in crack propagation, as it induces cell transformation obtaining larger volume and closing cracks thanks to compression.

4.3.1.2 Manufacturing techniques

1. Chemical vapor deposition (CVD): this is the best technique to obtain high purity engineered ceramics. It consists in starting using cold gasses, usually a mixture of silane and methane, then thanks to the presence of a heating source a solid ceramic material is obtained, and gaseous products are discarded. The process happens at high temperatures (1500-1600 C) and pressure (50-3000 mbar), so it's costly and the major drawback is that it's difficult to find these cold gasses.
2. Powder-based processes: ceramics powders are first mixed with additives to be kept together, then shaped mainly through the extrusion of the slurry or slip or tape casting, then de-hindered and finally sintered. Sintering is a diffusion-controlled process activated by temperature, exchanging atoms from one side to the other heating up powders and additives. In the first part of the process the density increases rapidly, but never reaches the theoretical value, which leads to the presence of pores, a big issue in ceramics, as while the porosity value increases, there is inverse proportionality between Young's modulus and porosity.

   To reduce the final porosity, liquid sintering aids are used. They form a droplet on the surface of the ceramic. If the angle between the droplet and the solid surface of the ceramic (also called theta) is lower than 90 degrees, the wetting of the surface happens, so compressive forces between particles arise, so the lower theta, the better. If theta is higher than 90 degrees there is no wetting and, on the contrary, tensile forces between particles are created. The sintering liquid is in a glassy phase at high temperature, but sometimes the sintering aid can reach its softening point, being not suitable anymore. Ceramics can also be manufactured with no sintering aid, only pressing with uni-action pressure or isostatic pressure, or both.

4.3.2 Glasses

By definition, glass is a non-equilibrium, non-crystalline state of matter that appears solid on a short time scale, but continuously relaxes towards the liquid state. Towards the softening point it behaves as a liquid. The key point in working with glass materials is focusing on viscosity. Glasses are good thermal insulators because phonons don’t propagate in their structure. Glasses have a very good recyclability and a material can be considered a glass if it has whatever structure that in suitable conditions is amorphous, such as ceramics, amorphous metals, organic compounds and polymers.

4.3.2.1 Glass structure

Silicate glasses are formed by chains of SiO4(4-) tetrahedrons connected by bridging oxygens. Considering silica, it’s possible to have it in crystalline or amorphous state. Starting from the liquid phase, the cooling down process can be performed in two ways:

1. Giving enough time to the liquid to crystallize in a stable state, causing a shrinking phenomenon, obtaining quartz
2. Not giving enough time to crystallize, having an undercooled liquid until the glass transition temperature Tg. For T>Tg a rubber-like product is obtained, while for T<Tg a brittle solid is the result.

The density of crystalline silica is higher than the one of amorphous silica, as in the amorphous structure the value is larger due to void spaces. Silica has the lowest thermal expansion coefficient in nature. Generally, the glass transition temperature can be expressed in the following way

$$T_g = \frac{2}{3} T_m$$

Equation 10. Approximation of the glass transition temperature

Where Tm is the melting temperature.

A glass is made up of three units:

1. Glass formers, materials that can easily form glass from the molten state forming an amorphous network. Silica is the main glass former, which has high viscosity at molten state and tetrahedrons are not moving one on the other. Very few glass formers, such as germania and boron oxide are present in nature, other than silica.
2. Glass modifiers, materials that don't form any glass alone, but can break bonds in the tetrahedron chain, so that the melting temperature decreases and, therefore, it's easier to work the glass. Examples of these kinds of materials can be found in alkali, earth-alkali and zinc oxides.
3. Glass intermediates, materials that don't form any glass alone, but in limited amounts they can take part to the glass former, such as alumina, titanium oxide and zirconia.

4.3.2.2 Mechanical properties and macroscopic defects

The biggest drawback of glasses is that this material is brittle. Macroscopic defects in glasses act as a stress concentration factor and, as the curvature radius of the defect in glass is very sharp, the value of true stress at the defect tip is higher than the nominal stress value. This is the reason why glasses break instantly in a brittle way. There's no possibility to increase the curvature radius, because glasses only behave elastically. Glasses and in general brittle materials have size dependent mechanical properties, so for larger diameters the probability to find defects increases.

4.3.2.3 Thermal properties

One of the major advantages in glass materials is the possibility to change the thermal expansion coefficient, tailoring it for different applications adding a dopant. For example, considering adding sodium oxide as dopant to the glass, the thermal expansion coefficient increases, and the melting temperature decreases, although the bond strength value decreases as well.

A very important parameter is the thermal shock resistance of the material (TSR)

$$TSR = \frac{\sigma_f k}{E\alpha}$$

Equation 11. Thermal Shock Resistance (TSR)

Where sigma f is the mechanical strength, k coefficient of thermal conductivity, E elastic modulus and alpha thermal expansion coefficient.

Having low values for thermal expansion coefficient is good for obtaining high TSR values, but generally glasses don't have good performances. The only change that is possible to make is modifying the thermal expansion coefficient value. A solution to increase the TSR is using glass ceramics that can reach zero-dur conditions.

4.3.2.4 Glasses and glass ceramics as joining materials

Glasses are suitable for high temperature applications, as they are characterized by high characteristic temperatures, can work in oxidized environments, and can join parts without applying any pressure. Moreover, at softening point glass is used as a glue, after the softening temperature Ts crystallization is partially induced so that it behaves as a joint.

4.3.2.5 Joining and integration materials

Focusing on SOC, to integrate the interconnection system, gas separation, thermomechanical stability, electrical insulation, mechanical robustness and chemical stability have to be ensured. For this purpose, glass-based sealants are used, as they are suitable for high temperatures, have good reliability, can be used as separator between fuel and oxidant and thermal expansion coefficient can be designed.

Glass in the amorphous state is thermodynamically unstable, reason why glass ceramic sealants are chosen instead of just glass.

4.3.3 Steels

Metal components are widely used in the renewable energy sector. A common steel has a carbon content percentage lower than 1%. Mechanical properties are related to the presence of dislocations, which can move freely if mechanical properties are poor. By interstitial and substitutional defects, movements of dislocations are stopped, the strength value is higher, and, moreover, without dislocations no plastic deformation occurs.

It’s possible to have three different lattice structures in steels:

1. Body centered cubic (BCC) metals, with the steel atom placed at center of the structure. This type has low ductile transition.
2. Face centered cells (FCC), which are denser in dislocations and have preferential slip planes, are considered highly ductile.
3. Hexagonal structures have high packing density, but a low value of possible slipping planes, not possessing high ductile qualities.

4.4 Materials for SOC

Since the performance of SOC is related to porosity, ionic or protonic conductivity and electronic conductivity of the electrolyte, compatibility of the materials inside the cell (integration) must be guaranteed in order to obtain good performances.

4.4.1 Materials and related issues for SOCs

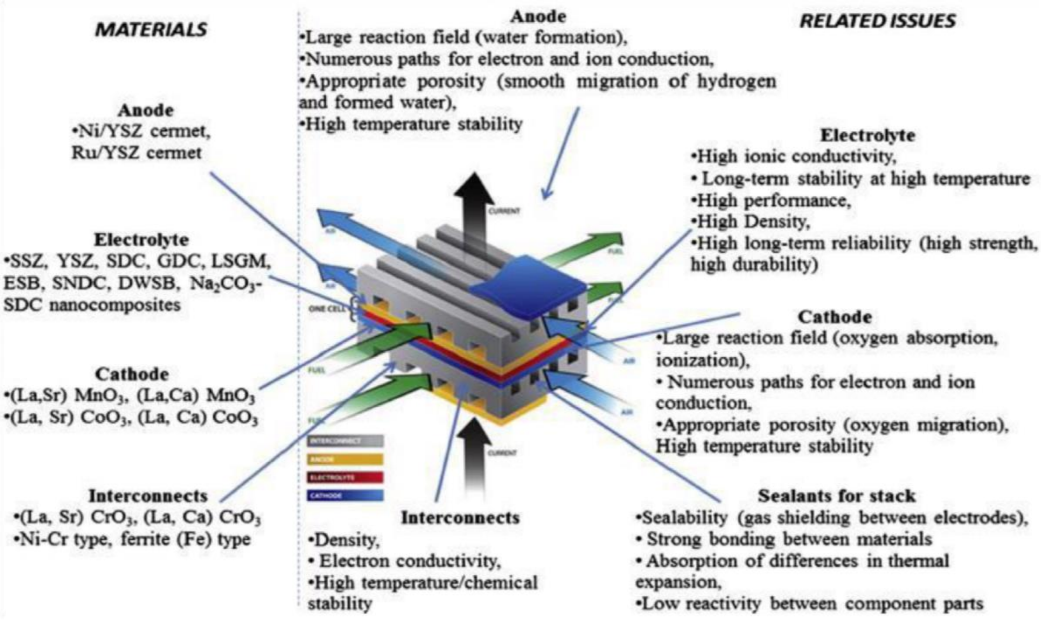

Figure 3. Summary of the material and the related issues of SOCs

1. The interconnects must provide electronic conductivity and high chemical stability, so they must be coated by a ceramic layer and show high temperature reliability. The most used materials are ferritic stainless steels
2. The sealant used is glass used as a high temperature glue due to integration issues. It must be tight to gas permeation. A good point is the possibility to

tailor the thermal expansion coefficient so that compatibility with other materials is ensured.

3. The electrolyte must have ionic conductivity only, it must be dense, show no permeation to gas and good mechanical reliability since the ceramic material always presents defects and is brittle. One of the main materials used is Yttria Stabilized Zirconia (YSZ), in which the matrix is doped with yttrium oxide.
4. The anode is usually a composite material between a metal and a ceramic. This kind of composite material is called cermet (Ni-YSZ or Ni-BZCY). Catalytic activity, electrical and ionic conductivity must be ensured. It also requires a large reaction field, as oxidation of hydrogen to water is needed. Appropriate porosity and high temperature stability are needed as well. Electronic conductivity is given by the presence of the metal, while the ionic conductivity by oxygen vacancies.
5. The cathode is made up of perovskites, whose structure is usually ABO3. perovskites can be modified to tailor its characteristics, as it’s a very flexible and versatile material. (LaSr)MnO3 (lanthanium strontium manganese oxide) or similar materials are used. The cathode must be porous. High values of electronic conductivity, minimum or no mismatch between the thermal expansion coefficients of the cathode and other components, good chemical compatibility, high oxide ion conductivity, good stability and high catalytic activity during oxygen reduction have to be ensured. These conditions are needed to start three elementary reactions happening at the cathode:
    a. Adsorption of oxygen at active sites
    b. Surface diffusion processes of the adsorbed oxygen towards the TPB
    c. Reaction of reduction of the adsorbed oxygen to a lattice oxygen ion. Having ionic conductivity and properly tailoring the porosity, it’s possible to extend the oxygen production reaction to the entire surface of the cathode.

4.4.2 Integration issues and challenges

Efficiency and durability can only be achieved by reliable joining and good integration. Issues regarding thermomechanical properties and functionality have to be addressed:

1. Corrosion must be limited, because the conductivity of the oxide scale is lower in respect to the one of the steels.
2. The presence of Chromium in the alloy, combined with the thermodynamic conditions of the SOFC, can form chromia, which contributes to the degradation of the oxygen electrode.
3. A good compatibility of the thermal expansion coefficient of the different materials must be ensured also for a temperature lower than the working temperature.

4.4.3 Functionalities

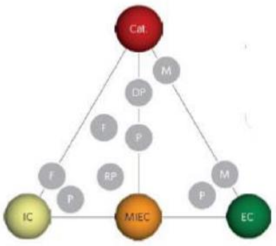

Figure 4. Functionalities of SOCs materials

Here four types of functionalities are displayed: electronic conductivity (EC), ionic conductivity (IC), catalytic activity (cat), mixed ionic and electronic conductivity (MIEC).

Metals are employed to provide electronic conductivity, while elements like fluoride (F) are used to both show ionic conductivity and mixed ionic and electronic conductivity and have a typical ceramic material structure. perovskites are electrically, ionic conductive and show catalytic activity, and allow to obtain all the functionalities needed in a SOC.

The anode in SOC is a composite, because it requires electronic conductivity, ionic conductivity and catalytic activity.

4.4.4 Ionic conductivity

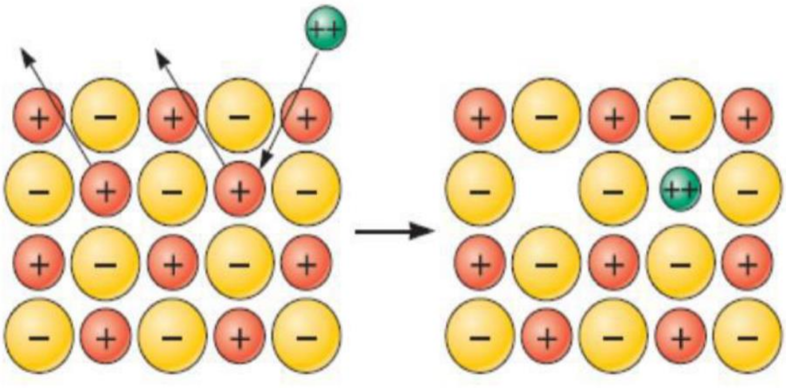

Figure 5. Creation of vacancies in an engineered ceramic

Basically, all materials can be conductors. The conductivity of a material is given by the sum of the charge, concentration of carrier species and mobility.

$$\delta = \sum cq\mu$$

For example, in YSZ, a processing of yttria oxide inside the zirconia oxide happens, having the substitution of tetravalent ions with trivalent ones, unbalancing the neutrality of the zirconia matrix creating oxygen vacancies, which is the main condition for the diffusion of other charged species. In this way, the hopping of ions through the electrolyte and the formation of vacancies can take place, as diffusion of charged species is a temperature triggered phenomenon. Mobility is strictly connected to the diffusion coefficient, temperature, and the Arrhenius state equation.

4.4.5 SOC sealant

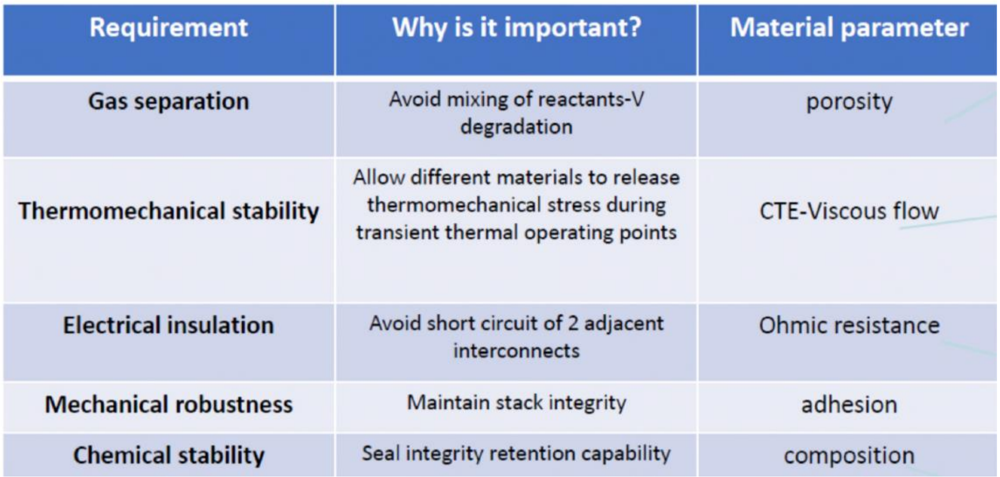

Requirement	Why is it important?	Material parameter
Gas separation	Avoid mixing of reactants-V degradation	porosity
Thermomechanical stability	Allow different materials to release thermomechanical stress during transient thermal operating points	CTE-Viscous flow
Electrical insulation	Avoid short circuit of 2 adjacent interconnects	Ohmic resistance
Mechanical robustness	Maintain stack integrity	adhesion
Chemical stability	Seal integrity retention capability	composition

Figure 6. Requirements for the SOC sealant

The phenomenology of glass formation refers to the glass transition from a supercooled liquid to a frozen one, obtaining a high viscosity amorphous material that is not thermodynamically stable. Glass transition is a kinetic transition with an internal timescale controlled by chemistry and an external scale controlled by the experiment itself, linked to the cooling rate, and so, having the most important role. In order to obtain glass, the cooling rate must be higher than the crystallization rate. Also, to assess whether the glass formation will happen it's needed to calculate the rate of nucleation as function of the temperature and to calculate the volume fraction of crystallization crystal growth in function of temperature is needed.

Requirements of SOC sealants are listed in the table. With glass it's possible to tailor the thermal expansion coefficient, but considering that it softens well below 1000 C, a more thermodynamically stable solution must be adopted, such as glass ceramics, which shows more crystalline structures. Glass ceramics must be designed considering the glass transition temperature Tg, the softening temperature and the thermal expansion coefficient.

4.4.6 SOC interconnects

Interconnects are needed for electrical connection, gas separation between electrodes and sealants to avoid gas leakages. The most important properties to consider are electrical conductivity and thermal expansion coefficient. The interconnect must be very reproducible, as many stacked cells are needed to reach a good voltage level. In the last 20 years interconnects have been made up of ceramic first, but this didn't constitute a cost-efficient solution, then it has been decided to employ stainless steel. Superalloys are very expensive and have quite high values for the thermal expansion coefficient, but other properties are good. The two main properties to consider are electrical conductivity, which has to be high, and thermal expansion coefficient. A compromise between price and electrical conductivity is found in Crofer 22, a state-of-the-art alloy that has high affinity with oxygen, forming a coating layer of chromia. It's a chromium rich ferritic steel with 0,03% C and 20-24% chromium, which is a ferrite stabilizer. Alloys have high electrical conductivity only at high temperatures, but this constitutes a problem, because chromia evaporates and poisons the active sites of the catalyst, which in the end is a big issue. In this case, chromium must be coated, having another interface.

In general, in coatings it's necessary to limit resistivity, chromia migration and oxidation rate. Also, generally, coatings are made up of perovskites and have two cations positioned in a specific location, being able to tailor both thermal expansion coefficient and electrical conductivity. One of the best solutions consists in having a double layer coating with a thin active anti-corrosion yttria layer and a thick spinel layer, which is the chromium blocking layer. The spinel structure is more complex than a normal perovskite and the state-of-the-art material in manganese cobalt. The most convenient method to produce this ceramic coating is the electrophoretic deposition, having a suspension of powder with a voltage difference, so that particles are positively charged, while the surface is negatively charged and, in the end, it's a self-limiting process, so the parts that were covered first will have a lower electrical field and the other parts will get covered.

In order to assess corrosion rates, it's possible to weigh the alloy without coating after oxidation and confront it with the coated alloy. If the coated alloy weighs less, the coating is effective. Double layer coatings are even more effective. Yttium chromide is a good compromise, as yttria is a very stable compound and won't evaporate. Moreover, coated interconnects are good precursors to obtain low area specific resistance (ASR) values for the whole cell. Good values are 0,2-0,55 ohm/m2 and ASR also decreases over time. Another technique is spray pyrolysis which allows to directly deposit particles on the surface. To obtain thicker coatings with this technique it’s possible to use lower temperatures and slow the manufacturing times.

5.Methodologies

5.1 Manufacturing techniques

5.1.1 Tape casting

Tape Casting was first introduced in the 1940s during the Second World War. In tape casting, sometimes referred to as the doctor-blade process, the slurry is spread over a surface using a carefully controlled blade referred to as a doctor blade. The tape casting process was firstly reported publicly in 1947 to produce thin ceramic sheets for usage of capacitor dielectrics and was shortly after applied to industrial production of ceramic capacitors. Many works on materials development and process improvement were published in the 1980s–1990s, see for example. Basically, this era was a period in which the technology matured, and new applications were explored, such as the production of thin membranes for fuel cells. A statistical design of experiments has also been conducted on the parameters like the weight fraction of ceramic powder, dispersant, plasticizer, binder and solvent in order to improve the process. A ceramic slurry contains different ingredients and each of them has a different impact on the rheological behavior of the slurry. The main ingredient in any slurry formulation is a powder. This is the only ingredient which determines the properties of a shaped material. As a ‘‘fluid forming technique” and, to increase the degree of formability, a solvent is needed to create a medium and carry powder under the casting blade, dissolve and assure a homogeneous distribution of all other slurry components. Another additive used in a ceramic slurry is the surfactant (standing for SURFace ACTive AgeNT), that actively modifies (or coats) the particle surface to obtain a desired characteristic, such as lower surface charge, higher surface charge, high/low surface energy, or specific surface chemistry. Both dispersant and deflocculant are categorized as surfactants. The binders are also used in ceramic slurries to simply impart the network that holds the entire chemical system together for further processing. Finally, other additives like plasticizers or sintering agents are usually added into any casting system to improve either the mechanical properties of the green tape (flexibility, plasticity, etc.) or the physical properties of the sintered tape (density, microstructure) or the heating kinetics. In principle, the parameters influencing tape casting are related to either the material content, i.e., the ceramic powder, solvent, dispersant, binder, plasticizer and deflocculant, or the machine configuration, i.e., the slurry height in the reservoir, the doctor blade height, substrate velocity, the doctor blade width and so forth. These parameters strongly influence the final properties of the tapes since they control the rheological behavior of the ceramic slurry.

Solid oxide fuel cells (SOFCs) are generally based on the same principle as the oxygen sensor, where the electrical energy is produced from a reaction of gasses such as hydrogen and oxygen or natural gas and oxygen with water as a by-product. The electrolyte in these fuel cells is the stabilized zirconia, which becomes a conductor of oxygen ions at elevated temperatures. In many cases the zirconia membrane, which is relatively large in the x and y directions and has a very thin cross section, is manufactured by tape casting. By tape casting of ceramic slurries directly onto the joining substrate, unnecessary handling steps may be avoided, and less binder and plasticizer must be added. [2]

5.1.2 Solid state and liquid state sintering

Sintering is categorized in the synthesis/processing element among the four basic elements of materials science and engineering. It is a processing technique employed to produce density-controlled materials and components from metal or/and ceramic powders by applying thermal energy. As material synthesis and processing have become crucial in recent years for materials development, the importance of sintering is increasing as a material processing technology. Sintering is one of the oldest human technologies, originating in the prehistoric era with the firing of pottery. Only after the 1940s, sintering was studied fundamentally and scientifically. Since then, remarkable developments in sintering science have been made. One of the most important and beneficial uses of sintering in the modern era is the fabrication of sintered parts of all kinds, including powder-metallurgical parts and bulk ceramic components. Sintering aims at producing sintered parts, with reproducible micro-structure, through the control of sintering variables. Micro-structural control means the control of grain size, sintered density, and size and distribution of other phases including pores. In most cases, the final goal of micro-structural control is to prepare a fully dense body with a fine grain structure.

The sintering of powder compacts with complex-shaped particles of different sizes cannot be explained in a simple manner. If spherical particles of the same size are assumed, the sintering of powder compacts can be represented as the sintering between two particles. In early studies, a sphere/plate geometry was also used for the explanation of initial stage sintering. The driving force behind sintering is largely determined by neck geometry and size; an examination of the geometrical relationship around the neck is first needed. The driving force of sintering appears as differences in bulk pressure, vacancy concentration, and vapor pressure. Diffusion is the most important sintering mechanism. The diffusion mechanism is related to the movement of atoms under a difference in vacancy concentration. A basic assumption in sintering is that the particles are sintered under a quasi-equilibrium state. In the case of diffusion, the diffusion gradient is in a steady state, and the time to achieve the steady state is negligible compared to that of a change in particle geometry.

Basically, sintering processes can be divided into two types: solid state sintering and liquid phase sintering. Solid state sintering occurs when the powder compact is densified wholly in a solid state at the sintering temperature, while liquid phase sintering occurs when a liquid phase is present in the powder compact during sintering. In addition to solid state and liquid phase sintering, other types of sintering, for example, transient liquid phase sintering and viscous flow sintering, can be utilized. Viscous flow sintering occurs when the volume fraction of liquid is sufficiently high, so that the full densification of the compact can be achieved by a viscous flow of grain–liquid mixture without having any grain shape change during densification. Transient liquid phase sintering is a combination of liquid phase sintering and solid-state sintering. In this sintering technique a liquid phase forms in the compact at an early stage of sintering, but the liquid disappears as sintering proceeds and densification is completed in the solid state. In general, compared with solid state sintering, liquid phase sintering allows easy control of microstructure and reduction in processing cost, but degrades some important properties, for example, mechanical properties. In contrast, many specific products utilize properties of the grain boundary phase and, hence, need to be sintered in the presence of a liquid phase. [3]

5.1.3 Laser sintering

The solid-state reactive sintering (SSRS) characteristic with the assistance of sintering aids (e.g., NiO) has been proven to be an effective method for achieving high-quality proton conducting oxide electrolytes at relatively low sintering temperatures (e.g., < 1400 °C). Instead of performing a long-term (e.g., > 10 h) SSRS in a conventional high-temperature furnace, a novel rapid laser heating process was used to perform SSRS, which was named as rapid laser reactive sintering (RLRS). This RLRS method was confirmed to be able to sinter protonic ceramics with well-engineered microstructures within a short time (e.g., < 10 s).

Proton conducting oxides (i.e., protonic ceramics) possess low transport activation energies which allow for high ionic conductivity at low operating temperatures (250–600 °C). However, because of the high refractory nature of the materials, state-of-the-art proton conducting oxides of yttrium-doped barium zirconates and cerates usually require sintering temperatures higher than 1700 °C to achieve acceptable relative densities. The high-temperature requirements make it very difficult to fabricate ceramic energy devices based on dense protonic ceramic electrolytes. On the other hand, the proton conducting oxides also need to be fabricated into highly porous nanostructures as electrode scaffolds for further improving device performance (e.g., direct hydrocarbon PCFCs), which requires even lower fabrication temperatures or new techniques which can sinter protonic ceramic under a specific temperature distribution instead of the conventional co-firing technique. Although the sintering mechanism is not clear, the addition of sintering aids can often decrease the sintering temperature to as low as 1350 °C, which makes it possible to prepare SOFCs by inexpensive co-fired techniques. Although the SSRS technique has been recently developed and successfully applied, it still needs long-term cofiring of the electrolyte and electrode (e.g., anode cermet) at a high temperature around 1400 °C. This high temperature usually eliminates the possibility of creating nanostructures for high-performance supporting electrodes when making half-cell using the co firing method. Furthermore, it is still a challenge to combine the PCFCs/PCECs with low-temperature and cost-effective stainless steel interconnects. By combining the selective laser sintering/melting technique and the solid state reactive sintering technique, a new rapid laser reactive sintering technique for selectively and instantaneously processing ceramics with well-controlled microstructures (fully dense and highly porous) has been developed, demonstrating the successful fabrication of dense large-grained (for electrolyte) and highly porous (for electrode scaffold) crack-free protonic ceramic parts with different configurations from inexpensive carbonates and binary oxides.

The rapid laser reactive sintering (RLRS) of protonic ceramics can be performed through four steps: mixing precursor solids, preparing precursor paste, depositing precursor layer and, finally, performing RLRS.

The RLRS process appears to be incredibly rapid and effective-processing times on the order of seconds can achieve the same crystal structures for BCZYYb and BZY20 ceramics as the state-of-the-art SSRS process, which take ~10 h at temperatures of 1400–1500 °C. [4]

The concept of laser sintering is referring to a method introduced in late 1980s as a new member of the additive manufacturing technologies. Laser sintering has been industrialized especially for processing of complex components because of its advantage of making three-dimensional (3D) net shape parts in one single operation. Sintered components can be made of a large variety of materials, such as plastics and metals. In addition, laser sintering enables production of special components that are difficult or even impossible to make by other conventional technologies. However, attempts to use laser sintering for processing ceramics, however, have not been equally successful despite the efforts made.

The laser sintering technique uses a high-energy laser beam to fuse powder granules directly into complex 3D net shape components in a layer-by-layer manner. Repeatedly a laser beam is scanning over a new single layer of free-packed powder granules and consolidating them via sintering or melt-solidification to each other and the previous consolidated substrate. The process scheme is governed by computer aided design (CAD) and computer aided manufacture (CAM) principles, so called CAD/CAM. As the laser beam moves quickly over the powder granules the process involves both a very rapid local heating of the powders and a subsequent rapid cooling of the melts. The laser sintering technique can be classified into three categories regarding binding mechanisms, namely solid-state sintering, liquid phase sintering or partial melting and melt-solidification. It is worth pointing out that laser sintering is a complicated process, and, in real practice, it is difficult to distinguish between these three types of general mechanisms. nature. Often, in the early stage of the laser sintering process, solid state sintering occurs, which transfers to liquid phase sintering or melt-solidification mechanisms later. Still, the preferred mechanism could be manipulated by adjusting the laser sintering parameters, like intensity and interaction time. The size distribution of powder granules can be controlled as well as using homogeneous composition to avoid local Tm variations.

In general, a laser sintering system consists of a laser source, a laser scanner, a powder loading unit, a building plate and a gas flow controller. Lasers with different wavelengths are selected to match the absorption characteristics of the corresponding powder granules. [5]

5.1.4 Spark plasma sintering

Another very interesting equipment in the laboratory facility can perform SPSS. The spark plasma sintering (SPS) process is an ECAS (electric current activated/assisted sintering) technique that combines the benefits of highly pulsed electric current (1000–8000 A), high pressure (up to 100 MPa), high temperatures (up to 2400 °C), and high heating rates (up to 1,000 K/min)3,11,12,13. With these characteristics, a wide range of materials can be fully compacted, from the polymers to ultra-high temperature ceramics14, such as TaC15, ZrB2 16, etc. With more than 6,000 archival publications (as indicated by Web of Science®), the SPS process is now a well-established and stable technology allowing the fabrication of small and large size samples for sintering times between 5 and 60 min depending on the material and the targeted application17. Despite its advantages, the SPS technique is low productive because of its commonly utilized batch processing schematics. [6]

This technique has been reported to be very effective in the sintering of little samples of ceramics (0,5-1 inch at a maximum), while it has reported issues in sintering larger components due to the presence of thermal gradients within the sample structure, making it mechanically unstable in the end. Though it is a very attractive and fast technique, it hasn’t been chosen for the purpose of the case study, since the sizes needed for the cell stack are bigger than the ones feasible with SPSS.

5.2 Imaging and spectroscopy

5.2.1 Sputter coating

Coating of samples is required in the field of electron microscopy to enable or improve the imaging of samples. Creating a conductive layer of metal on the sample inhibits charging, reduces thermal damage and improves the secondary electron signal required for topographic examination in the SEM. Fine carbon layers, being transparent to the electron beam but conductive, are needed for x-ray microanalysis, to support films on grids and back up replicas to be imaged in the TEM. The coating technique used depends on the resolution and application.

Sputter coating for SEM is the process of applying an ultra-thin coating of electrically-conducting metal – such as gold (Au), gold/palladium (Au/Pd), platinum (Pt), silver (Ag), chromium (Cr) or iridium (Ir) onto a non-conducting or poorly conducting specimen. Sputter coating prevents charging of the specimen, which would otherwise occur because of the accumulation of static electric fields. It also increases the number of secondary electrons that can be detected from the surface of the specimen in the SEM and therefore increases the signal to noise ratio. Sputtered films for SEM typically have a thickness range of 2–20 nm.

Benefits for SEM samples sputtered with metal: Reduced microscope beam damage, increased thermal conduction, Reduced sample charging (increased conduction), Improved secondary electron emission, Reduced beam penetration with improved edge resolution, Protects beam sensitive specimens. [7]

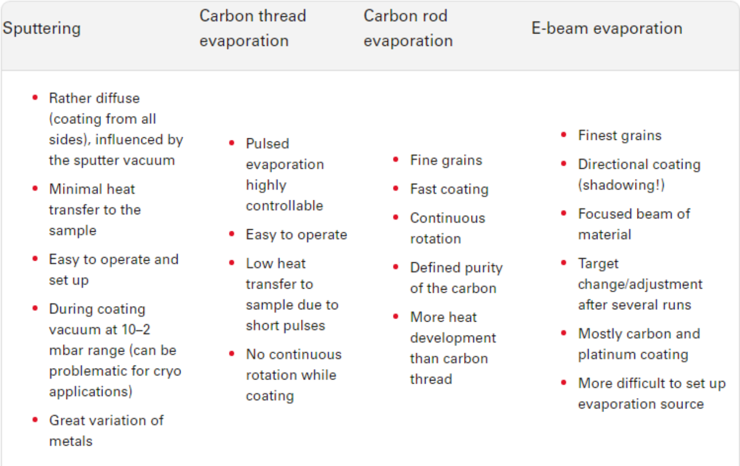

Sputtering	Carbon thread evaporation	Carbon rod evaporation	E-beam evaporation
• Rather diffuse (coating from all sides), influenced by the sputter vacuum • Minimal heat transfer to the sample • Easy to operate and set up • During coating vacuum at 10–2 mbar range (can be problematic for cryo applications) • Great variation of metals	• Pulsed evaporation highly controllable • Easy to operate • Low heat transfer to sample due to short pulses • No continuous rotation while coating	• Fine grains • Fast coating • Continuous rotation • Defined purity of the carbon • More heat development than carbon thread	• Finest grains • Directional coating (shadowing!) • Focused beam of material • Target change/adjustment after several runs • Mostly carbon and platinum coating • More difficult to set up evaporation source

Figure 7. Different sputtering techniques

Sputter coating is done to charge a non-conductive sample, as both YSZ and BZCY aren’t electrically conductive, so that it’s possible to have an image resulting from the SEM. It’s needed to enable the machine from the computer and turn it on from the back.

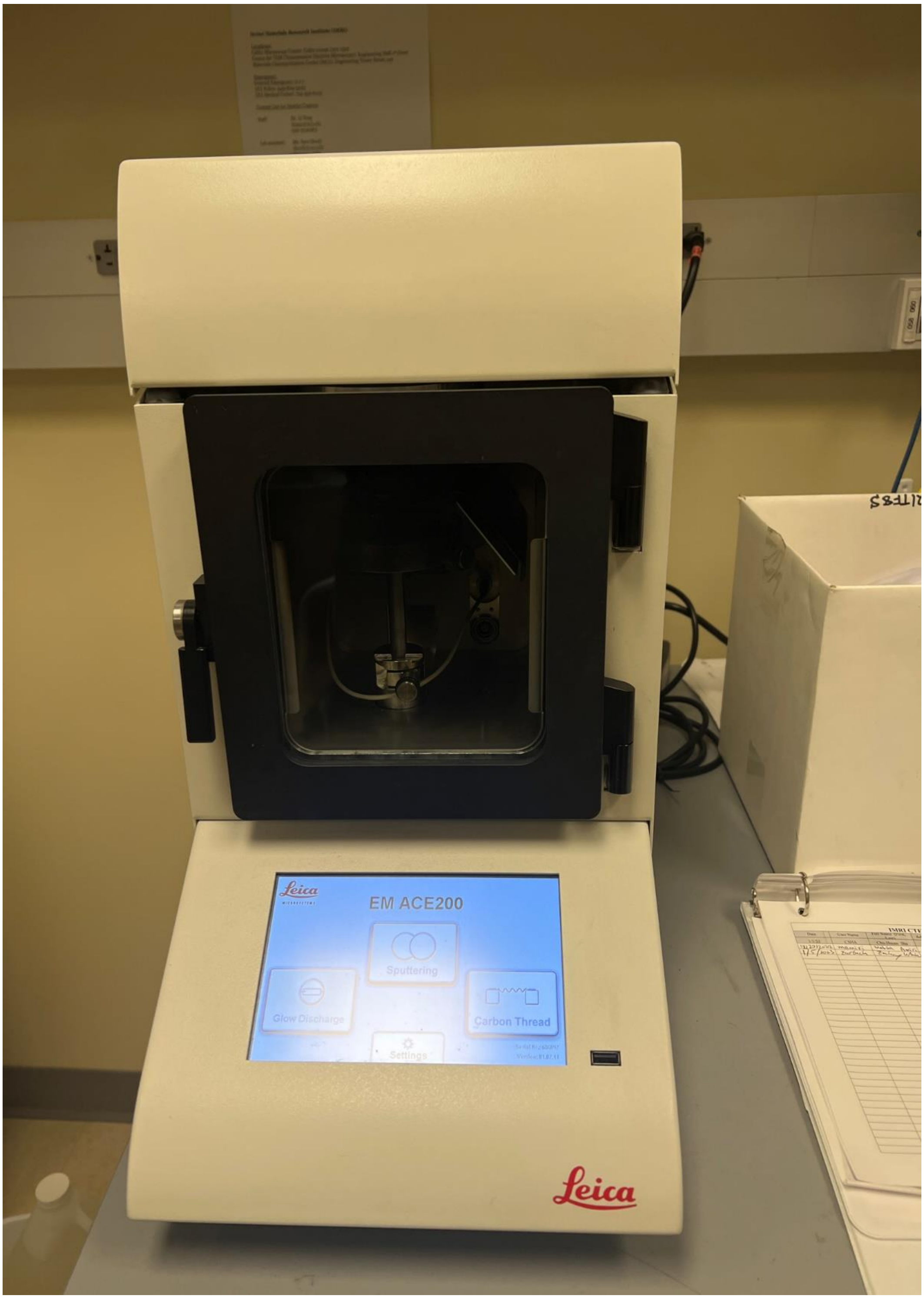

Figure 8. Leica sputter coater

There is also a glow discharge mode available on this equipment, and it’s done to reduce the contamination. The SEM sample preparation begins with putting the stage that is inside the sputter coater to go down. As a first step, the stage is unscrewed. The small plates on the stage need to be locked. There are 16 places available for sputter coating.

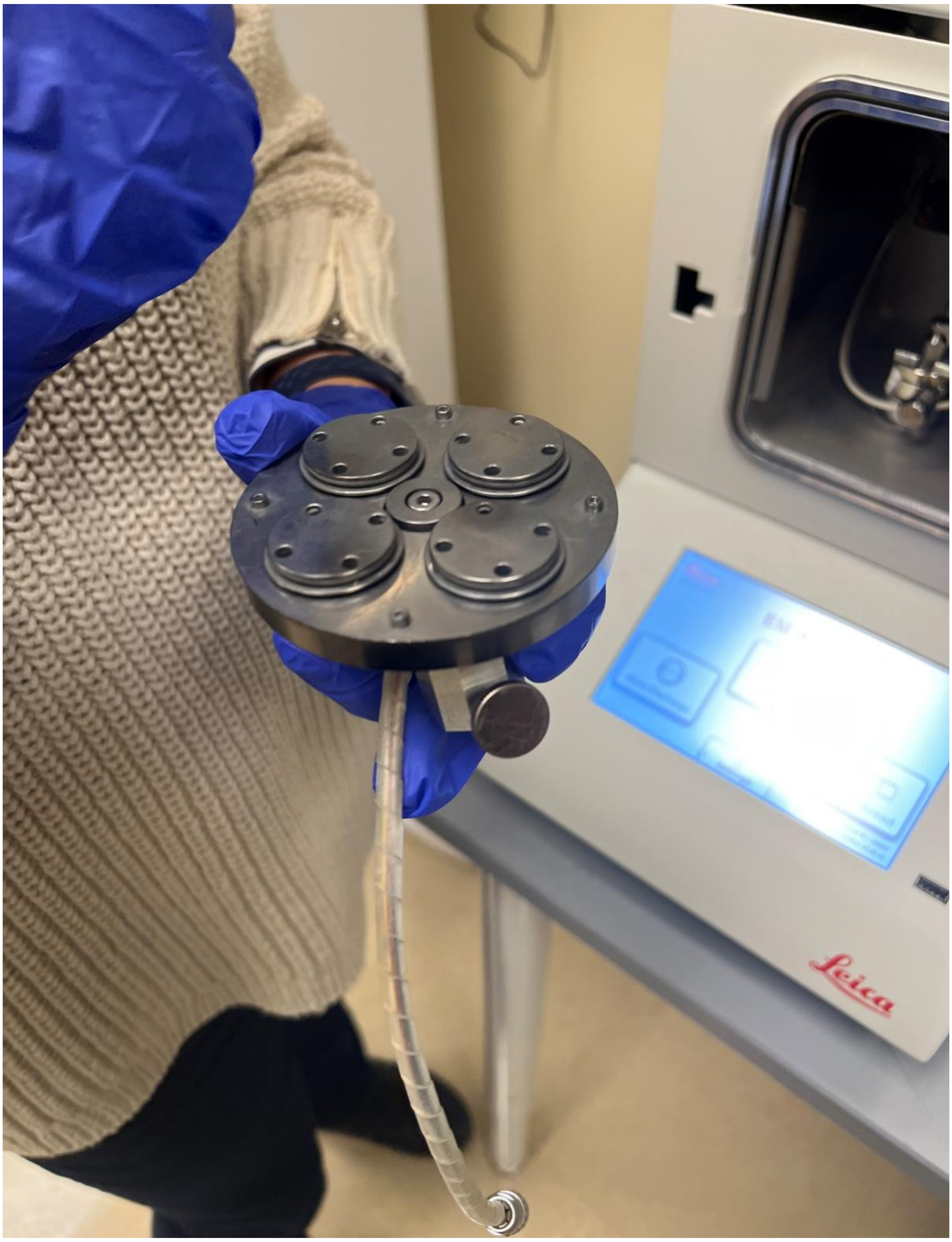

Figure 9. Stage of the sputter coater

The stage needs to be plugged to the bottom. Make sure it’s tight and the red dot corresponds to the plug. The stage can be placed back on. The machine needs a restart, because it must load up again the initial conditions as the samples have been mounted.

5 different rotation speeds are available and it’s possible to test them all. The speed between 2 and 3 is suitable for sputtering. The “sputter” plug only must be used.

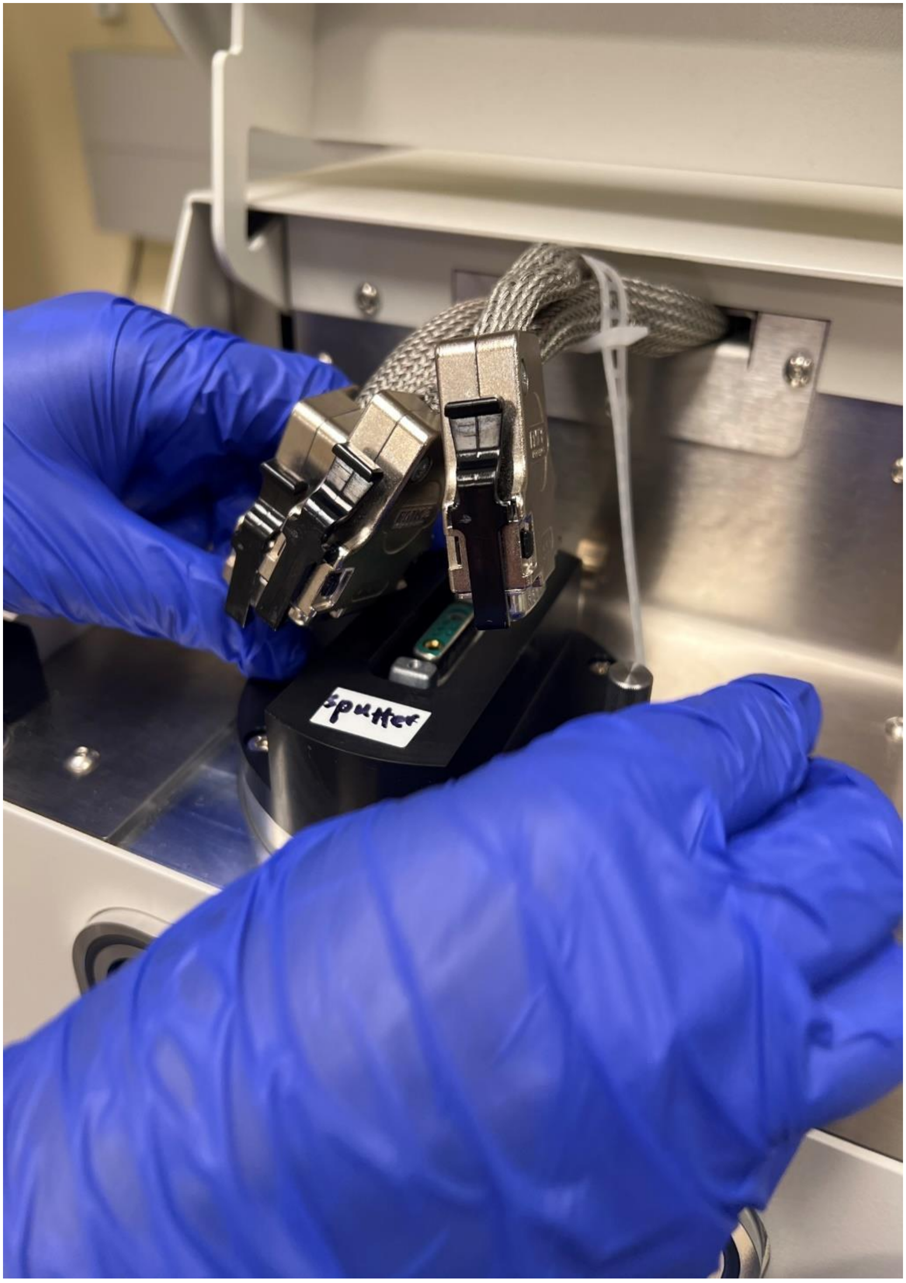

Figure 10. Sputter plug of the sputter coater

It’s also possible to control the thickness of the coat. We want a coat of at least 4 nm.

Quartz is installed as a crystal to perform coating.

The height difference between the average stage (the center of the stage) to the crystal is important. If the sample is above the center, a negative value on the screen is needed, if below a positive one. If the stage is put all the way down and the upper sample is analyzed, a value of -20 mm is chosen.

Then it's possible to close the door. If a good value of frequency for quartz is 5,99-6 GHz, therefore it needs to be tested.

For sputtering, Platinum-Palladium is chosen. A value of 4 to 8 purge cycles is chosen. These are the cycles where the argon in the chamber is replaced.

2.0 mbar should be shown if the pump button is pressed. Opening the argon valve is the last step before starting. Also remember to close it after the sputtering to prevent leakage.

The particles can be sputtered in a directional or in diffuse way. Both should work. As the start button is pressed, the argon starts flowing into the chamber. Once it's done and the thickness has reached the target value the vent button is pressed. Use tweezers to take out the sample.

5.3 Scanning electron microscopy

Scanning electron microscopy (SEM) is an important electron microscopy technique that can achieve a detailed visual image of a particle with high-quality and spatial resolution. SEM is a multipurpose state-of-the-art instrument which is largely employed to observe the surface phenomena of the materials. The sample is exposed in SEM to the high-energy electron beam and gives information about topography, morphology, composition, chemistry, orientation of grains, crystallographic information, etc. of a material, and therefore SEM is a useful tool to be used for the characterization of materials. Morphology indicates the shape and size, while topography indicates the surface features of an object or "how it looks", its texture, smoothness or roughness. Likewise, composition means elements and compounds that constitute the material, while crystallography means the arrangement of atoms in the materials. The sample is shot in a SEM using high-energy electron, and the outcoming electrons/X-rays are analyzed. These outcoming electrons/X-rays give information about topography, morphology, composition, orientation of grains, crystallographic information, etc. of a material. Morphology indicates the shape and size, while topography indicates the surface features of an object or “how it looks”, its texture, smoothness or roughness. Likewise, composition means elements and compounds that constitute the material, while crystallography means the arrangement of atoms in the materials. SEM is the leading apparatus that can achieve a detailed visual image of a particle with high-quality and spatial resolution of 1 nm. The SEM instrument is based on the principle that the primary electrons released from the source provide energy to the atomic electrons of the specimen which can then release as the secondary electrons (SEs) and an image can be formed by collecting these secondary electrons from each point of the specimen, the basic requirement for SEM to operate under a vacuum to avoid interactions of electrons with gas molecules in order to obtain high resolution. In addition, the primary electrons produced and emitted from the electron gun are accelerated by heating or applying high energy in the range of 1−40 keV. These emitted electrons are focused and confined to a monochromatic beam (to a diameter of 100 nm or less) by magnetic field lenses and metal slits within a vacuumed column. The confined primary electrons are scanned across the sample surface by scanning coils in a raster pattern. Once the primary electron beam hits the sample surface, it will interact with the near-surface area of the sample to a certain depth in many ways. The impinging electrons accelerated towards the specimens have substantial quantities of kinetic energy, which lose their energy inside the sample by generating several signals from the interactions of electrons with the specimen. If high voltages are applied, it will generate electrons with high energy and will thus penetrate farther into the sample and generate a larger interaction volume. In consequence, it will emit a variety of signals due to Coulomb (electric charge) field interaction of incoming electrons with specimen nucleus and electrons. The signals are gathered by electron collectors (detectors), which are then manipulated by the computer to form the required image. According to the detected signal (secondary electrons, backscattered electrons or X-rays), different information about the sample could be observed. The two routinely used electrons for sample image creation are the backscattered and secondary electrons. However, secondary electrons are considered the most important electrons, indicating sample morphology and topography, while backscattered electrons are used for demonstrating the contrasts in multiphase samples composition. After this the electrons are excited to the higher energy levels; when it comes back to the lower energy levels, it emits X-rays, having a specified wavelength, depending on the difference in energy level of various elements. In this way each element generated a characteristic X-ray after the impinging of an electron beam. SEM is non-destructive, as the generation of X-rays does not lead to any loss in the volume of the specimen; therefore, one can repeatedly analyze the same material. [8]

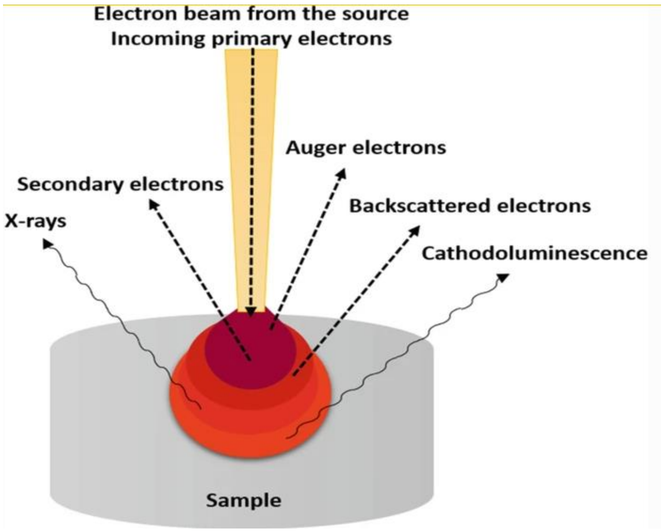

Figure 11. SEM working principle

In the laboratory facility of the Materials Research Institute of UCI, a SEM training with a copper sample has been performed in order to better understand how to use this instrument for further research on YSZ and BCZY samples.

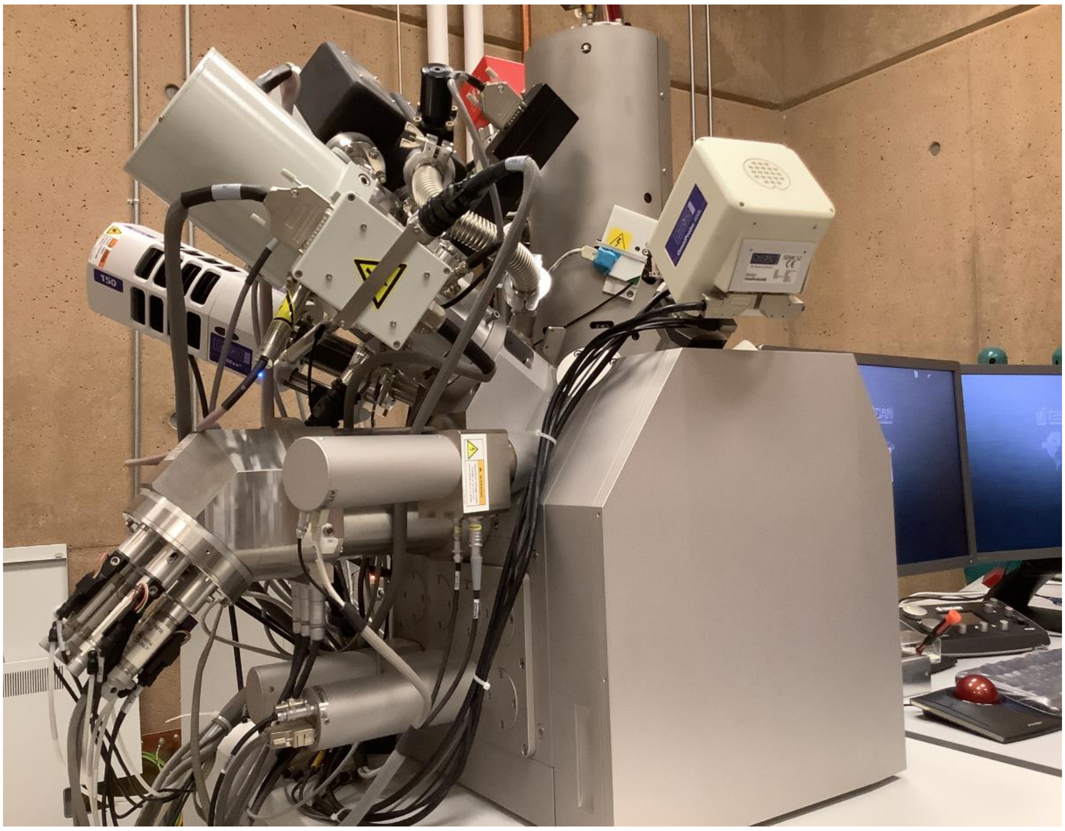

Figure 12. Gaia Tescan SEM in UCI IMRI facility

The SEM has a separate computer with which it’s possible to control the microscope. It’s an ion beam microscope. In standby conditions the pump won’t work so it won’t be in vacuum conditions and can save the lifetime of the machine. The vacuum and stand-by conditions need to be checked first. For that, two bars at least to be green. The stage needs also to be in home position, so z=80 and x and y rotations are 0. A check of the section on the right of the screen is needed. Open the stage control and check the number mentioned. There is a button associated with the camera. We can see an objective lens from which the electron beam comes out. The sample must be dry, must be conductive, secured, stable to the electron beam.

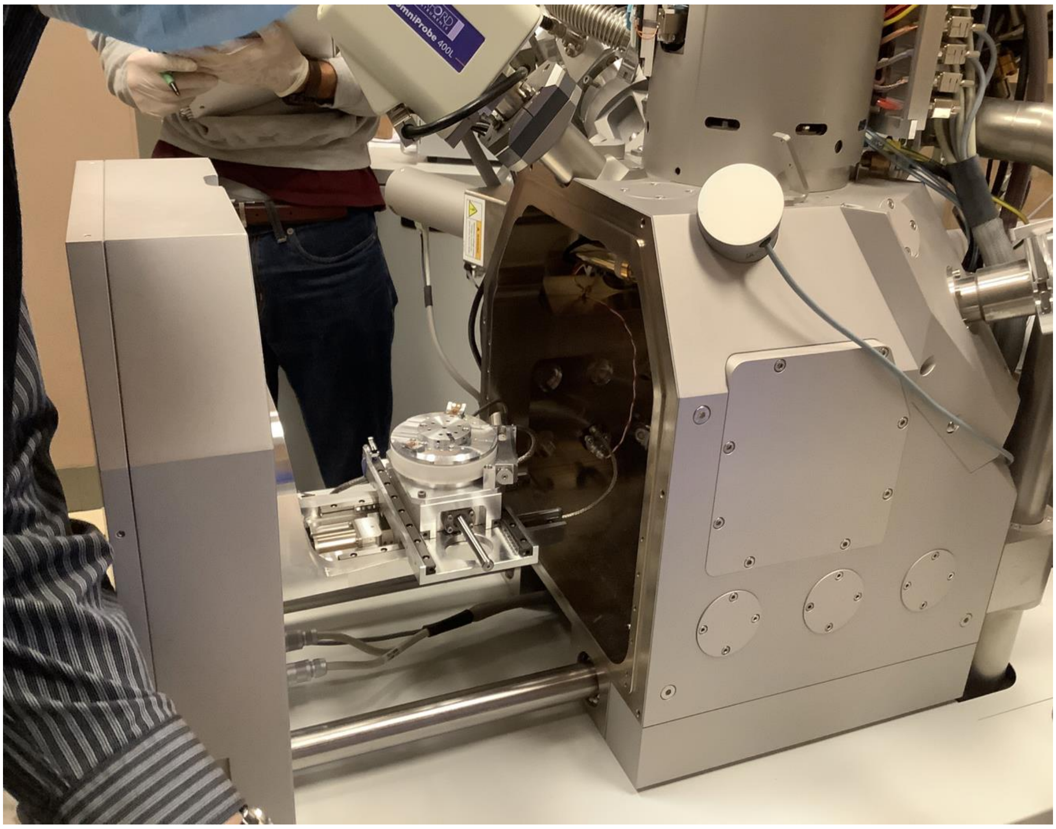

Figure 13. Loading the stage of the SEM

There are 7 positions in which it's possible to place the samples, making sure the samples are positioned at the same height and securing them with a screwdriver. After closing the door slowly, press the pump and wait two minutes until a noise is heard, while holding the door. Now all the bars should have turned green. In this way, it's possible to make sure the vacuum is ok. Go to the preset under SEM. It's possible to choose the parameters based on the type of sample and the intended type of analysis. In this demonstration, a copper sample is used. If a high-resolution image is needed, values between 1 to 10 must be used. Then it's needed to click beam on and the beam comes down to the sample. The stamps on the beam are changing the mode to FIELD mode. Adjust brightness and contrast too. Put on minimum magnification. In this way it's possible to find the sample. On the screen it's possible to see where the beam is hitting. As the samples are rotating, they need to be stopped with the dedicated button, trying to move the specimen and center it. The central button of the mouse is useful to move the sample clicking on it, and, if scrolled, to adjust the time frames shown (slower pace or faster). With a prolonged press on the right button, it's possible to change the size of the window. It's important to measure specimen height and find the minimum distance. "z" is the height from the beam point to the surface of the specimen. The lenses minimize the beam size to a certain focal point, the distance between the bottom of the core piece and the crossover of the cross point is called walking distance, which can be changed and is used to measure “z”. To calculate “z”, it’s possible to use imaging. The image is not only associated with the sample, but also to the beam. It’s not possible to get a resolution better than the sample size. The beam becomes smaller on the specimen. To obtain the best image, the focal point must be directly on the specimen. Resolution mode rather than FIELD mode must be used to measure the sample height. In resolution mode it’s not possible to see the image, because the focus point is not adjusted. A change in the height of the support is needed. Now the numbers shown must be close to the specimen height. It’s also possible to change the stage and the z with WD and Z. Now the sample will move up and will stop automatically in the middle. A much more accurate measurement of the sample height is obtained. Now in SE mode the image is not so clear, change mode to in beam SE. Now let’s get the sample even closer, reducing WD. Getting the best image quality. Alignment let’s click adjustment.

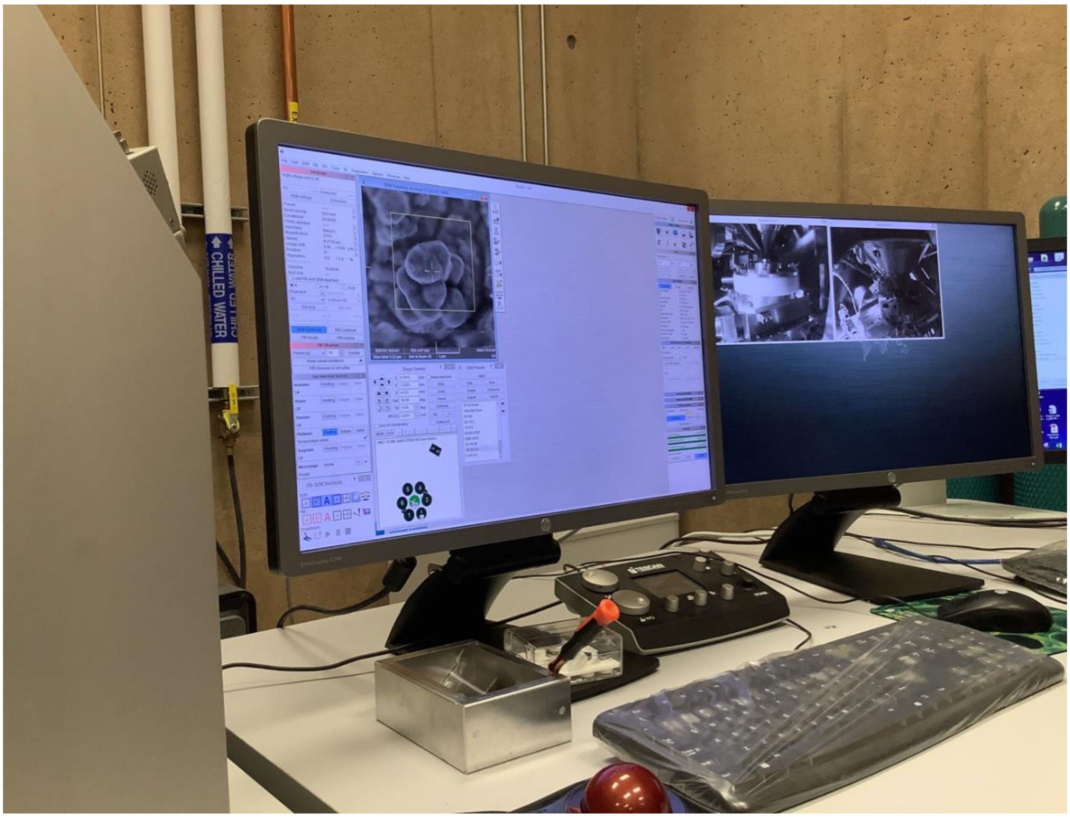

Figure 14. Gaia Tescan software GUI

Longer exposure times can help with details. The flattest the sample the better will be the result on all the planes. It’s possible to save the displayed image. Then to shut down, turn off the beam. Put the sample in first, slowly open the microscope and collect the samples.

5.4 X-ray diffraction

X-ray diffraction (XRD) is a powerful nondestructive technique for characterizing crystalline materials. It provides information on structures, phases, preferred crystal orientations (texture), and other structural parameters, such as average grain size, crystallinity, strain, and crystal defects. X-ray diffraction peaks are produced by constructive interference of a monochromatic beam of X-rays scattered at specific angles from each set of lattice planes in a sample. The peak intensities are determined by the distribution of atoms within the lattice. Consequently, the X-ray diffraction pattern is the fingerprint of periodic atomic arrangements in a given material.

X-ray diffractometers consist of three basic elements: an X-ray tube, a sample holder, and an X-ray detector. X-rays are generated in a cathode ray tube by heating a filament to produce electrons, accelerating the electrons toward a target by applying a voltage, and bombarding the target material with electrons. When electrons have sufficient energy to dislodge inner shell electrons of the target material, characteristic X-ray spectra are produced. These X-rays are collimated and directed onto the sample. As the sample and detector are rotated, the intensity of the reflected X-rays is recorded. A detector records. and processes this X-ray signal and converts the signal to a count rate, which is then output to a device such as a printer or computer monitor. X-ray powder diffraction is most widely used for the identification of unknown crystalline materials (e.g., minerals, inorganic compounds). Determination of unknown solids is critical to studies in geology, environmental science, material science, engineering, and biology.

The interaction of the incident rays with the sample produces constructive interference (and a diffracted ray) when conditions satisfy Bragg’s law:

$$n\lambda = 2d\sin(\theta)$$

where n is an integer, λ is the wavelength of the X-rays, d is the interplanar spacing generating the diffraction, and u is the diffraction angle. This law relates the wavelength of electromagnetic radiation to the diffraction angle and the lattice spacing in a crystalline sample. These diffracted X-rays are then detected, processed, and counted. By scanning the sample through a range of 2(theta) angles, all possible diffraction directions of the lattice should be attained due to the random orientation of the powdered material.

There are some strengths and some limitations of X-ray powder diffraction (XRPD). Strengths: powerful and rapid (<20 min) for identification of an unknown mineral, provides unambiguous mineral determination in most cases, requires minimal sample preparation, wide availability of XRD units, relatively straightforward data interpretation, nondestructive, fast, and easy sample preparation, high-accuracy for d-spacing calculations, can be done in situ, allows characterizing single crystal, poly, and amorphous materials, standards are available for thousands of material systems; limitations: homogeneous and single-phase material is best for identification of an unknown, access to a standard reference file of inorganic compounds is required, material, in tenths of a gram quantity, must be ground into a powder, for mixed materials, detection limit is » 2% of sample, for unit cell determinations, indexing of patterns for non-isometric crystal systems is complicated, peak overlay may occur and worsens for high angle "reflections".

XRD analysis can easily detect the existence of defects in a particular crystal, its resistance level to stress, its texture, its size and degree of crystallinity, and virtually any other variable relating to the sample's basic structure.

Proper sample preparation is one of the most important requirements in the analysis of powder samples by X-ray diffraction. This statement is especially true for soils and clays that contain finely divided colloids, which are poor reflectors of X-rays, as well as other types of materials such as iron oxide coatings and organic materials that make characterization by XRD more difficult. Sample preparation includes not only the right sample treatments to remove undesirable substances, but also appropriate techniques to obtain desirable particle size, orientation, thickness, and other parameters. Analysis of powders by XRD requires that they are extremely fine grained to achieve good signal-to-noise ratio (and avoid fluctuation in intensity), avoid spottiness, and minimize preferred orientation. Reduction of powders to fine particles also ensures enough particle participation in the diffraction process.

Important factors in sample preparation are: Sample properties also influence the quality of a powder

pattern by either reducing intensities or distorting intensities; Preferred orientation or texture: Texture means that the powder particles do not have an arbitrary shape but a strongly regular anisotropic shape, typically platelets or needles. On preparation these are then preferably oriented along the sample surface massively changing the peak intensities. Several techniques may be employed to minimize this effect: The most efficient way is to form a slurry in a highly viscous liquid such as nail varnish. In such a liquid, the random orientation is retained on drying. Alternatively, the anisotropic particle shape can be reduced by grinding in a ball mill. This should be done with great care as excessive grinding can easily break down the particle size to nanometer size and lead to amorphization. It is recommended to try the effect of subsequent 5 minutes grinding intervals to optimize the process on respective samples. In the case of coatings or thin films preferred orientation is often a desired effect. In this case Rietveld refinement can be used to determine the degree of texture; Crystallite size and strain: the broadness of a diffraction peak corresponds to the mean crystallite size in a reciprocal manner. The smaller the average crystallite size, the broader the reflections and the lower the absolute intensities. This effect becomes visible below an average crystallite size of less than 200 nm. Related to crystallite size broadening is strain broadening. Strain broadening occurs due to the presence of defects in crystals. Such strain can be introduced by substitution of constituting atoms but also by special thermal treatment. It is possible to distinguish strain broadening from size broadening as the angle dependence is much larger than in the latter case; Sample preparation height: Rotating sample holders improve the measurement statistics and thus provide the best results. However, they are not available for all

machines. The most serious error during sample preparation is to fill the sample holder too high or too low. Both result in a significant shift of peak positions, which can make the interpretation difficult. [9]

5.5 Raman spectroscopy

Raman spectroscopy was named in the honor of its inventor, C.V. Raman, who, along with K.S. Krishnan, published the first paper on this technique. Raman spectroscopy (RS) is a versatile method for analysis of a wide range of forensic samples. It resolves most of the limitations of other spectroscopic techniques. It can be used for both qualitative as well as quantitative purposes. Qualitative analysis can be performed by measuring the frequency of scattered radiations while quantitative analysis can be performed by measuring the intensity of scattered radiations.

Raman spectroscopy is a scattering technique. It is based on the Raman Effect, i.e., frequency of a small fraction of scattered radiation is different from frequency of monochromatic incident radiation. It is based on the inelastic scattering of incident radiation through its interaction with vibrating molecules. It probes the molecular vibrations.

In Raman spectroscopy, the sample is illuminated with a monochromatic laser beam which interacts with the molecules of the sample and originates scattered light. The scattered light having a frequency different from that of incident light (inelastic scattering) is used to construct a Raman spectrum. Raman spectra arise due to inelastic collision between incident monochromatic radiation and molecules of the sample. When a monochromatic radiation strikes a sample, it scatters in all directions after its interaction with sample molecules. Much of this scattered radiation has a frequency which is equal to frequency of incident radiation and constitutes Rayleigh scattering. Only a small fraction of scattered radiation has a frequency different from frequency of incident radiation and constitutes Raman scattering. When the frequency of incident radiation is higher than frequency of scattered radiation, Stokes lines appear in the Raman spectrum. But when the frequency of incident radiation is lower than frequency of scattered radiation, anti-Stokes lines appear in the Raman spectrum. Scattered radiation is usually measured at right angles to incident radiation. Raman spectrophotometers can be dispersive or non-dispersive. Dispersive Raman spectrophotometer uses prism or grating while non-dispersive Raman spectrophotometer uses an interferometer. Thermoelectrically cooled photomultiplier tubes and photodiode array detectors were used in early models of dispersive Raman spectrophotometers. Advances in instrumentation and technology replace these detectors with more sensitive charge transfer devices (CTDs) such as charge-coupled devices (CCDs) and charge-injection devices (CIDs). Depending on the area of use, Raman spectrophotometers can be categorized into two broad classes: lab-based spectrophotometers and in-field, in-situ or down-field use Raman spectrophotometers which include portable and hand-held devices or remote or stand-off systems. The basic principle is same in each case and these systems are differentiated by versatility of an instrument and size and relative cost of its components. More compact components are used in on-site Raman spectrophotometers. Benchtop, handheld, portable, remote or stand-off Raman spectrophotometers are available for on-site analysis and research purposes. Low sensitivity due to weak Raman scattering is the major problem associated with this technique. However, sensitivity can be enhanced using Resonance Raman Spectroscopy (RRS) and Surface Enhanced Raman Spectroscopy (SERS).

Raman spectroscopy has established itself as a reliable and non-destructive technique for the qualitative and quantitative analysis of a variety of drugs of abuse and illicit substances of forensic interest. Technique is capable of analyzing solid and liquid samples quite rapidly and without removing from packaging and thereby maintaining the integrity of forensic samples. The simplification of spectra caused by resonance allows the easy identification of species contained in complex mixtures. However, low sensitivity due to weak Raman signals and strong fluorescence due to impurities or colored packaging material can be very well addressed by combining two developments of the technique namely resonance Raman and surface enhanced Raman spectroscopy. [10]

Procedure

To calibrate the instrument, the usage of a silica sample is needed. The Raman spectroscopy uses a light scattering technique.

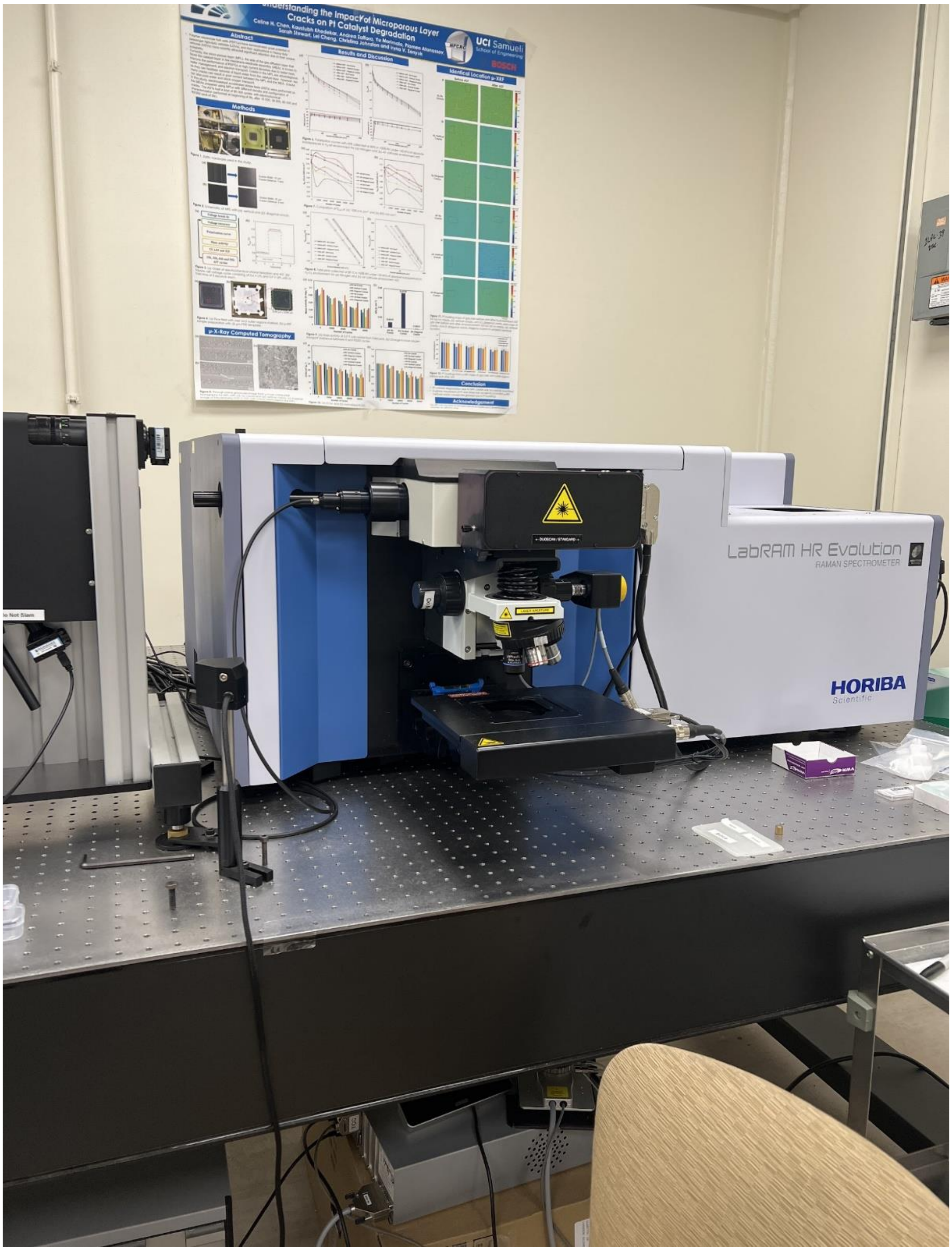

Figure 15. Raman spectrometer

The instrument has a zoom option and it's possible to calibrate for focus and lens that are planned to be used. Lithium MCM will be used in today's test, which is a cathode material. The software used is called "LabSpec 6 HORIBA scientific". In order to set the instrument correctly it's worth finding scientific papers that contain information on a Raman spectroscopy performed on the material analyzed. The instrument has four different lasers.

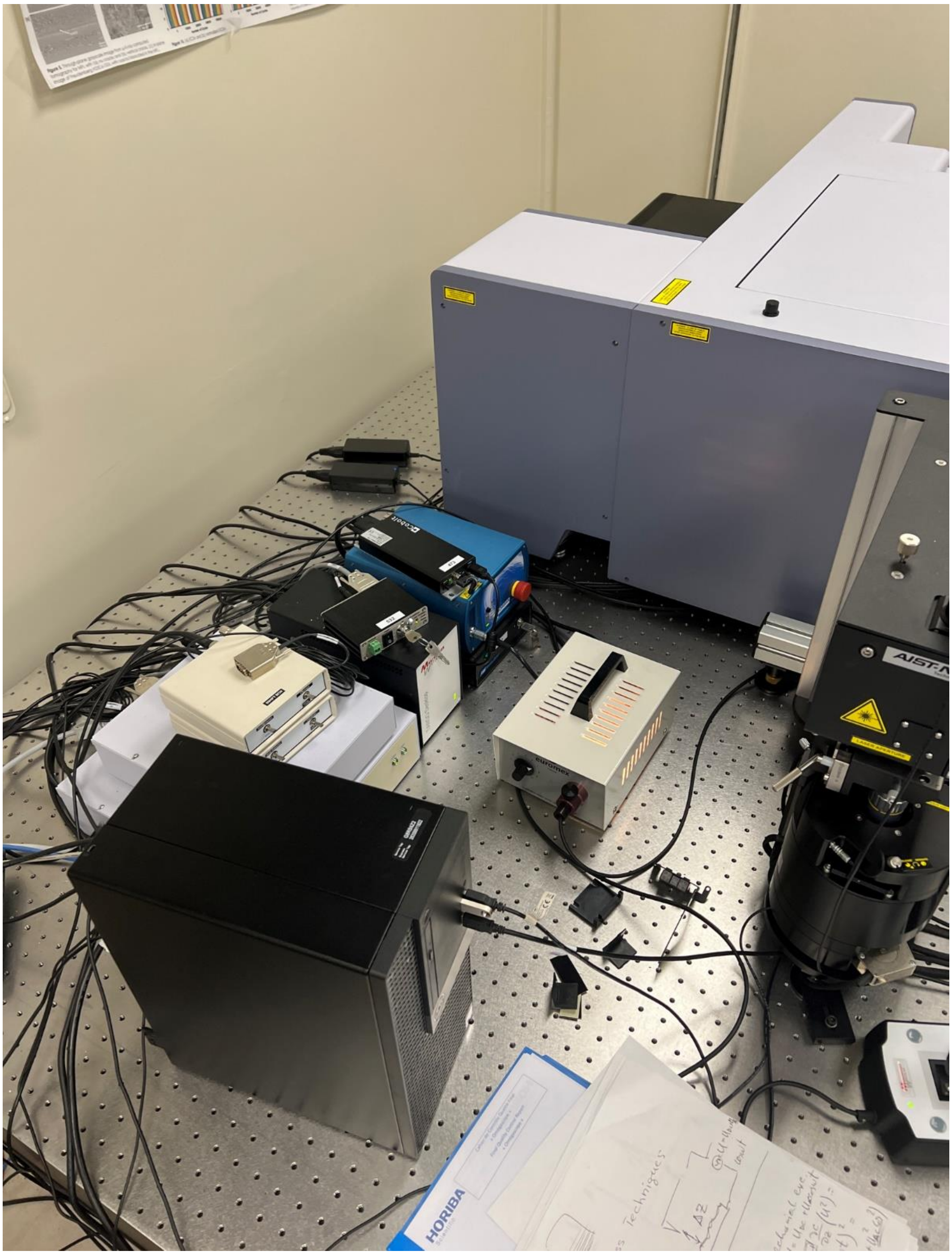

Figure 16. The four lasers of the spectrometer

There is a guide to use the software too. When on the software there is a red icon, it means that the machine needs to be calibrated. Green light means the instrument is on. The silica sample will be put under the instrument

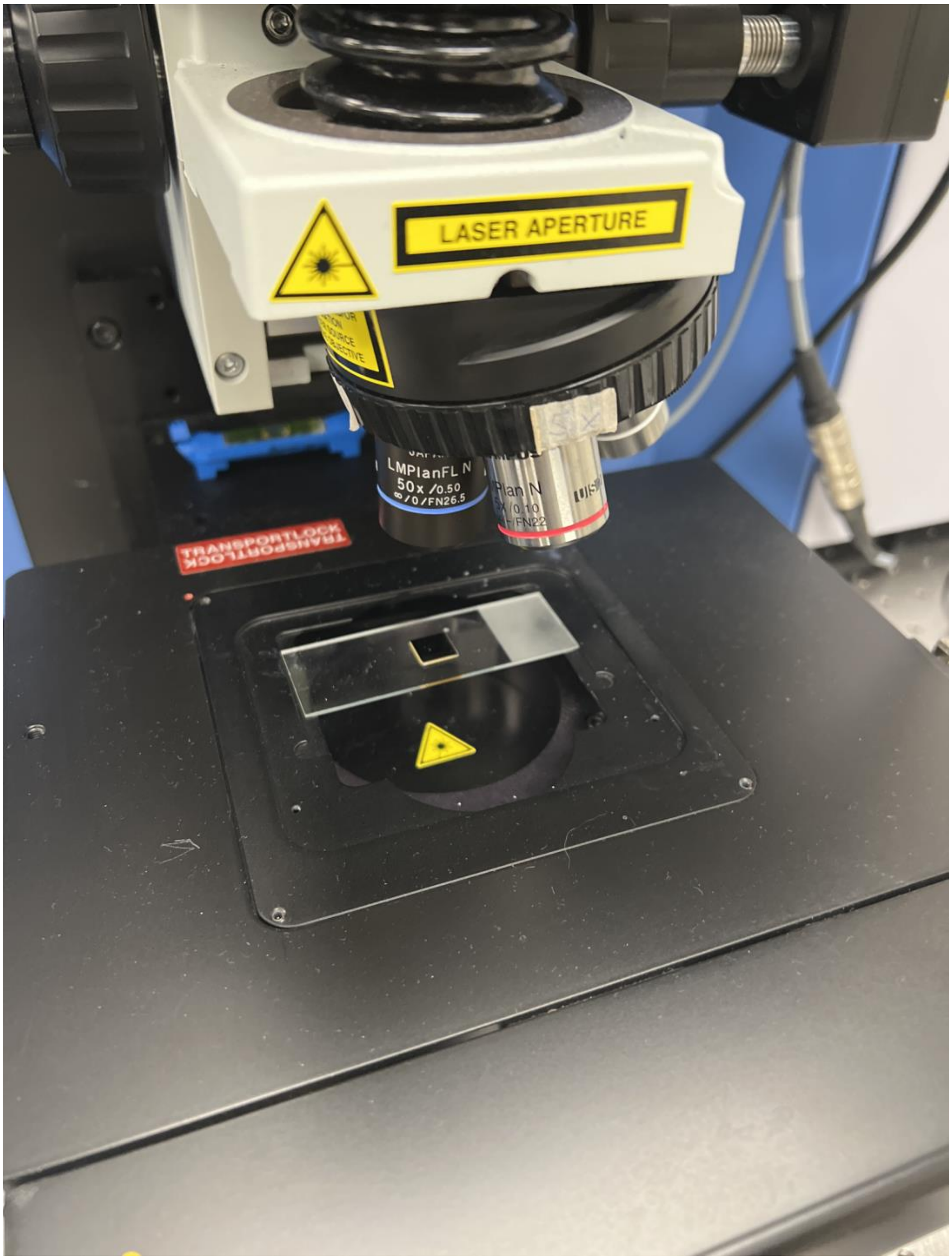

Figure 17. Main laser

At first, the zoom is set at 10x. If the sample is approached too fast with the objective, it could end up damaging the sample and problems of this kind come with the 100x lens.

The instrument can have fine movements controlled with this controller in the picture

Figure 18. Controller of the spectrometer

On the software, it’s possible to click on video and then start video and then, acting on the controller, focus on the sample. To zoom it’s needed to twist the instrument clockwise. When it’s focused, the light dot on the sample will be minimized. Now, it’s possible to see the sample on screen.

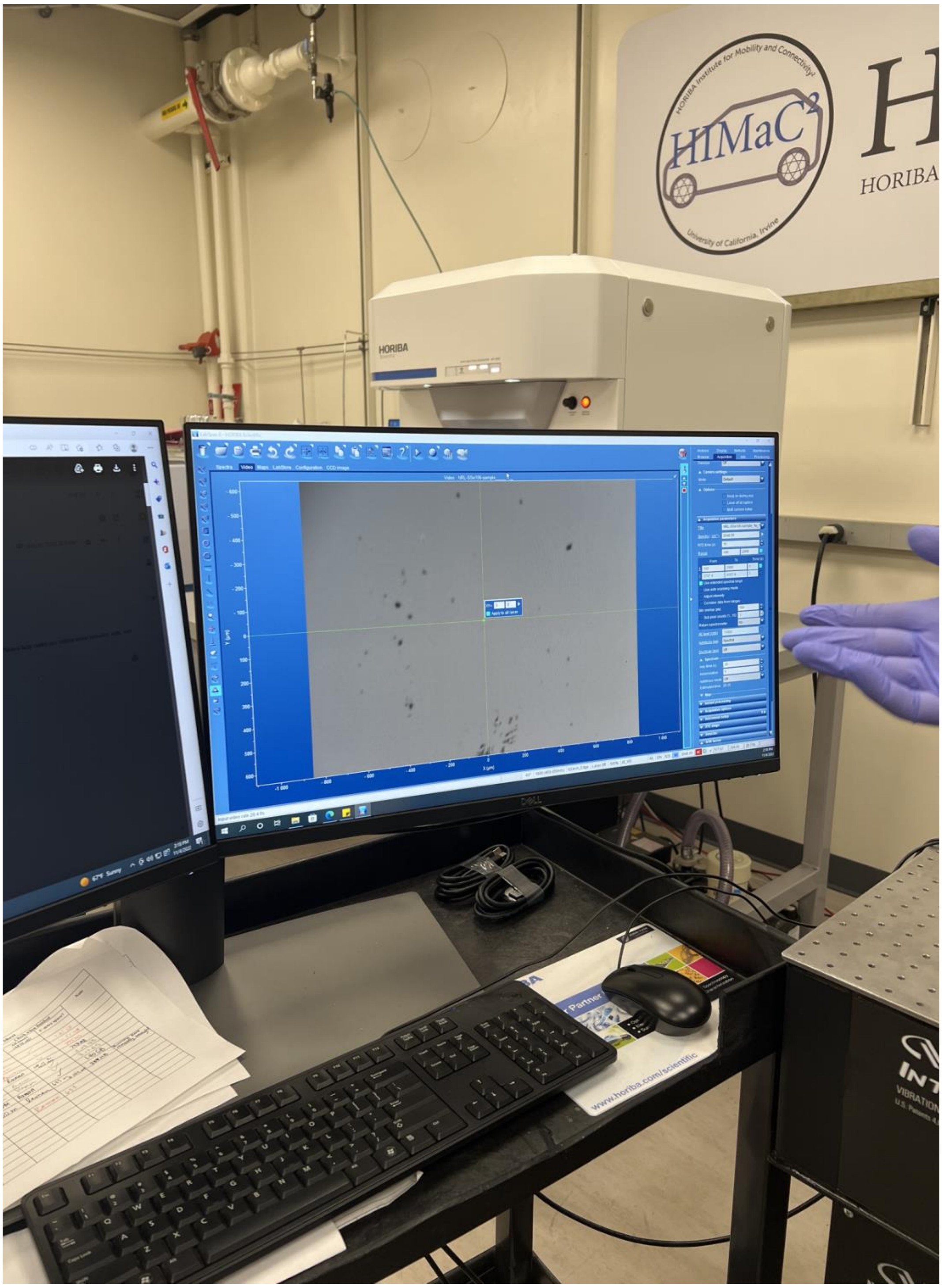

Figure 19. Sample picture on the screen

To check if the sample is focused, it’s worth going to the edge of the sample moving the controller.

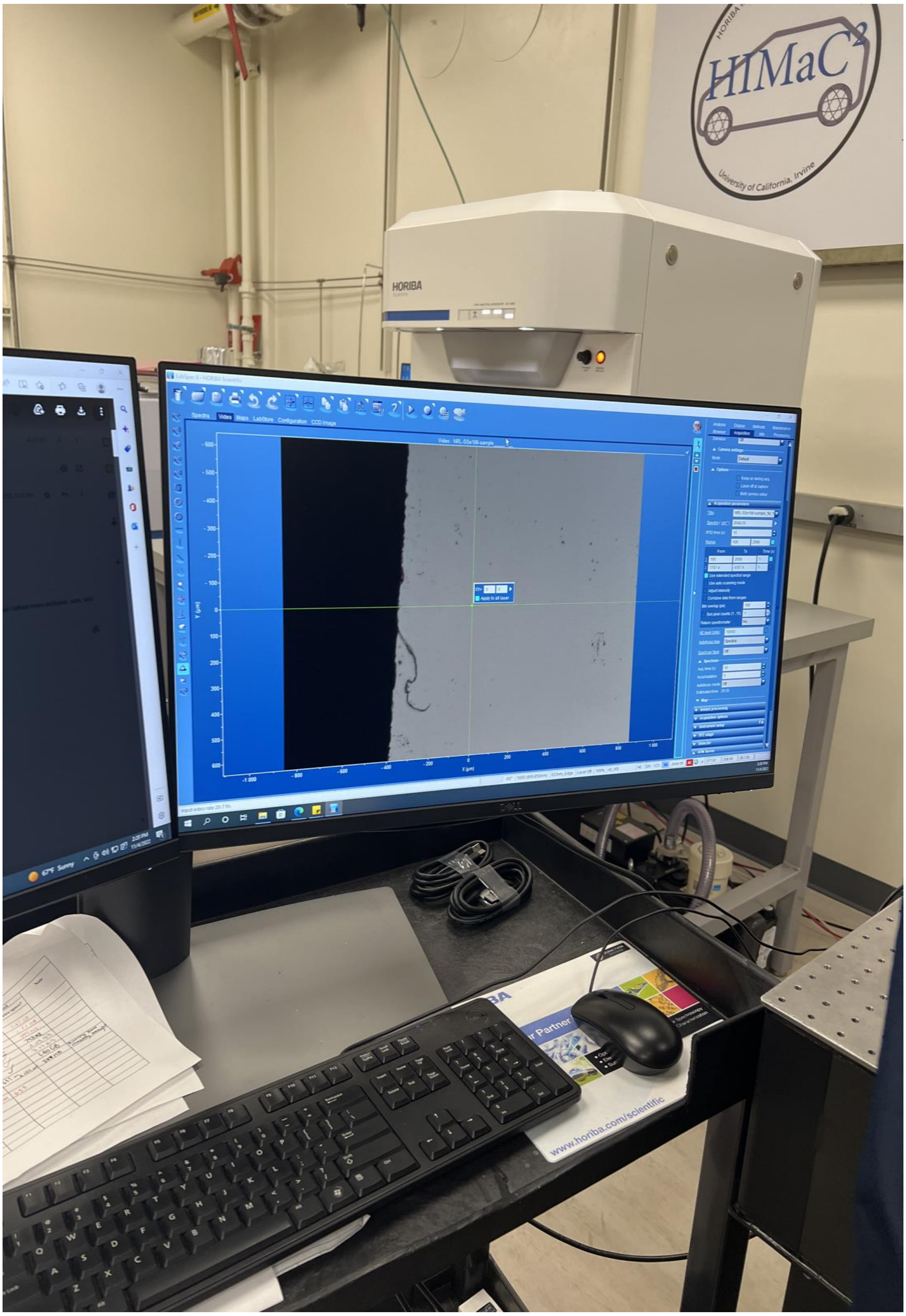

Figure 20. Sample picture on the screen

Once the sample appears to be focused with the 10x zoom, it’s possible to move to higher zoom values (50,100x…). Starting at 10x can be helpful to focus and find the sample in an easier way.

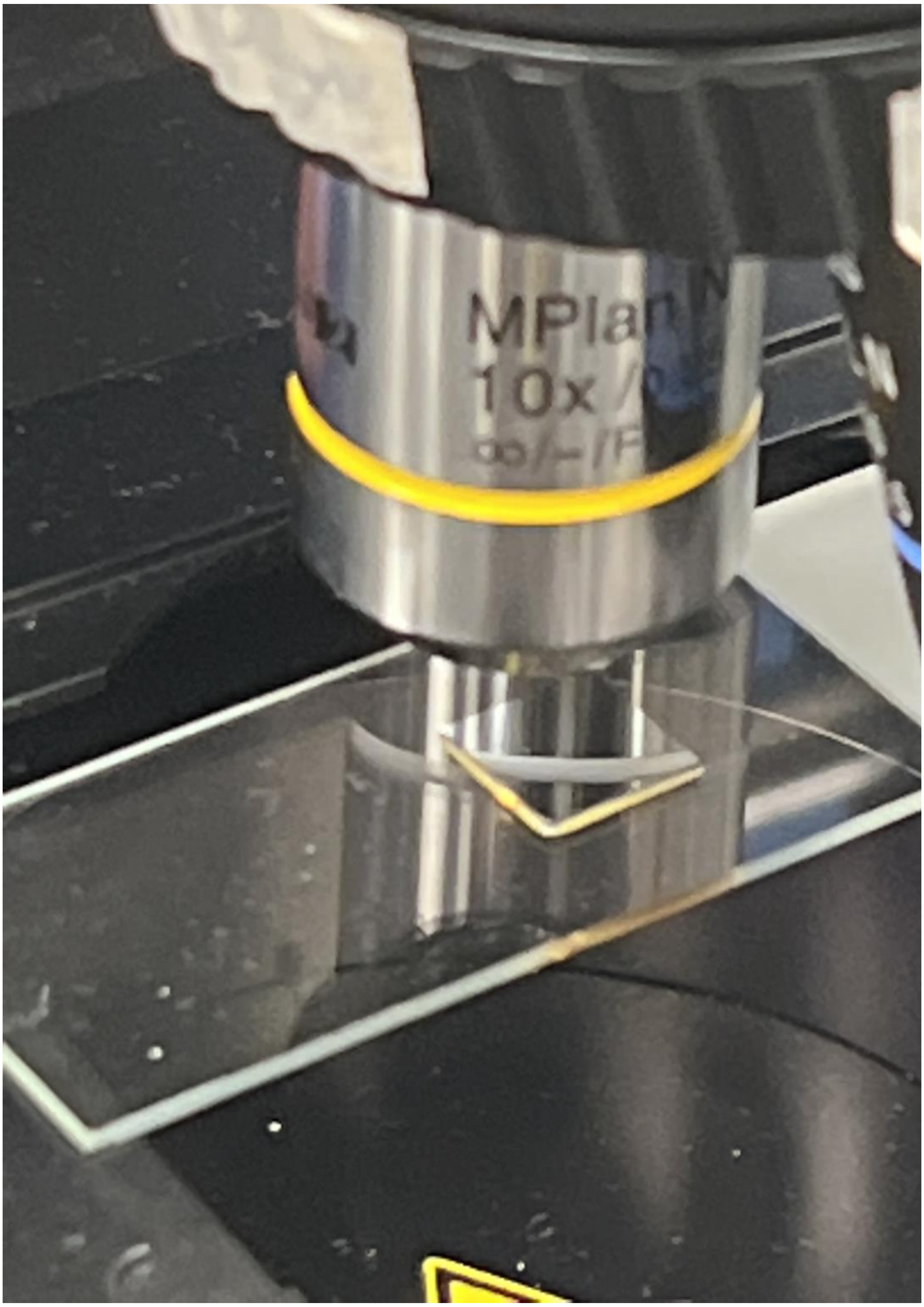

Figure 21. Zoom value

Also' it's needed to specify which laser is going to be used. The lens now is very close to the sample, so it's recommended not to use the manual adjustment of the height of the instrument, as the sample doesn't have to be damaged. Turning up the intensity of the light with the optical light can be useful in getting a brighter image on screen. Make sure the laser and objective chosen on the software are the ones planned to be used.

After stopping the calibration, it's possible to stop the video and take a picture of the sample.

There are now a bit of options: choose current laser/grating to start the auto calibration with the laser functioning. When taller samples are present it's needed to be more careful.

The auto calibration is passed, a message will pop up on the screen. The fingerprint for silica is 520 cm-1, which is its characteristic Raman shift. If it's not at 520 with silica a re-calibration is needed.

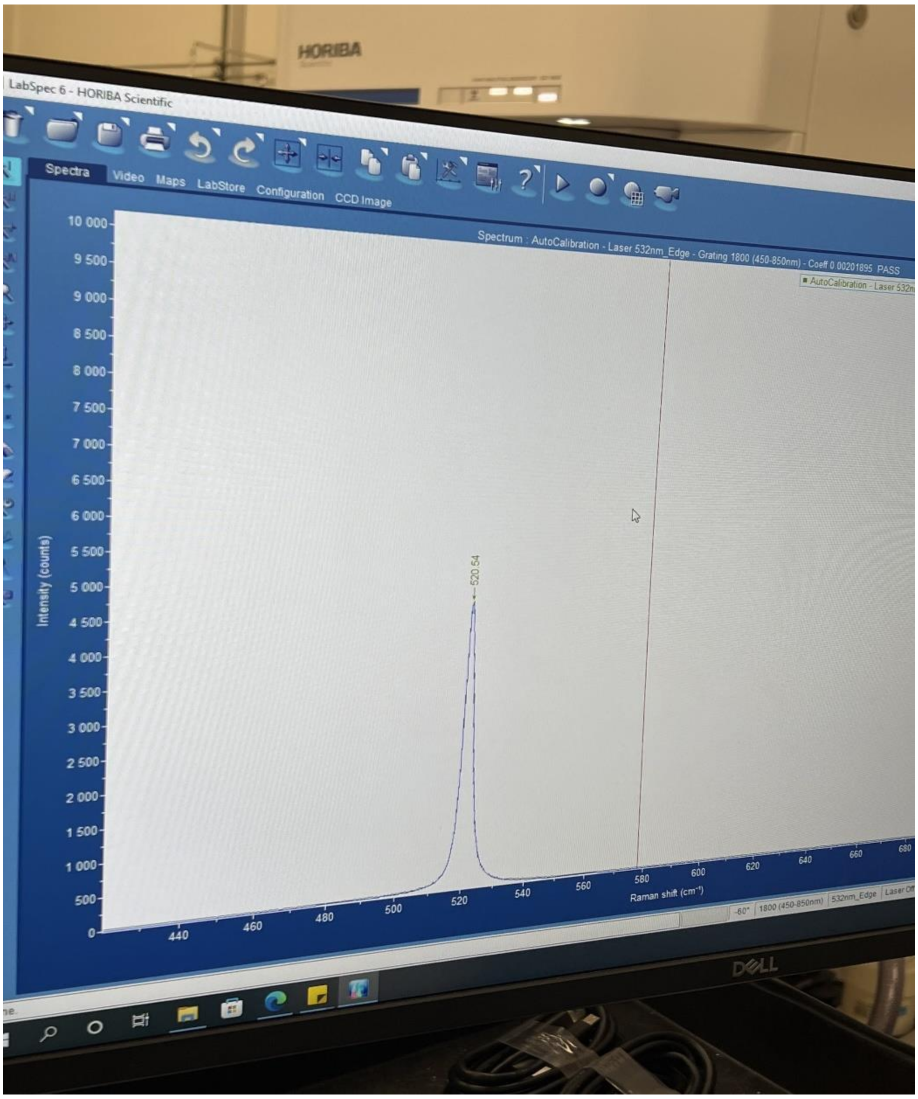

Spectrum : AutoCalibration - Laser 532nm_Edge - Grating 1800 (450-850nm) - Coeff 0.00201895 PASS

Figure 22. Characteristic Raman shift for silica

Now, it's possible to analyze the cathode sample. The vacuum pen is used to pick up battery materials and, in general, to hold materials without touching them (it sucks the materials). In this case a normal pin is used. Click video again on the software. The image now appearing is not the one of the cathode samples, but it’s of the silica sample. Click the video camera icon again. It’s possible to use the knob when far from the sample. The light is more scattered on the cathode sample surface, so it means it’s not focused. Let’s center the sample a little bit more. This is an image of the cathode sample.

The sample is not touched by the instrument if it’s possible to still see a little light. The green dot is the center of the measurement. Now click stop all so that we can get the image.

When collecting the spectrum, it’s possible to click on “spectrum acquisition”. But before that, it’s advisable doing a real time display to avoid other noise sources. The real time display shows if the peak is expected to be on the sample, so if it’s not coming from where expected it might be a noise. Click acquisition on the right side of the screen.

Here, it’s possible to name the sample and to set the duration for the real time display (RTD) (1 second). The range is set between 1000 and 3000, this is where the peak is expected to happen. The acquisition time will be 10s and 2 accumulations. The longer the acquisition time, the better the spectrum.

Make sure to choose have correct laser and objective on the software before making real time measurements and acquisition.

This is a non-destructive method, if done properly.

When doing the real time display, check if the noise disturbance is ok. The signal is constituted by the peaks, the second requirement is that the intensity must not exceed 65000 counts. Then that the spectrum is stable.

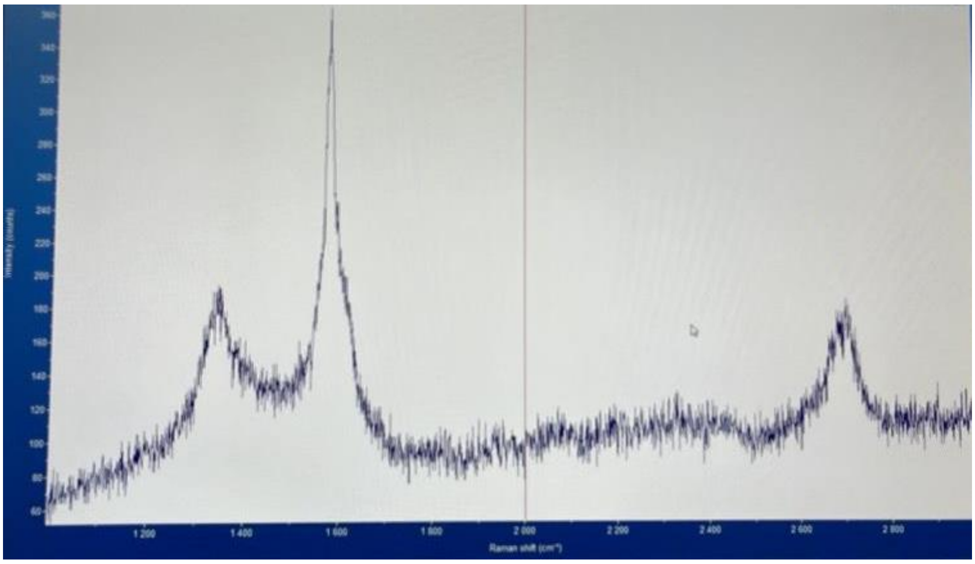

Figure 23. Result of the Raman spectrum acquisition

It's also possible to use EFM together with the Raman spectroscope.

5.6 Energy Dispersive Spectroscopy

Energy-dispersive X-ray spectroscopy (EDS, also abbreviated EDX or XEDS) is an analytical technique that enables the chemical characterization/elemental analysis of materials. A sample excited by an energy source (such as the electron beam of an electron microscope) dissipates some of the absorbed energy by ejecting a core-shell electron. A higher energy outer-shell electron then proceeds to fill its place, releasing the difference in energy as an X-ray that has a characteristic spectrum based on its atom of origin. This allows for the compositional analysis of a given sample volume that has been excited by the energy source. The position of the peaks in the spectrum identifies the element, whereas the intensity of the signal corresponds to the concentration of the element.

As previously stated, an electron beam provides sufficient energy to eject core-shell electrons and cause X-ray emission. Compositional information, down to the atomic level, can be obtained with the addition of an EDS detector to an electron microscope. As the electron probe is scanned across the sample, characteristic X-rays are emitted and measured; each recorded EDS spectrum is mapped to a specific position on the sample. The quality of the results depends on the signal strength and the cleanliness of the spectrum. Signal strength relies heavily on a good signal-to-noise ratio, particularly for trace element detection and dose minimization (which allows for faster recording and artifact-free results). Cleanliness will impact the number of spurious peaks seen; this is a consequence of the materials that make up the electron column.

Sensitive to low concentrations—minimum detection limits below 0.1% in the best cases; Affords a high degree of relative precision—typically 2–4%; Non-destructive in most situations; Usually requires minimal sample preparation effort and time; Delivers complete analyses of complex samples quickly, often in under a minute. [11]

6.Other analysis techniques

6.1 Rheology

Rheology is the study of the flow of matter, primarily in the liquid state, but also as soft solids or solids under conditions in which they respond with plastic flow rather than deforming elastically in response to an applied force. Most low molecular weight liquids, solutions of low molecular weight inorganic salts, molten metals and salts, and gasses exhibit Newtonian flow characteristics, i.e., at constant temperature and pressure, in simple shear, the shear stress (s) is proportional to the rate of shear (c_) and the constant of proportionality is the well-known dynamic viscosity (l).

There has been a growing recognition of the fact that many substances of industrial significance, i.e., foams, emulsions, dispersions and suspensions, polymeric melts and slurries, do not conform to the Newtonian postulate of linear relationship between (s) and (c_) in simple shear. Accordingly, these fluids are variously known as non-Newtonian, non-linear, complex, or rheologically complex fluids.

A rheometer is a precision instrument that contains the material of interest in a geometric configuration, controls the environment around it, and applies and measures wide ranges of stress, strain, and strain rate. It’s an instrument that measures both viscosity and viscoelasticity of fluids, semi-solids, and solids. It can provide information about the material’s viscosity, defined as a material’s resistance to flow deformation and is a function of shear rate or stress, with time and temperature dependence; viscoelasticity, a property of a material that exhibits both viscous and elastic character. [12]

The Discovery series Hybrid Rheometer (DHR) from TA Instruments offers precise measurements of both viscosity and viscoelasticity of various materials, e.g., high viscosity fluids, pastes, polymer solutions and melts, and soft solids and as a function of temperature. Typical applications include viscosity measurements of LED encapsulants, solder pastes, fluxes, underfill, die-attach adhesives, glob top encapsulants, etc. for the electronic packaging industry; curing profiles of thermoset plastics and UV-curing adhesives and encapsulants; and rheology and viscoelasticity of polymers. [13]

6.2 Thermo-gravimetric analysis

Thermogravimetric analysis (TGA) is an analytical technique used to determine a material’s thermal stability and its fraction of volatile components by monitoring the weight change that occurs as a sample is heated at a constant rate. [14]

6.3 Differential scanning calorimetry

Differential scanning calorimetry (DSC) is a powerful analytical tool for the identification of various physical properties and thermal transitions of polymeric materials. DSC is used to estimate the melting and mesomorphic transitions along with their entropy and enthalpy. Characterization of glass transition temperature (T_g) and other effects that show either changes in heat capacity (C_p) or latent heat of polymeric materials can be performed using DSC. This analytical tool measures thermal transitions, C_p, and enthalpy through calorimetry. Since its invention in the 1960s, DSC has become a trendy thermal analytical tool used in a broad heating kinetic range related to heating and cooling at different heating rates and isothermal conditions.

Calorimetry is derived from the combination of calorie and metering. Thermal analysis is used to examine the energy changes in a material, which is estimated by measuring heat flow to and from the material. Calorimetry is an essential technique used to make a direct estimation of enthalpy connected with a typical process of interest.

Among different kinds of calorimeters, differential scanning calorimeter (DSC) is the most extensively used.

In other words, the device is a thermal analysis instrument that regulates the temperature and heat flow connected with sample material transitions as a function of time and temperature. During a temperature change, DSC measures a heat amount, which is radiated or absorbed primly by the specimen on the basis of the temperature difference between the sample and reference. DSC can be broadly classified into two major classes: heat-flux DSCs and power-compensated DSCs (PC-DSCs).

The specimen is enclosed inside a pan, and an empty reference pan is placed on a thermoelectric disk surrounded by a furnace in a heat-flux DSC. Both furnaces are heated at a linear heating rate. The heat transfer is performed on the specimen and reference pan through the thermoelectric disk, but because of a heat capacity (C_p) of the sample, there would be a temperature difference between the sample and reference pans. Area thermocouples measure this temperature difference, and the consequent heat flow is determined by the thermal equivalent of Ohm's law:

$$q = \frac{\Delta T}{R}$$

where R is resistance of the thermoelectric disk, ΔT is temperature difference between sample and reference, and q is sample heat flow. However, the PC-DSC has sample and reference pans in separate furnaces. Independent heaters heat these furnaces. The instrument attempts to maintain the same temperature of the sample and reference pan, but the difference in temperature between these two pans is measured and plotted as a function of temperature or time. DSC thermal analysis technique can determine the heat of fusion, melting point, cold crystallization, structural phase transitions, crystallinity, the onset of melting, offset of melting, degradation temperature, crystallization kinetics, phase transitions, thermal curing kinetics, and thermodynamic analysis of biomolecules. [15]

6.3.1 Differences between TGA and DSC and the combination of the two techniques with STA

A TGA instrument measures a sample’s mass as it’s heated or cooled; DSC measures how much energy a sample absorbs or releases during heating or cooling. When using them together, the “‘bonus information essentially labels what type of reaction produced a given signal,”. “With the singular techniques, there are a number of reactions that give similar signal responses.” As an example, he points out that the decomposition or burning of a sample generates the same signal from TGA, even though the processes are endothermic and exothermic, respectively, which DSC readily distinguishes. “And while it is certainly possible to run the techniques in parallel or sequentially and obtain the same information, you save time by running both simultaneously.”

7.Electrolyte

Electrolyte is one of the essential and fundamental constituents in a SOC. It plays a very critical role in the transfer and balancing of charges between the positive and negative electrodes. The interaction between the electrodes and the electrolyte in all electrochemical processes significantly influences the electrode-electrolyte interface state and the internal structure of the active materials. Therefore, the properties of the electrolyte-solution system are crucial to determine the electrochemical behavior of the device. A good electrolyte will help to achieve a high-power density, high energy density and long cycling life.

Aqueous electrolytes have smaller potential windows (≤ 1 V) compared to 3.5–4 V. In addition, aqueous electrolytes are reported to have high conductivity due to its high dynamic viscosity. However, its suffer in low energy density, cycling stability, corrosion and leakage problems (Yu et al., 2013). Although organic and inorganic electrolytes can be operated at high voltages, they still suffer from lower conductivity and cycling stability (Armand et al., 2011). Solid-state electrolytes may prevent the leakage of liquid electrolytes, but they also suffer from low ionic conductivity (Dou et al., 2018). Each electrolyte inherently has its benefits and disadvantages which ultimately need to be considered for the design of a high-performance supercapacitor for the desired application. The choice of electrolyte, therefore, plays a critical role when it comes to the performance. [16]

7.1 YSZ Electrolyte

Zirconia is the most popular material in the ceramic application. It's widely used as a thermal barrier coating, selective laser sintering, gas sensor, polymer membrane filler, structural components, solid electrolytes, and medical application. Usually, this ceramic material is used in cubic or tetragonal form and stabilized with aliovalent cations like calcium (Ca^{2+}) and yttria (Y^{3+}) to become a good O^{2-} conductor because of high mechanical strength, high chemical stability, high corrosion resistant, high ionic conductivity, high thermal barrier, and low thermal conductivity properties. Since 1960, numerous research and development has highlighted the YSZ electrolyte fabrication via process yttria oxide doped to zirconia. The introduction of yttria oxide increases the concentration of oxygen vacancies, which improves the crystallography of electrolyte with increase the mobility of protons inside the YSZ and reduce the energy loss because of the lowering ohmic resistance on solid electrolyte. Besides, the introduction of yttria enhanced the mechanical and chemical stability of zirconia in a typical operating environment, which fulfills the requirement of the electrochemical system with high performance. These main criteria of YSZ electrolyte make this ceramic-based material is chosen as one of the pioneers as solid electrolyte usually applied in SOFCs application. However, the high conductivity is achieved in the high operating temperature of SOFCs (~800–1000°C) prominent in the problem of cell degradation. Therefore, the low-to-intermediate SOFCs application is urgent to enhance the durability and lifetime of the system, reduce the cost of manufacturing and operating, easy to handle, facilitate retirement and expand the consumption to the portable and transportation sector. The main challenge in order to lower the temperature of SOFCs operation is maintaining the excellent conductivity property of YSZ electrolyte with low ohmic resistance and polarization resistance. The potential of YSZ electrolyte in SOFCs application is explored in various modifications as a solid electrolyte such as reducing the film of electrolyte component, introducing the metal oxide inside the YSZ, and fabricating bilayer electrolyte in order to enhance the performance towards lowering the operating temperature of the SOFCs. [17]

7.1.2 Manufacturing Procedure

The procedure described as follows has been used to prepare the material of the electrolyte, which is an ion conductive solid oxide. The most established material for electrolytes of this type is certainly Yttria Stabilized Zirconia. A powder of YSZ has been chosen to start off, as an optimal composition of powder, solvents, disperser, binders and plasticizers has to be found in order to obtain a homogeneous slurry. When the optimal composition will be reached, it’ll be possible to study the PCC slurry composition, which involves BCYZ.

Components	Composition
Terpineol	15 mL
YSZ powder	5 g
Ethanol/Isopropanol (50/50)	2,5 mL
PVB	2 g
Phthalate	6 mL
PEG (1,084 g/mL)	25 g

Table 1. Indicative composition of the YSZ slurry

As a first step, solvents have been poured in a separate container (isopropyl and ethanol) in order to better measure the quantity needed in the mixture with a pipette. Then the disperser (alpha terpineol) has been added to cause electrostatic repulsion between particles in the material.

Then, yttria stabilized zirconia powder is put on a folded paper with the aid of a spoon and placed into a scale. The aim in preparing a slurry is basically making the material spreadable for tape casting and then sintering. Solvents have been mixed along with the YSZ powder in a little container, which has been taped to a zirconia balls container. Zirconia balls are needed to crush the powder in a better way and are employed to make sure there is no contamination and, avoid other kinds of reactions. After that, the two taped containers have been ball milled for 24 hours. Then, a binder has been added to the mixed slurry. The binders can be PEG (polyethylene glycol), polyvinyl butyrate and bento n-butyl phthalate. Also, a plasticizer has been added to make the bonds of the binder more flexible.

The following step regarding the preparation of the electrolyte material consists in the tape casting process.

In this case study, tape casted has been firstly performed on the YSZ slurry that has been mixed on the ball-mill overnight.

Figure 24. Tape caster in the UCI ISEB facility

The surface of the tape caster has been cleaned with a solvent (isopropanol), which has helped in making a piece of PTFE (Teflon) stick to the surface. Then, the completely mixed slurry that has been left overnight has been spread manually over the Teflon surface as homogeneously as possible. The doctor blade has further spread the slurry mechanically with a certain thickness and has been placed at the beginning of the PTFE piece. A doctor blade that produces a sample that is 400 µm thick has been employed. Speed and the stop point of tape casting have been chosen. The more homogeneous the slurry spreads under the doctor blade, the better the result. When the tape casting is finished, it's worth collecting the remaining slurry from the specimen in order to put it again in the box. Finally, the slurry has been dried with the heating mode of the tape caster at 80 °C and left to further dry overnight in the laboratory. The dried slurry check step has been very important, as it highlighted some critical aspects of the composition. As a matter of fact, the tape casted and dried slurry couldn't be removed properly from the Teflon surface, as it already presented cracks. It means that the composition of the slurry must be revised and modified in order to obtain the right quantities of binders, plasticizers and other additives. This result was expected, as the slurry wouldn't spread very homogeneously on the Teflon surface while tape casting with the doctor blade. It has been decided, together with the rest of the research group, that another type of binder, the PVB, must be employed, therefore an order has been placed to receive it.

Another trial in the slurry preparation has been made following the already mentioned modalities. This time, two main modifications have been done: in the first place, it has been chosen to employ just one type of plasticizer, which is the phthalate and, secondly, to increase the quantity of new utilized binder (PVB), keeping in mind that a more flexible and kept-together slurry is needed in order for it to be peeled from the Teflon piece without cracking, and, ultimately, to obtain a more homogeneous slurry. These decisions have been made based on a scientific paper found on ResearchGate. [18]

Components	**Amount (wt.%)**
YSZ	50
Water	20.5
Dispersant	2.0
Binder	25.0
Surfactant	0.5
Antifoaming	0.5
Isopropyl ethanol	1.5

Table 2. Reference YSZ slurry composition in wt.%

Since the goal is not having a water-containing slurry, as the final application will be destined to a protonic conductive electrolyte, the water has been replaced with solvent.

Also, since the percentages reported are mass-based, the following formula has been used to retrieve the precise quantities in mL of the liquid components, starting from defining the YSZ powder quantity, which is 5g:

$$\frac{\left(\frac{\% \cdot 10}{100}\right)}{\rho\left[\frac{g}{mL}\right]}$$

Equation 12. Quantity of the liquid components in the slurry

Where ρ is the density of the liquid.

In the following table, the new composition of the YSZ slurry is displayed. Also, it's worth noticing that the disperser quantity has been reduced, while the solvent quantity has been increased.

Components	**Composition**
Alpha-Terpineol	0,16 mL
YSZ powder	5 g
Isopropanol	2,8 mL
PVB	2,5 g
Phthalate	0,144 mL

Table 3. YSZ-1 composition

The YSZ powder, solvent and disperser have been put into a clean container together with zirconia balls and will be ball-milled for at least 24 hours.

It has been noticed that the PVB powder quantity is high, the presence of too much powder into this formulation can compromise the final result, as there can be issues in its dissolution. So, it has been decided to reduce its value to 1,25 g in a new trial (YSZ-2) and, along with that, dissolve separately the PVB adding 0,5 mL of solvent and then adding it to the composition. Therefore, the total quantity of solvent is 3,3 mL and the final composition is displayed below

Components	Composition
Alpha-Terpineol	0,16 mL
YSZ powder	5 g
Isopropanol	3,3 mL
PVB	1,25 g
Phthalate	0,144 mL

Table 4. YSZ-2 and YSZ-3 composition

The slurry has finally been ball-milled for more than 24 hours. The procedure followed for tape casting is the same as the previously used one. This composition has shown much better results starting from its spreading on the Teflon foil, being much more homogeneous. Moreover, after the tape casting the slurry has been dried for 20 minutes, showing no cracks on the surface. The only element that is worth mentioning is the presence of air bubbles. For this reason, a new sample (YSZ-3) with the same composition as YSZ-2 has been made removing all air from the slurry putting it in a vacuum with a negative gauge before the tape casting step. The result after tape casting in this case has been even better, as there were no more air bubbles, nor cracks on the surface.

It has also been decided to create a new sample increasing the solvent quantity of 500 µl to the pre-existing slurry.

The new composition therefore is:

Components	Composition
Alpha-Terpineol	0,16 mL
YSZ powder	5 g
Isopropanol	3,3 mL
PVB	2,5 g
Phthalate	0,144 mL

Table 5. YSZ-4 composition

The slurry with added solvent has been then ball-milled for 30 minutes and then tape casted. The result reported a homogeneous slurry with no cracks after drying. All the samples have been left in the laboratory for them to air dry overnight.

The substantial difference in the binder quantity made this change possible.

After 24 hours, the new samples have been checked using tweezers and a sharp cutter to peel the dried slurry off the Teflon foil. The three slurries peeled off effortlessly. The key point in obtaining a slurry suitable for sintering is therefore adding more binder.

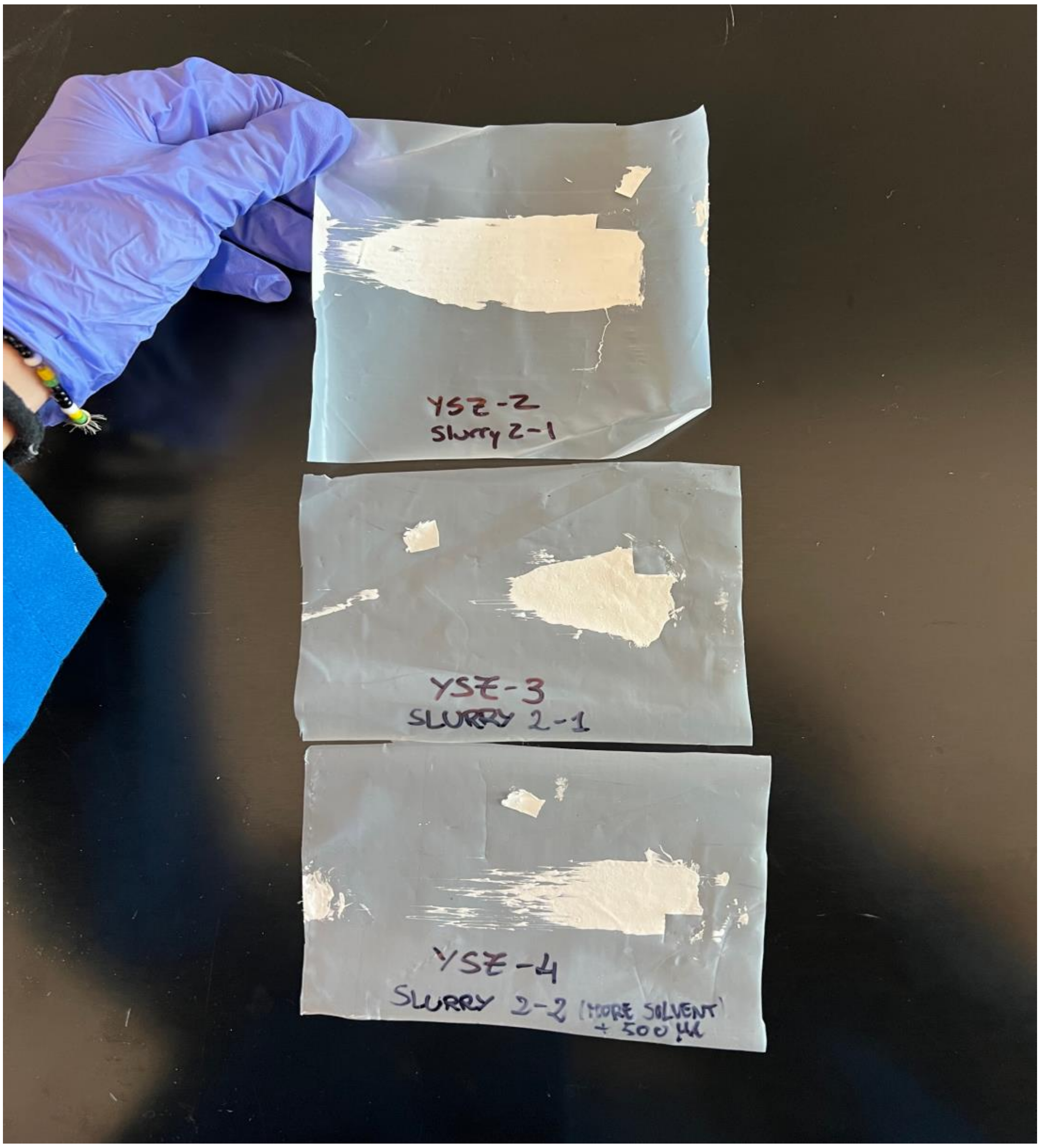

Figure 25. Tape casted and dried YSZ-2,3,4

The next steps will consist of doing rheology on the vacuumed slurries, one with more solvent and the one with the original composition. Also, they'll be sintered first in a furnace and then, if possible, with a CO2 laser.

Two additional YSZ slurries have been made for comparison reasons. One slurry (YSZ-5) has the same characteristics of the YSZ-4 slurry, with more solvent in it, the other one (YSZ-6) starts from the composition of the previous but the quantities of binder and dispersant have been modified slightly, following the trend of less dispersant and more binder, choosing to subtract 0,4% of the Alpha-Terpineol dispersant and adding 0,4% of PVB binder. Therefore, the new composition is displayed in the following:

Components	Composition
Alpha-Terpineol	0,11 mL
YSZ powder	5 g
Isopropanol	3,3 mL
PVB	2,54 g
Phthalate	0,144 mL

Table 6. YSZ-6 composition

The two slurries have been vacuumed to remove all the air from the composition to avoid the formation of bubbles.

It has been worth noticing that, during the tape casting step, the new YSZ slurry with more binder and less dispersant spreader less homogeneously on the Teflon piece and after drying in the heater for ten minutes it presented cracks on the surface. This result means that an optimal percentage regarding both binder and dispersant quantities exists and has been found in the last trials.

An additional laboratory regarding **rheology** on the prepared YSZ slurry has been done in order to better characterize the material. A guided procedure to properly turn on the rheometer has been followed. Firstly, it has been ensured that the air supply is on. It should read 30 psi for the air bearing and should never be turned off for any purpose. Then, the black bearing lock is removed by holding it in place while turning the draw rod knob at the top in a counterclockwise fashion. Once the bearing lock is removed, make sure that the spindle rotates free of friction. At this point, the rheometer can be turned on. Also, it’s needed to ensure that the water supply for the Peltier plate cooling is turned on and the water is clean, and the pump is fully submerged. After the instrument has finished the system check, the instrument control software, TRIOS, can be started from the desktop. The instrument inertia must be determined. This value is unique for each bearing assembly. An acceptable range for this value is ~21–22 µN·m·s2. The value for the instrument should not change by more than 10% of the original Inertia value. This calibration should be performed monthly. Then, a geometry unit is selected between 20 mm and 40 mm parallel plates.

It has to be ensured that the shaft was set to the home position by holding down the lock button on the rheometer until a sound is heard. Attach test geometry by sliding it up the drive shaft and hold it stationary while turning the draw rod at the top in a clockwise direction. Line up the line on the geometry with the line on the rheometer.

The geometry inertia must be determined too. The value of the inertia for each measuring system differs because they all have been uniquely engineered and have different masses. It is important to calibrate the inertia value for each geometry, particularly if high frequency oscillations are being used, or if low viscosity fluids are being measured.

Also, the bearing friction correction must be performed after instrument inertia and geometry inertia. A magnetic bearing is used to set the drive shaft afloat and provide virtually friction free application of torque to the sample. However, there will always be some residual friction. With most test materials, this is insignificant, but in about 1% of the low viscosity samples, this inherent friction causes inaccuracies in the final rheological data. To overcome this, the software has a bearing friction correction that should be activated. The bearing friction value without any geometry attached is ~0.25 – 0.3 μNm/(rad/s). With attaching a geometry, this value may rise up to about 0.3 – 0.5 μNm/(rad/s). Bearing friction correction can be found just below the Geometry Inertia calibration.

The geometry gap must be then zeroed. The upper geometry should be at the testing temperature before zeroing the gap. This will account for the change in dimensions due to the coefficient of thermal expansion of the testing geometry/system. Zero gap needs to be performed every time when the geometry is removed or replaced.

Gap Compensation needs only to be used when testing over a temperature range.

Mapping must be performed too. Due to the micron-level tolerances needed to make the magnetic bearing to work, any bearing will have small variations in torque behavior around one complete revolution of the shaft. They are consistent over time unless changes occur in the magnetic bearing. By combining the absolute angular position data from the optical encoder with microprocessor control of the motor, these small variations can be mapped automatically and stored in memory for subsequent real-time corrections in the test. To create a mapping, the software rotates the drive shaft at a fixed speed, monitoring the torque required to maintain this speed through a full 360° of rotation. These variations in torque can then be accounted for automatically by the microprocessor, which is in effect carrying out a baseline correction of the torque. This results in a very wide operating range of the bearing without operator intervention – a confidence check in bearing performance. Perform a rotational mapping on the geometry when the test procedure will be applying either a flow or transient (Creep or Stress Relaxation) mode of deformation. There are three levels of rotational mapping – fast, standard, and precision. It is also possible to perform multiple mapping iterations. Standard should be good for most applications. The magnitude of the torque correction varies with the instrument type, but typically has an absolute maximum in the range 0.2 to 1 μN.m. As the torques in your procedure drop, the error from an unmapped bearing increase, so it may become necessary to perform precision mappings to keep these errors to a minimum.

The oscillation mapping will perform a baseline subtraction only when using the continuous controlled strain mode and will improve the performance for low torque, low displacement data. This calibration is recommended when performing oscillatory tests on low viscosity samples.

Then a procedure is set and saved and ready to proceed with sample preparation. The amount of sample volume that is required, based on the dimensions entered in the geometry step for a cone, parallel plate and concentric cylinder systems, can be found in the Geometry Information step. After loading a sample, the gap is closed, its size is variable and should be between 500 microns and geometry diameter (microns)/10.

Trimming the gap is needed when extra material is loaded and close the gap to a value of 5% larger than the required gap, so that excess material is expelled from between the upper geometry and lower plate, i.e. overfilled state. Then the bearing is locked with the bearing lock button on the Front Panel in order to keep the geometry from rotating and trim the excess material using a right edged tool. Then lower the gap to the final test gap.

Finally, a test can be run. In the post experiment it’s needed to: ensure plates have cooled before touching them, unscrewing the draw rod from the geometry unit before raising the Head, thoroughly clean the geometry unit and Peltier plate, lace cleaned geometry unit in its container and place bearing lock on.

In this test on the YSZ slurry, the temperature must be set at ambient temperature, so 25 C. Also, the duration of the test is changed, performing a test of 5 minutes. A viscosity-shear force plot will be displayed after the test.

The parameters measured are displayed directly on the machine.

The goal of setting the gap sizes is to have the top part of the machinery to sit right on top of the sample without having to squish it and having excess on the sides. Then the top part of the machine will also spin to measure the friction. Or as an alternative, we can also clean the excess.

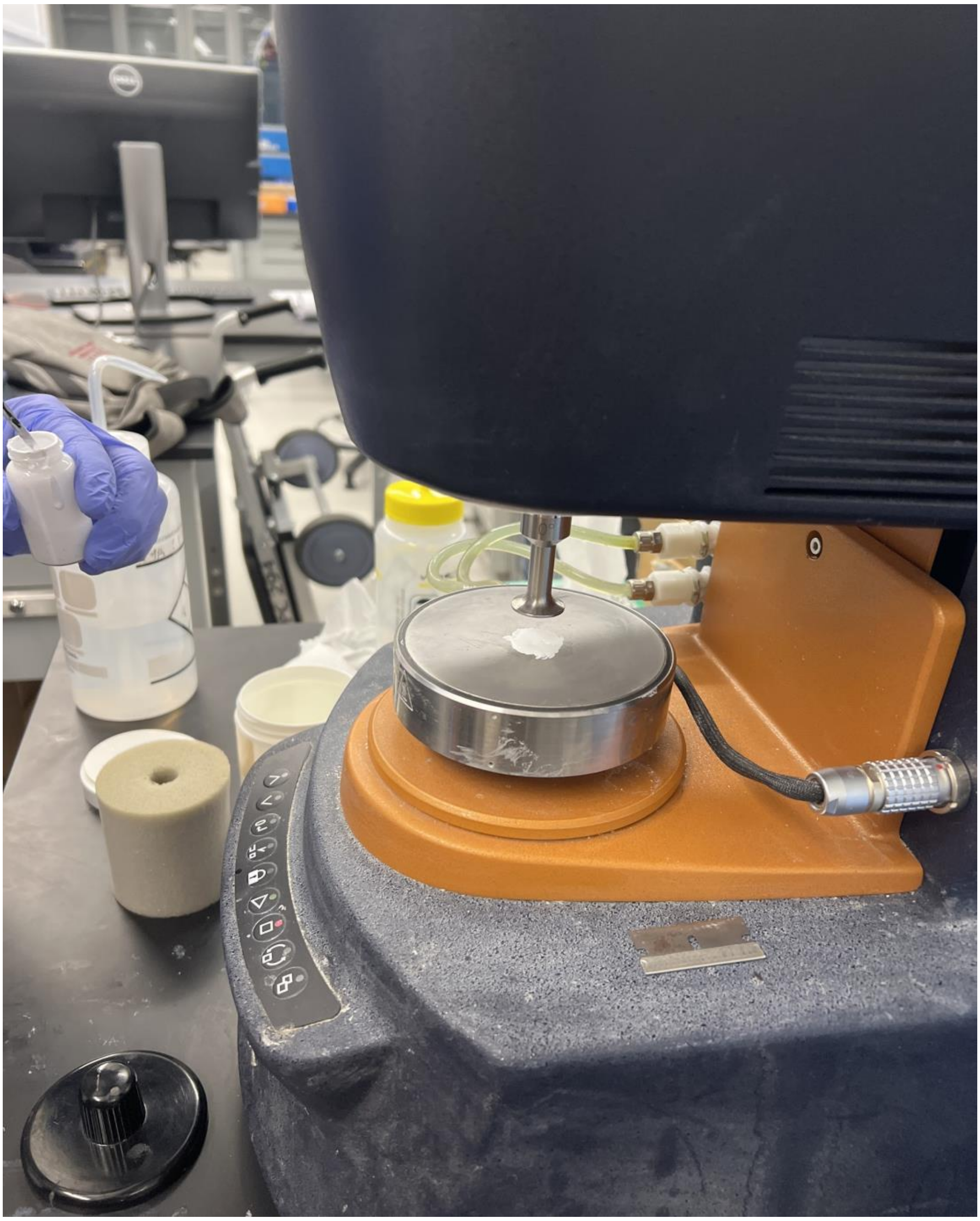

Figure 26. Rheometer set-up in the UCI TEMPR facility

In this test, the excess was cleaned. As the time set for the test passes, results will be shown on the already mentioned plot.

Inaccuracy in the measurements can be given by the excess on the sides and the fact that the slurry can dry in the process. Anyways, there shouldn't be a big error range, so the result is somehow still precise enough.

Results for a 5-minute test are saved. Then, the same test is repeated for a shorter time in order to get a higher accuracy. The rheology can be useful if different deposition techniques other than tape casting are used, as parameters for more novel techniques are in need to be set and, consequently, are highly needed. The purpose of the rheology performed in this way is just to have more information on the prepared slurry. Also, a thermo-gravimetric analysis on the slurry will be performed (add more information on this process, you have notes).

The software used to generate plots and control the equipment is called "TA instruments Trios".

It has been noted that the slurry without the addition of the binder is more spreadable. Very low viscosity values were obtained, while the binder increases the value of viscosity drastically. For this reason, the slurry results to be harder to spread over surfaces.

The results of this experiment reported two plots: the first plot shows a steep down in the curve, which is related to an inaccuracy of the test due to the machine getting stopped by dried parts and excess.

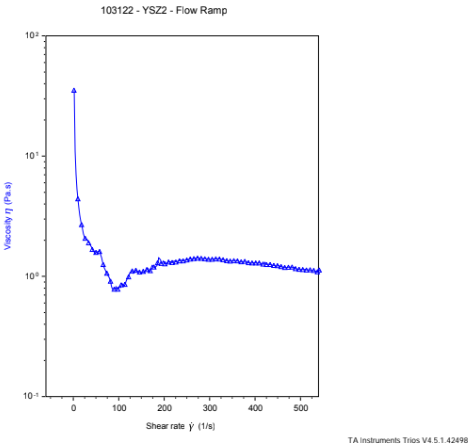

Figure 27. First attempt of YSZ rheology

While the second plot shows a more accurate and normal trend, as the test was much smoother.

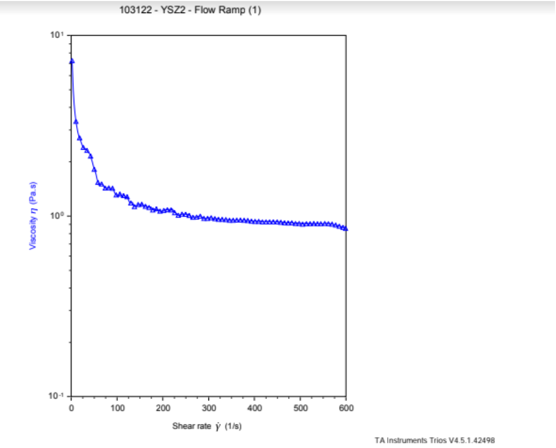

Figure 28. Second attempt of YSZ rheology

Changing the plasticizer from a powder form to a liquid form can help in lowering the viscosity, also having more solvent rather than binders in the formulation represents a valid strategy.

Rheology has been performed on the slurries relative to YSZ-4 (on this plot called YSZ STD), which contains more solvent, following what above-mentioned, and the last YSZ slurry produced following the more binder and less dispersant trend. The results of rheology performed on the two samples is here displayed

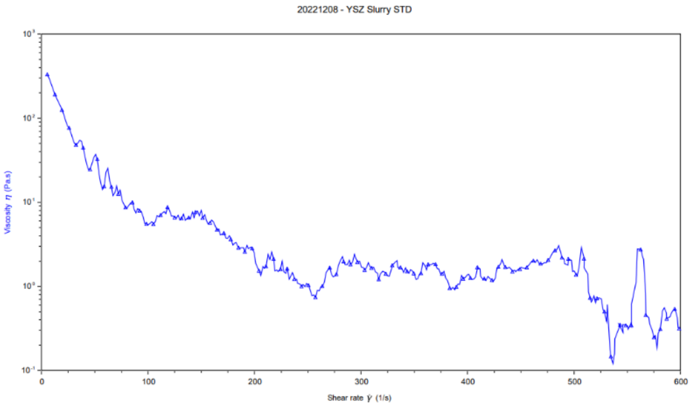

Figure 29. Rheology on YSZ-4

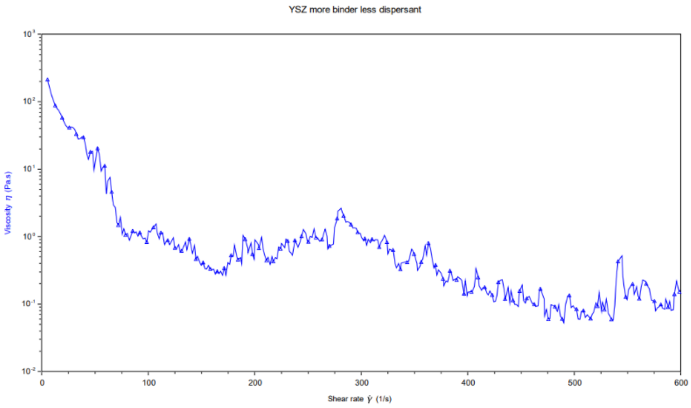

Figure 30. Rheology on YSZ-6

Both slurries have shown lower values of viscosity as expected. As a matter of fact, they were spread more homogeneously during tape casting, but the best result in terms of homogeneity has been obtained with the YSZ-4 (here called YSZ STD), demonstrating that increased quantities of binder result in less homogeneous slurries and, therefore, in a less smooth tape casting process, also indicating that an optimum point in the binder quantity exists. So, as a general rule, lower values of viscosity allow to obtain a smooth tape casting process, and, particularly, a reduction in viscosity corresponding to a shear rate of 100 1/s is an indicator of a well performing slurry.

To get a better understanding of the manufacturing process to employ in the fabrication of the electrolyte, the UCI ceramic material research group has been contacted. The group gave an insight on their processing techniques of engineered ceramics. It has been noted that solid state sintering is the process the research group prefers, as they observed that eliminating the binder from the composition would be advisable, as organic components are difficult to manage. However, the temperatures needed for sintering without using any binder are around 1600 °C for zirconia and alumina compounds, which are the most suitable ceramics that can stand these working temperatures and can ultimately be also laser sintered. The goal of the solid-state sintering is to avoid obtaining grain boundaries, as they are detrimental for conductivity. This goal can be achieved through solid state sintering. The starting point in understanding the manufacturing process was defining the suitable composition for the YSZ slurry. Later, barium zirconates will be studied as well. If solid state sintering will be chosen as the sintering technique for this case study, temperatures of 600-700 °C have to be reached. The research group also claimed that the high temperatures involved are very localized with the traditional solid-state sintering and it's possible to gain much more control of the process while employing very little quantities of PVA and avoiding the formation of bubbles, as there is no liquid part associated with the preparation of a slurry. This research group stated that they make very little usage of sintering aids and would only indicate magnesium oxide for treating zirconia or alumina. Also, the smaller the powder used, the better the whole process.

The ceramic research group discouraged the choice of laser sintering because of two main reasons: the high temperatures reached in this process can make almost all the engineered ceramics unsuitable for this kind of process and that the sizes reached with these techniques won't be suitable for the final purpose of the cells that will be produced.

For the sintering step, it has been chosen to adopt traditional furnace sintering of the tape casted YSZ slurry, while it has been advised to later perform a solid-state sintering in the furnace for the Barium Zirconate powders. In the laboratory facilities of the Engineering Tower there is a YAG laser available for use, though it must be booked weeks in advance before the effective usage in order to prepare the equipment and then clean it after the laser sintering, as it uses an argon inert atmosphere. The ways to perform sintering with this YAG laser are mainly two: this laser can spray powders while the laser beam is on, but ceramic powders are not suitable for this kind of sintering, as the powders would be stuck in the nozzles. Another way is depositing a layer of ceramic slurry, laser sinter and then depositing another layer manually until the desired thickness is reached. A minimum value of thickness must be reached to guarantee mechanical stability to the sample. In the end, YAG laser sintering is feasible, but it surely takes a lot of time to be completed and evaluating the time schedule for the whole project this option has been excluded.

The laboratory facility is also equipped with gas atomizers, which make the spheralization process feasible in order to get more packed and dense powders.

In this case study, tape casted and dried YSZ slurry samples will be sintered in the furnace and then, Barium Zirconate powders will be first compacted and then furnace sintered. For this purpose, the furnace must reach 1600-1700 C, so it must be high temperature, though the optimal values for YSZ slurry sintering are reported to be around 1450 °C. [19]

Since a manual for the high temperature furnace hasn’t been found on the internet, some trials must be made to get the right heating and cooling rates for the sintering and may vary among different ceramics.

7.2 BZCY Electrolyte

Doped perovskite barium zirconate materials and doped barium cerate-zirconate solid solution ($BaCe1xZrxO3\text{-}\delta$) are the most widely used proton-conducting electrolytes, especially the doped $BaCe1{-}xZrxO3\text{-}\delta$ family, owing to their high proton conductivity, high ionic transference number, and low sintering temperature. Electrolyte materials must be chemically compatible with both fuel electrode and air electrode components during fabrication and operation. Although incompatibility between the electrolyte and air electrode materials has been frequently reported in the literature, it is now less of a concern as many high-performance air electrode materials are available for use.

Perovskite oxides represent a large category of complex oxides with the characteristics of flexible composition and rich properties. Many perovskites show mixed H+, O2– , and e– conductivity, possess good catalytic activity for various fuels, including H2 and hydrocarbons, and good resistance to coke deposition and sulfur poisoning. Nickel (Ni) is the most promising fuel electrode catalyst due to its low cost, high electronic conductivity, good thermal conductivity, and excellent thermal/ chemical compatibility with ceramic proton conductors.

Low operating temperature, low electrolysis voltage, and high partial pressure of water are beneficial for reducing electronic leakage and improving faradaic efficiency in the electrolysis mode. Other improvements involve the introduction of proton conductivity instead of increasing oxygen-ion conductivity in the air electrode. The concept of triple conducting oxides (TCOs) has emerged. TCOs enable the electrochemical reactions to occur anywhere on the entire surface of the air electrode. With the reduction of electrolyte thickness and the discovery of more active air electrodes, there is a noticeable trend of pushing the operation of PCECs to lower temperatures ($\leq$ 500°C). The oxygen ion bulk diffusion, which exhibits considerable activation energy, could unavoidably become the rate limiting step at lower temperature. To better serve the SOCs at lower temperature, surface modification, which improves the electrochemical activity while maintaining the bulk properties, for promoting the catalytic activity may effectively boost the performance in the near future. Other strategies to improve performance consist of infiltration, substitution and exsolution of nanoparticles, and insertion of a catalyst layer or functional layer. Infiltration or exsolution can produce finely dispersed nanoparticles to maximize the active surface area. The insertion of a catalyst layer above the fuel electrode layer can protect the fuel electrode from coking and thus enhance reforming activity. The insertion of a functional layer between the fuel electrode and electrolyte significantly increases the TPB length and reduces interfacial resistance. Usually, interfacial reactions during electrode manufacturing or subsequent operation are considered unwanted and should be avoided to attain the desired phase structure of each component. On the other hand, they can be utilized to obtain secondary phases with beneficial physicochemical characteristics. The performance and stability optimization achieved by nanocomposite formed in-situ via parent phase transformation can be attributed to aspects such as intimate nanocontact between derivative phases, alleviated CTE mismatch between electrode and electrolyte, and better physic-chemical compatibility between parent, derivative, and electrolyte phases. The introduction of nano-catalysts via various strategies has dramatically enhanced its resistance to coke deposition and sulfur poisoning at moderate temperatures.

Advanced materials optimization and architecture innovation are carrying the development of PCECs from laboratory exploration to the next phase. Significant breakthroughs are expected in promising protonic energy conversion and storage applications beyond the current technologies. Scaling up the footprint of the cells and readying them for in-field demonstration will be needed to demonstrate the advantages of PCECs in the future. [20]

Protonic ceramic cells (PCCs) typically use acceptor-doped Ba(Zr,Ce)O3 as electrolytes, which allow for reducing the operation temperature to 400–600 C owing to an increased ion conductivity at intermediate temperatures. In fuel cell mode (PCFC) these cells have the advantage of water formation at the cathode, hence no fuel dilution occurs, and this leads to high fuel utilization and increased efficiency. Potential applications for PCCs can be found in either mobile or stationary fields. Interestingly, with adjusted catalytic activity at the anode side, a wide range of fuels such as ammonia and different hydrocarbons and alcohols can be used instead of hydrogen. Some works have shown that multilayer structures are used to reduce the electrolyte thickness down to 10–20 mm, supported by a much thicker, porous anode. Two key results must be achieved: the combination of tape casting and reactive sintering is able to produce large-area anode/electrolyte membrane assemblies and that the achieved total proton conductivity of the electrolyte is suitable for PCFCs. The cation composition is decisive for the performance of the components. Several groups have investigated partial Ce substitution in BZY, because increasing the Ce content facilitates the sintering and leads to higher proton retention at elevated temperatures. However, while BaZrO3 is thermodynamically stable against decomposition, BaCeO3 is less chemically stable. Since a compromise between processability, stability, and resulting conductivity needs to be achieved, it’s important to explore the selected combination of manufacturing routes.

As for sintering, to obtain a fully densified electrolyte layer on a composite porous support, a sintering temperature of 1500 C or slightly lower has been proven to be sufficient. Although sintering at higher temperatures might be beneficial, especially regarding the grain growth and the reduction of the grain boundary resistance of the electrolyte layer, it increases the risk of Ba evaporation and associated functional disadvantages. During the co-firing two important properties need to be ensured: gas tightness of the electrolyte layer and flatness of the bi-layer assembly. In general, it can be summarized that temperatures above 1500 C are not beneficial. The sintering involving a transient liquid phase in the NiO-rich anode as well as in the NiO-poor BZCY electrolyte layer is a complex process, but with appropriately chosen conditions dense anode–electrolyte assemblies with minimized secondary phase content can be achieved. In general it is found that NiO addition to Ba(Zr,Ce,Y)O3d is beneficial for sintering properties and grain growth but decreases the bulk proton conductivity. [19]

Due to delays in the sintering phase of the YSZ samples, it has been chosen to proceed with the production of the BZCY slurry in little quantities, since the powder itself is very costly. The powder consists of ceria and yttria doped barium zirconate.

The exact formulation is $BaZr_{0.7}Ce_{0.2}Y_{0.1}O_{3-\delta}$, meaning it contains 70% barium zirconate, 20% ceria and 10% yttria.

Given the successful results in the tape casting of the last two YSZ slurries, their composition has been taken as a reference to scale the components' quantities. It has also been chosen to use 1 g of BZCY powder, to prove the tape casting step is feasible. Therefore, since the starting powder quantity was 5 g, the quantity of every component has been divided by 5 for sake of simplicity. Also, it has been decided to make two different slurries (both called BZCY-1) in which the only difference resides in the solvent used: one contains only ethanol, the other only isopropanol.

The new compositions therefore are:

Components	Composition
Alpha-Terpineol	0,032 mL
BZCY powder	1 g
Ethanol	0,558 mL
PVB	0,25 g
Phthalate	0,028 mL

Table 7. BZCY-1 with ethanol

Components	Composition
Alpha-Terpineol	0,032 mL
BZCY powder	1 g
Isopropanol	0,558 mL
PVB	0,25 g
Phthalate	0,028 mL

Table 8. BZCY-1 with isopropanol

The powder has been put in two containers along with the different solvents and zirconia balls, and ball-milled for 24 hours. After 24 hours it's possible to add binder and plasticizer, then ball-mill again for 24 hours and, finally, tape cast.

After 24 hours it has been noted that one of the ball-milled jars exploded and it was the one that contained isopropanol as solvent, demonstrating the right choice in separating the two types of solvents in two separate containers. The cause of the explosion hasn't been already understood, but supposedly an uncontrolled reaction happened overnight and melted the container. Further analysis may be conducted on the residues of this slurry.

The other jar containing ethanol as solvent was intact, therefore PVB and phthalate were also added. The jar was put again on the ball-mill for 24 hours.

After the mixing, tape casting was performed, obtaining a sample of 400 μm that was possible to be peeled off the Teflon piece. After that, a furnace for sintering has been found. The furnace used is Sentro Tech Corp and can go up to 1500 C.

Before sintering, the addition of sintering aids has been discussed. In BZCY slurries it's crucial to add sintering aids in order to get a good density, while keeping its conductivity and other physical properties. In this first trial, no sintering aid has been added in order to study its behavior in the furnace.

The sample has been sintered for 10 hours, with a heating rate of 100 C/h, up to 1400 C. The result is the sample becoming black, confirming the decision to add sintering aids. Also, it has been reported that in order to sinter BZCY a reducing atmosphere is needed, which is not possible to obtain with the above-mentioned furnace. The reason why the BZCY sample turned black while sintering has been attributed to the presence of humidity and, since Barium Zirconate presents OH- transport, along with the absence of a reducing atmosphere, it produced the above-mentioned result.

A topic of concern is the addition of a barrier layer on the electrolyte surface. BZCY ceramics are usually sintered at 1450 C in reducing environment alone and supported on FeCr alloy metal support, and key characteristics such as Ba loss, sintering behavior, and chemical compatibility with metal support are determined. Critical challenges are identified for this fabrication approach, including Contamination of the electrolyte with Si and Cr from the metal support, incomplete electrolyte sintering, and evaporation of electrolyte constituents. Various approaches to overcome these limitations are proposed, and preliminary assessment indicates that the use of barrier layers, low-Si-content stainless steel, and sintering aids warrant further development.

There is a tradeoff between stability in the presence of carbon dioxide vs. high conductivity, sinterability and grain growth, with the Ce:Zr ratio being a key controlling factor. Doping with Y and Yb yields improvement in conductivity.

Co-sintering is an attractive option for fabricating MS-SOCs due to the conventional low-cost, high-throughput manufacturing techniques used to deposit the ceramic layers (e.g., tape-casting, screen- printing, aerosol spray deposition), and the relatively high processing temperature resulting in a dense electrolyte layer with high conductivity.

The limited work on co- sintering BZCY with stainless steel support indicates, however, that significant challenges exist for this approach. Co-sintered BZCY-Ni anodes supported on ferritic stainless steel, finding that interdiffusion between the anode and steel layers was a significant issue and resulted in contamination of the Ni catalyst and melting of the stainless steel. It's possible to minimize interdiffusion via addition of a ceria barrier layer. Also, BZCY survives sintering in reducing atmosphere (required to avoid oxidation of the stainless steel) but reacts deleteriously with the metal support. A large amount of Si and a minor amount of Cr from the stainless steel migrated into the BZCY layers. After sintering, the electrolyte layer was composed of a mixture of BZCY and a significant amount of Ba2SiO4. Furthermore, BZCY achieved only 73% of theoretical density and experienced significant Ba evaporation after sintering at 1450 C in reducing atmosphere.

Complete symmetric MS-SOFCs with yttria-stabilized zirconia (YSZ, Tosoh) ceramic layers were prepared by tape casting, de-binding in air, and sintering in reducing atmosphere (2% hydrogen in argon). Commercial powders were used as sintering aids: Co3O4, ZnO, NiO (all <50 nm, Sigma-Aldrich) and LiF (<10 mm, Sigma-Aldrich). Sintering aid powders were used as-received, with the exception of LiF, which was attritor milled with iso- propyl alcohol for 1 h to reduce particle size before use.

Higher sintering temperature is expected to be required for full densification of BZCY ceramics. Over-densification of the metal is a concern when sintering at higher temperature, especially above 1450 C. This is not surprising, as the stainless-steel melting point is around 1525 C. To be compatible with co-sintering on metal support, the ceramic layer will ideally densify completely at 1450 C or below.

Si and Cr migration from the stainless steel to the BZCY electrolyte does occur during co-sintering, leading to formation of Ba2SiO4 and BaCrO4, and depletion of Ba from the proton conducting phase. This is expected to be detrimental to electrolyte performance, as the conductivity of BZCY is known to be highly sensitive to Ba content, reaction with Cr is known to be detrimental, and Ba2SiO4 and BaCrO4 are inactive and would block the proton transport pathway. Si migration increases and Cr migration decreases dramatically with increasing Ce and Yb content, Si, and to a lesser extent Cr, migration can be curtailed by lowering the sintering temperature below 1450 C. Si evaporates from the metal and migrates via vapor diffusion, presumably creating a Si- saturated atmosphere throughout the vicinity of the cell. In contrast, Cr is expected to migrate via solid state diffusion, consistent with the linear gradient in Cr concentration from the metal support to the exposed side of the electrolyte. Reducing the sintering temperature appears to be a promising approach if densification can be achieved at lower temperature. The use of sintering aids to achieve this goal is discussed. To summarize, lowering the sintering temperature and Si content of the stainless steel are both viable approaches to minimizing migration. [21]

Barrier layers have been used to block undesired migration of elements between adjacent layers in a variety of SOFC architectures. Here, we find that this is an effective approach for reducing Si and Cr migration from the stainless-steel support to the ceramic layers. Our initial trial uses CGO as the barrier layer, chosen because it was previously reported that BZCY and CGO do not significantly inter-diffuse or react with each other when sintering in reducing atmosphere at 1400 C. Si and Cr content appear to be reduced. [22]

Lowering the sintering temperature is desirable for several reasons including: 1) minimizing Si and Cr migration (Section Si and Cr migration); 2) preventing over-densification of the metal support (Section Metal support); 3) reducing Ba evaporation (Section BZCY); and 4) reducing processing cost. As discussed above in Section Sintering behavior and Section Si and Cr migration, increasing Ce and Yb content enhances sintering, but also dramatically increases contamination of the electrolyte layer with Si. The use of **sintering aids** is another approach to reduce sintering temperature that is widely used for BZCY processing in air. The effectiveness of various sintering aids (Coe, Zne, and Ni-oxides and LiF, all 2 wt%) is compared. All sintering aids significantly enhanced densification in air. The oxide sintering aids were much less effective in reducing atmosphere, however, providing final density less than 90%. LiF is a very effective sintering aid in reducing the atmosphere, providing a final density of 94%. LiF enhances sintering in air through a liquid phase mechanism. The ceramic layer sintering was so enhanced by LiF addition that the shrinkage was no longer matched well to the metal support, leading to cracking and curvature of the ceramic layers. Improving metal shrinkage at 1300 °C and below will be a subject of future effort. So, too much LiF is in the end detrimental. [21] Approaches for co-sintering metal-supported proton-conducting solid oxide cells with Ba(Zr,Ce,Y,Yb)O3-d electrolyte. Ruofan Wang a, Grace Y. Lau a, Dong Ding b, Tianli Zhu c, Michael C. Tucker a,*

Another sample of BZCY slurry has been made (BZCY-2), this time following the old composition of the YSZ powder and using 5 g of BZCY powder. Moreover, manganese oxide (MnO2) has been chosen as sintering aid in 2%wt quantity and has been added during the second step along with the binder and the plasticizer.

Components	Composition
Alpha-Terpineol	0,16 mL
BZCY powder	5 g
Ethanol	2,8 mL
PVB	2,5 g
Phthalate	0,144 mL
Manganese Oxide	0,215 g

Table 9. BZCY-2 composition

The tape casting step has revealed some critical points of the sample, the major one having obtained a non homogeneous slurry. As a matter of fact, it has been noticed that the sintering aid didn’t mix well, as it was added during the second step and, supposedly, the quantity of the powders contained in the composition was too much. Moreover, after leaving the tape-casted slurry to dry overnight, it became bumpy due to the non-homogeneity, although it was possible to peel the dried slurry off of the Teflon foil, which indicates the presence of a sufficient quantity of binder.

.

Figure 31. Tape casted and dried BZCY-2

Although this slurry didn't give good results, it has been decided to add 1,2 mL more of ethanol for it to mix in a better way.

Similar to what has been already mentioned for the YSZ slurry, the binder quantity has been reduced and dissolved with 1 mL of ethanol before being added to the composition. Initially, the quantity that was intended to be added to the composition was just 0,5 mL, but it wasn't enough to dissolve the binder.

Components	Composition
Alpha-Terpineol	0,16 mL
BZCY powder	5 g
Ethanol	3,8 mL
PVB	1,25 g
Phthalate	0,144 mL
Manganese Oxide	0,2 g

Table 10. BZCY-3 composition

Another slurry has also been made using isopropanol as solvent, assessing whether the explosion that occurred in a previous trial has been accidental or it's correlated to the usage of the mentioned solvent.

Components	Composition
Alpha-Terpineol	0,16 mL
BZCY powder	5 g
Isopropanol	3,8 mL
PVB	1,25 g
Phthalate	0,144 mL
Manganese Oxide	0,2 g

Table 11. BZCY-4 composition

It was worth noticing that while dissolving the PVB with the two solvents, ethanol performed better in the task, as the binder dissolved faster and in a more homogeneous way in comparison to isopropanol.

After leaving the two samples on the ball-mill for more than 24 hours, the slurries have been vacuumed and then tape casted. The BZCY slurry containing ethanol performed sensibly better than the one containing isopropanol as solvent, as this last one presented several non-homogeneities after being tape casted.

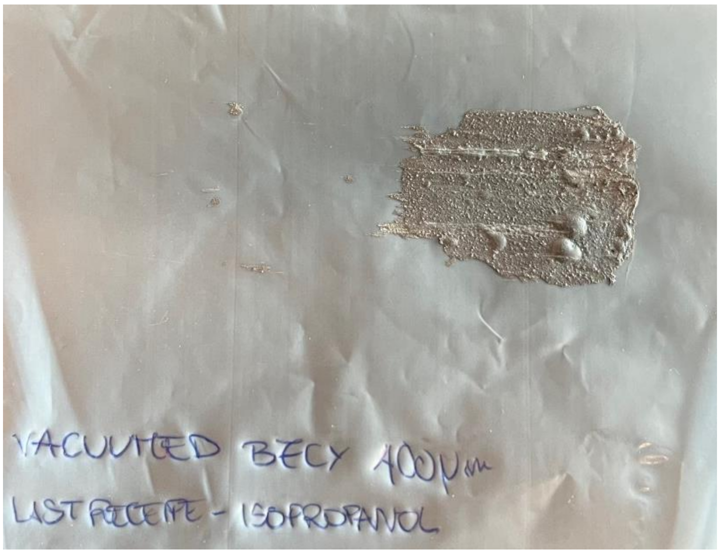

Figure 32. Tape casted and dried BZCY-4 400 μm

The slurry containing ethanol appeared very homogeneous and the tape casting step was completed easily.

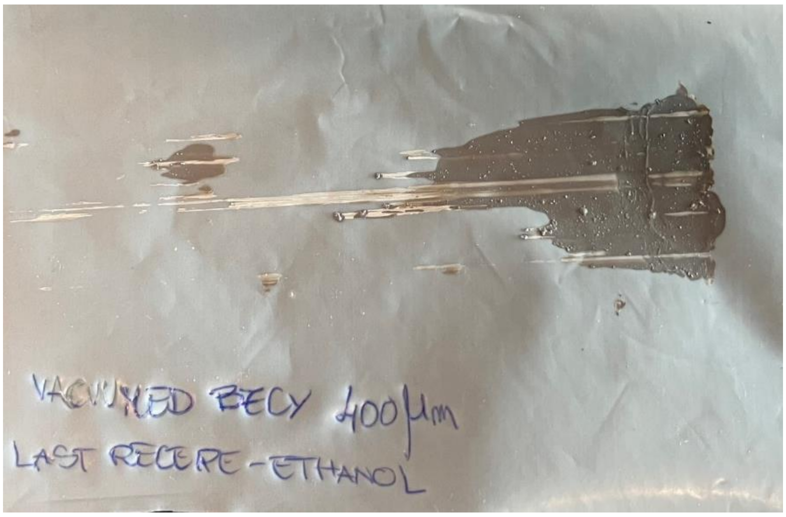

Figure 33. Tape casted BZCY-3 400 μm

Since this slurry has been the best performing one, it has been decided to reduce the thickness value of the doctor blade to 200 µm and, having noticed again an overall good performance, the value of thickness has been further reduced to 100 µm, obtaining a good result as well.

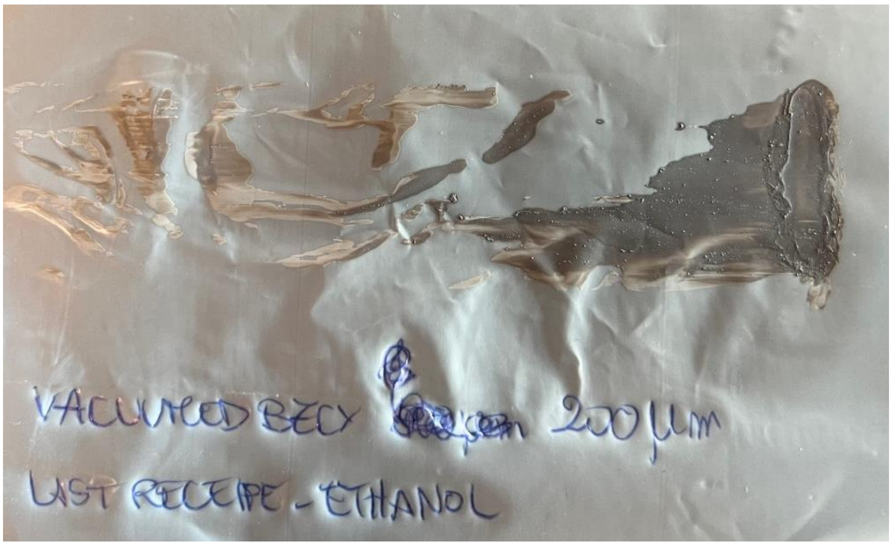

Figure 34. Tape casted and dried BZCY-3 200 µm

.

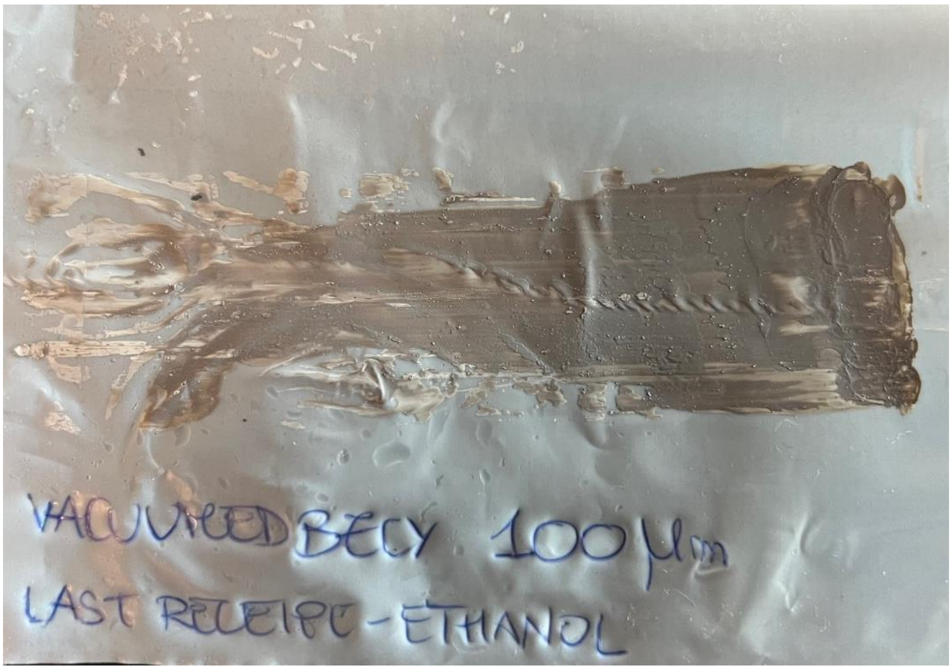

Figure 35. Tape casted and dried BZCY-3 100 µm

All the samples have been dried for 10 minutes each with the dryer of the tape casted at around 80 C and left air-drying overnight.

The choices of dissolving the PVB with ethanol separately before adding it to the composition and increasing the quantity of solvent constitute a winning strategy.

Sintering has been performed on the following samples, covering them with a tile to apply weight and flatten them

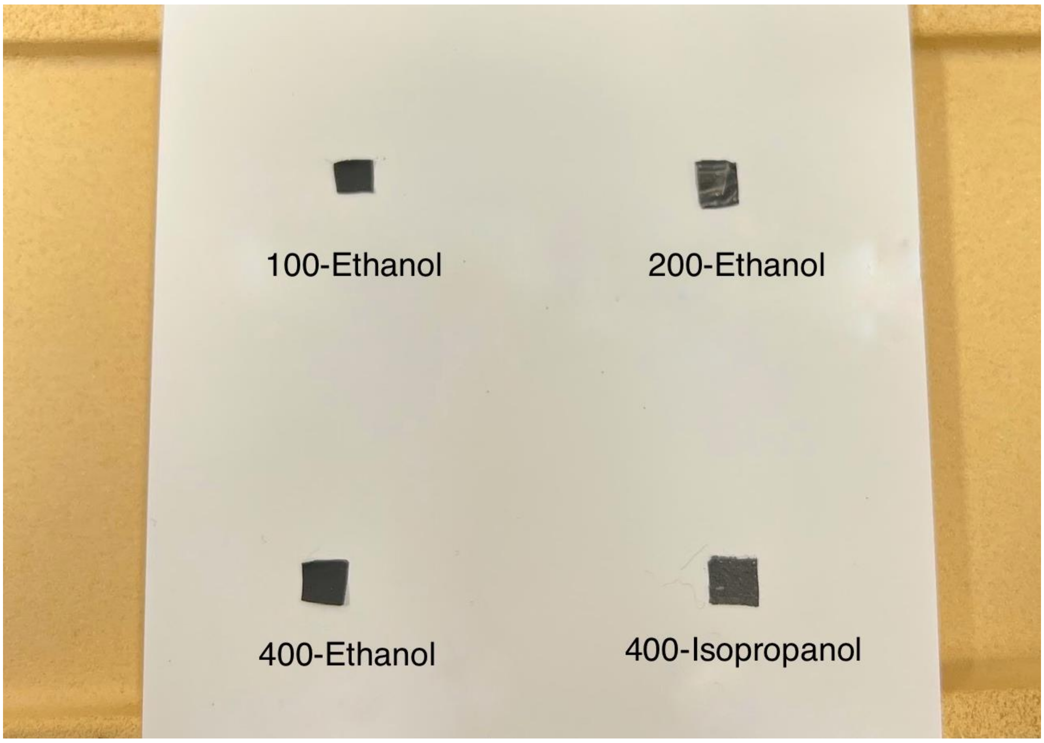

Figure 36. Pre-sintering display of BZCY-3,4 samples

It has been decided to perform sintering dividing the process in three steps (or segments). Step one consists in heating up to 525 C at 100 C/h for one hour, step two further heating up to 1450 C at 100 C/h for four hours and step three consists in cooling down to 25 C at 100 C/h for 14,5 hours.

After sintering, the samples dissolved and it has been hypothesized that the added weight had a negative impact on the thermal treatment and, also, the sintering process didn't involve any reducing atmosphere.

It has been decided to follow the sintering protocol of the Tucker group [21], which includes a de-binding step having a dwell at maximum sintering temperature. Since all the samples dissolved in the previous trial it has also been decided to lower the maximum sintering temperature to 1350 °C.

The process has been divided into five segments this time. Segment one consists in starting with a ramp up from 25 °C to 525 at 100 °C/h, the second segment is another ramp up from 525 to 1350 °C at 100 °C/h, the third segment is a dwell type at 1350°C for two hours, the fourth segment is a ramp from 1350 down to 25 °C at 100 °C/h.

In the following pictures, the BZCY samples of various thicknesses have been treated following the previously mentioned protocol, obtaining a successful sintering, since the samples all turned into a brown color, just as mentioned in the paper.

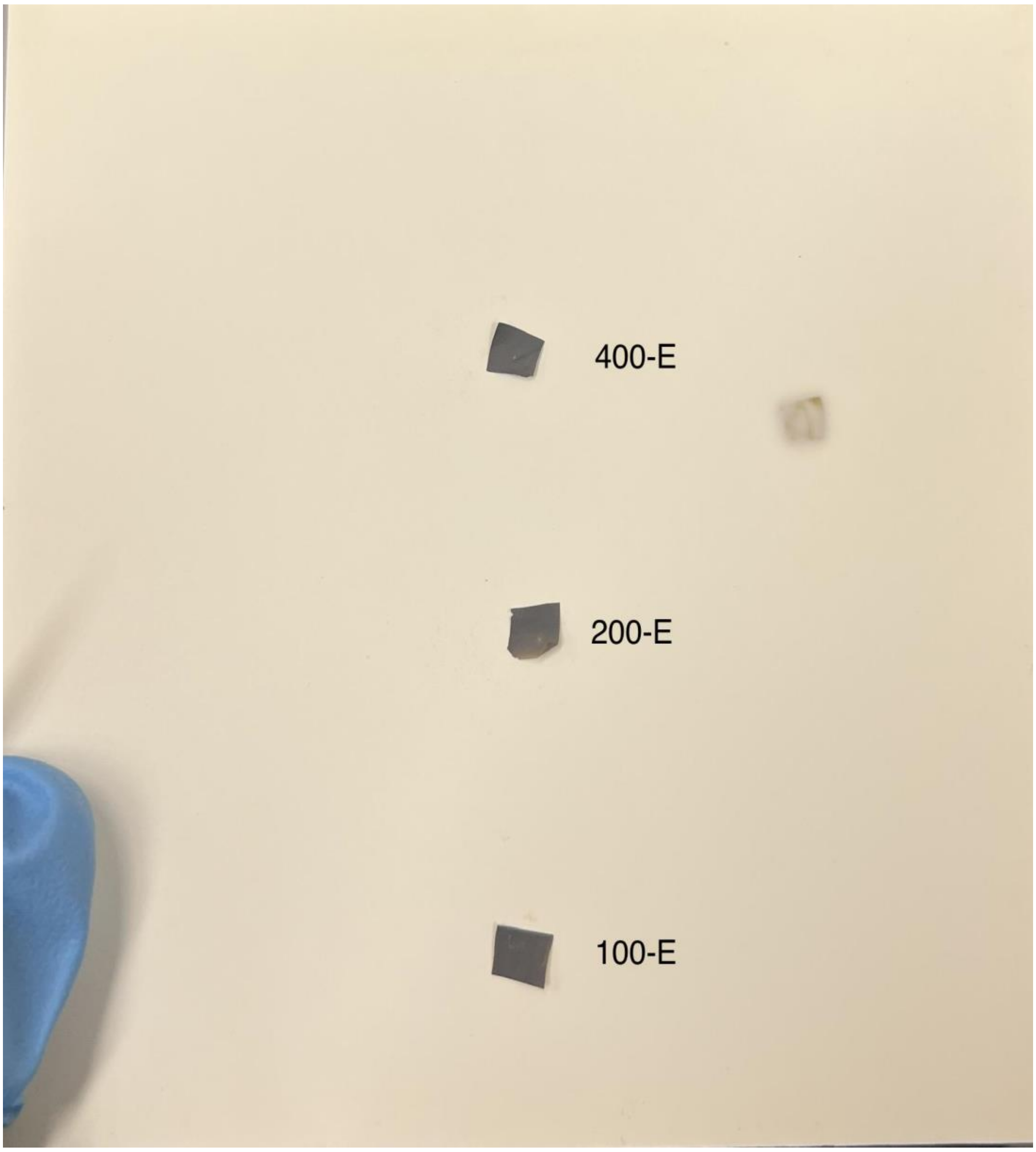

Figure 37. Pre-sintering display of BZCY-3 samples

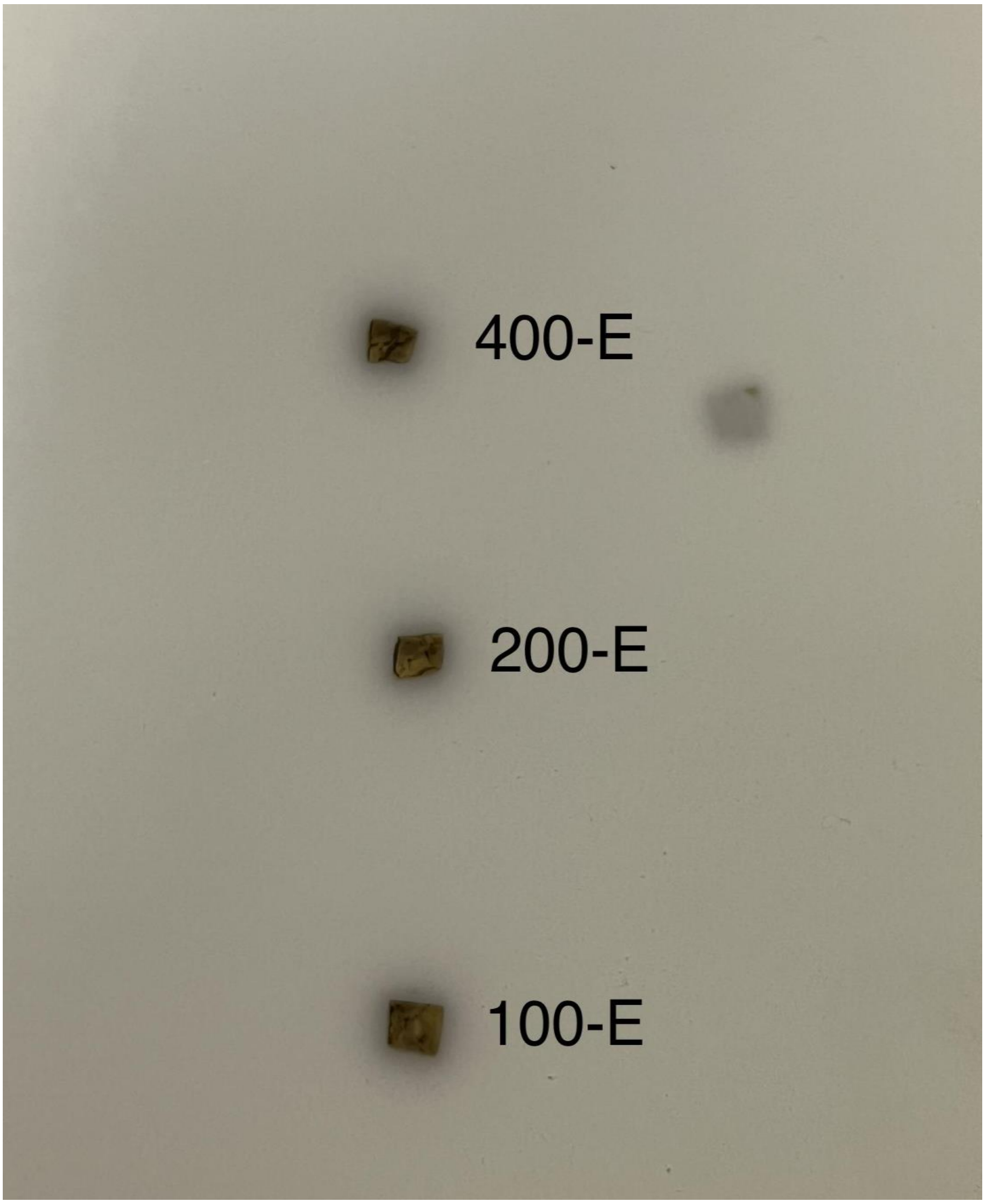

Figure 38. Sintered BZCY-3 samples

After having performed rheology on the two well performing BZCY slurries, it has been decided to further reduce the binder quantity to obtain lower values of viscosity, and, ultimately, to make the tape casting process even smoother, eventually allowing to reduce the thickness values of the tape casted layer. The new compositions are displayed in the following, keeping in mind that the same procedures regarding the addition of components, dissolving with 0,5 mL of solvent the binder, ball milling and vacuuming have been followed. The quantities have also been adjusted starting from a quantity of 2,5 g of BZCY powder, therefore scaled down by two, to use less BZCY powder due to its limited availability and high cost.

Components	Composition
Alpha-Terpineol	0,08 mL
BZCY powder	2,5 g
Ethanol	3,3 mL
PVB	0,315 g
Phthalate	0,077 mL
Manganese Oxide	0,1 g

Table 12. BZCY-5 composition

Components	Composition
Alpha-Terpineol	0,08 mL
BZCY powder	2,5 g
Isopropanol	3,3 mL
PVB	0,315 g
Phthalate	0,077 mL
Manganese Oxide	0,1 g

Table 13. BZCY-6 composition

At the end of the ball-milling process, it has been possible to tape cast only the slurry containing isopropanol, as the ethanol dried out during the process. The slurry has been tape casted with a doctor blade thickness of 100, 20, 15, 10 and 5 μm . All the samples have been left air drying. The dried slurry didn't peel off in the end, surely due to the presence of way less binder in respect to the other compositions.

Since the Teflon foils are not available anymore, an order has been placed for it to be shipped to the university.

In the meantime, it has been then decided to create a slurry with reduced quantity of BZCY powder only containing ethanol, increasing the binder quantity and reducing the solvent, finding a point in between the well performing composition and the last one mentioned. In the first step, 2,1 mL of ethanol have been added and, in the second step, an additional 0,5 mL of solvent is used to dissolve the PVB.

Components	Composition
Alpha-Terpineol	0,08 mL
BZCY powder	2,5 g
Ethanol	2,6 mL
PVB	0,4725 g
Phthalate	0,077 mL
Manganese Oxide	0,1 g

Table 14. BZCY-7 composition

On this slurry, rheology will be performed to assess the values of viscosity and shear rate.

Rheology on BZCY slurries. This has also been noticed performing rheology on the BZCY samples. The analyzed slurries were the ones relative to the decreased quantity of binder, one containing ethanol as solvent and one containing isopropanol, in respect to the starting composition. It has been chosen not to perform rheology on the starting slurry, as it would have reported too high viscosity values, it has been decided to rather compare the behavior of the two well performing slurries to highlight the differences regarding the different solvent usage.

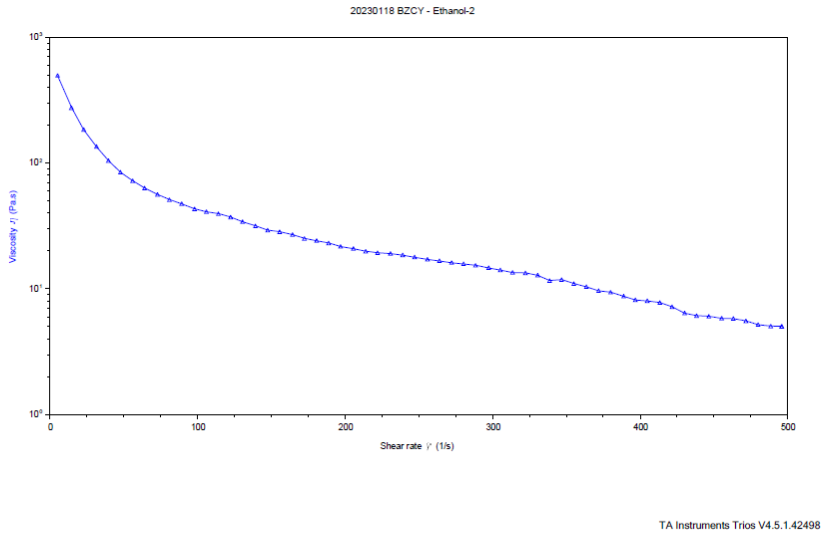

Figure 39. Rheology result of BZCY-3 with ethanol

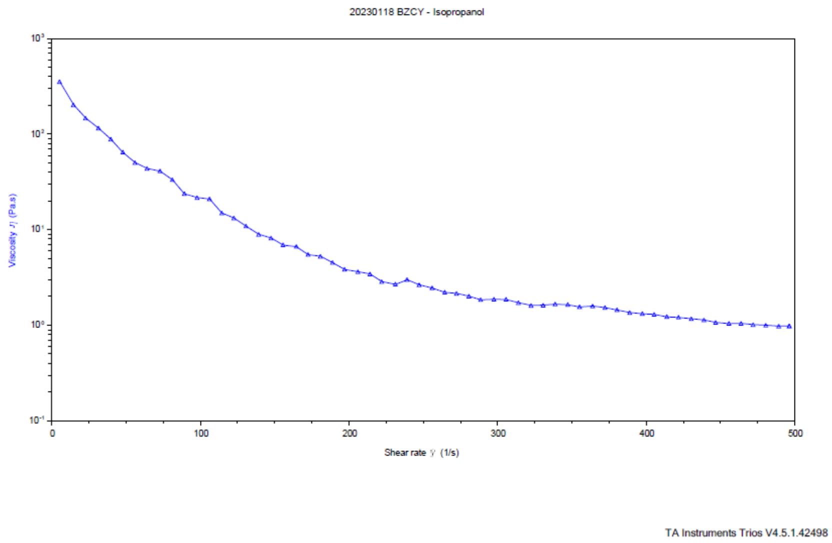

Figure 40. Rheology result of BZCY-4 with isopropanol

The BZCY slurry containing isopropanol showed slightly better characteristics in terms both of viscosity and shear rate, as its value is lower than that of the one containing ethanol. This was an unexpected result, as the slurry containing ethanol was tape casted in a smoother way and appeared to be overall more homogeneous and less bumpy (see pictures in the tape casting section). This reveals that although viscosity can be a good indicator of a well performing slurry in tape casting, it's not the only factor to consider and it's worth having a handful of different experimental trials to determine what works best.

Generally, in respect to the previously analyzed YSZ slurries, the BZCY slurries still reported higher values of viscosity, which led to the decision of further reducing the binder quantity.

Another slurry has been created reducing the binder quantity, but, in the end, it had an unsuitable value of viscosity, as it was too low to be successfully tape casted. Therefore, it has been decided to make modifications on the solvent quantity only, rather than the binder amount, in order to better dissolve the PVB separately before adding to the whole composition. The solvent has been added gradually to the PVB to assess the minimum amount needed, obtaining a gel-like density.

Components	Composition
Alpha-Terpineol	0,16 mL
BZCY powder	5 g
Ethanol	5 mL
PVB	1,25 g
Phthalate	0,144 mL
Manganese Oxide	0,2 g

Table 15. BZCY-8 composition

The tape casted samples range from 20 to 5 μm in thickness.

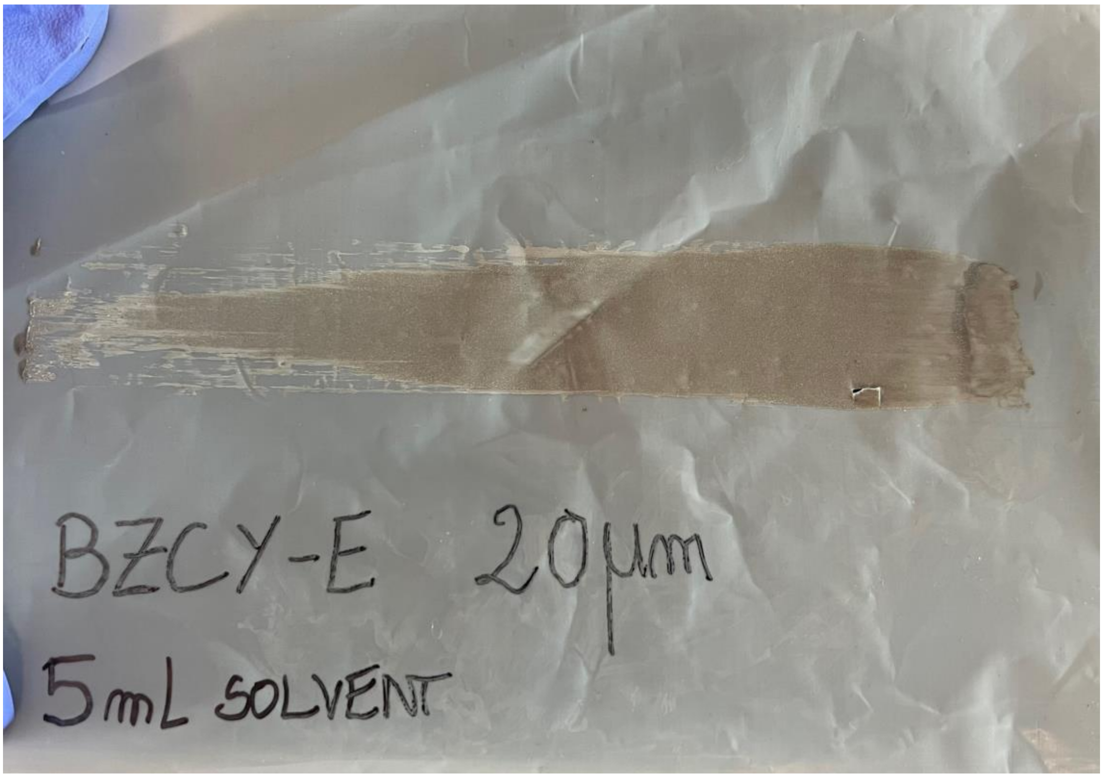

Figure 41. Tape casted and dried BZCY-8 slurry 20 μm

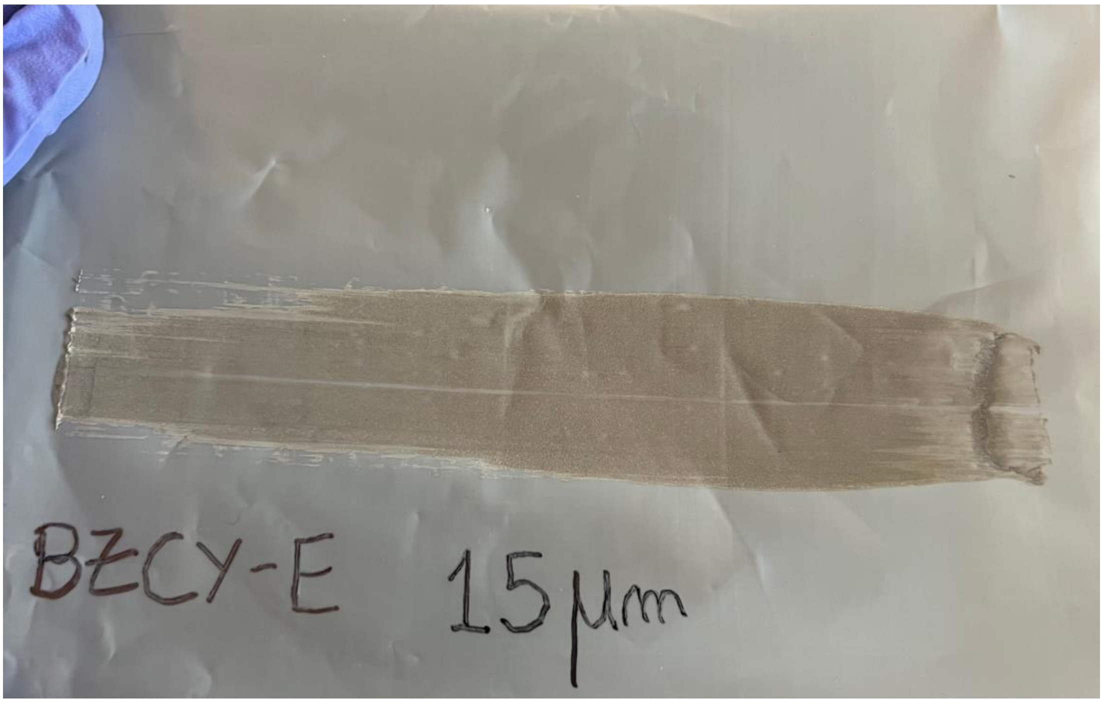

Figure 42. Tape casted and dried BZCY-8 slurry 15 µm

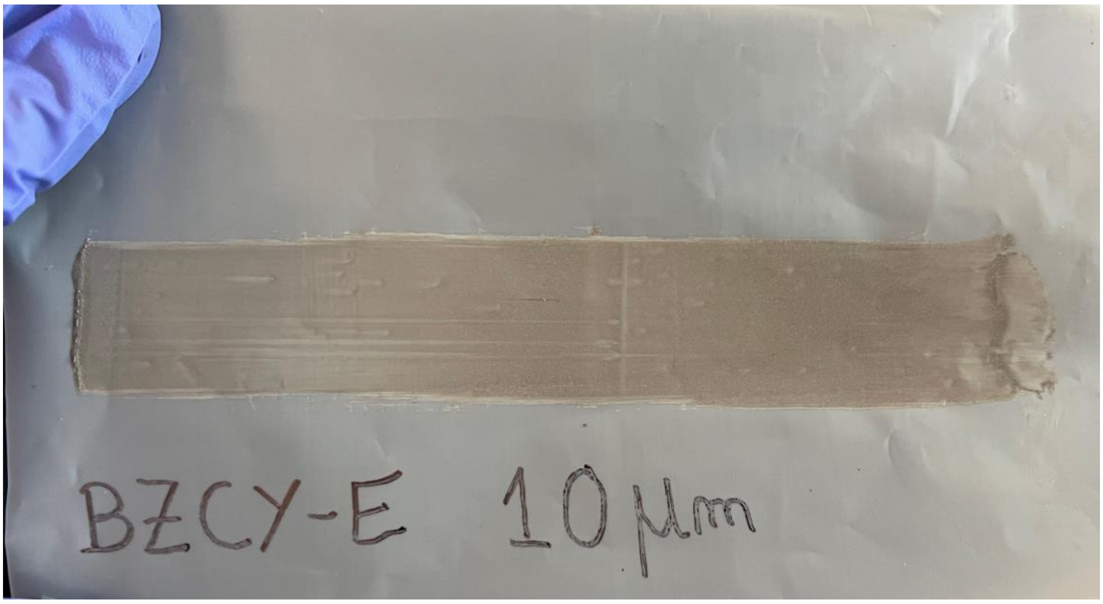

Figure 43. Tape casted and dried BZCY-8 slurry 10 µm

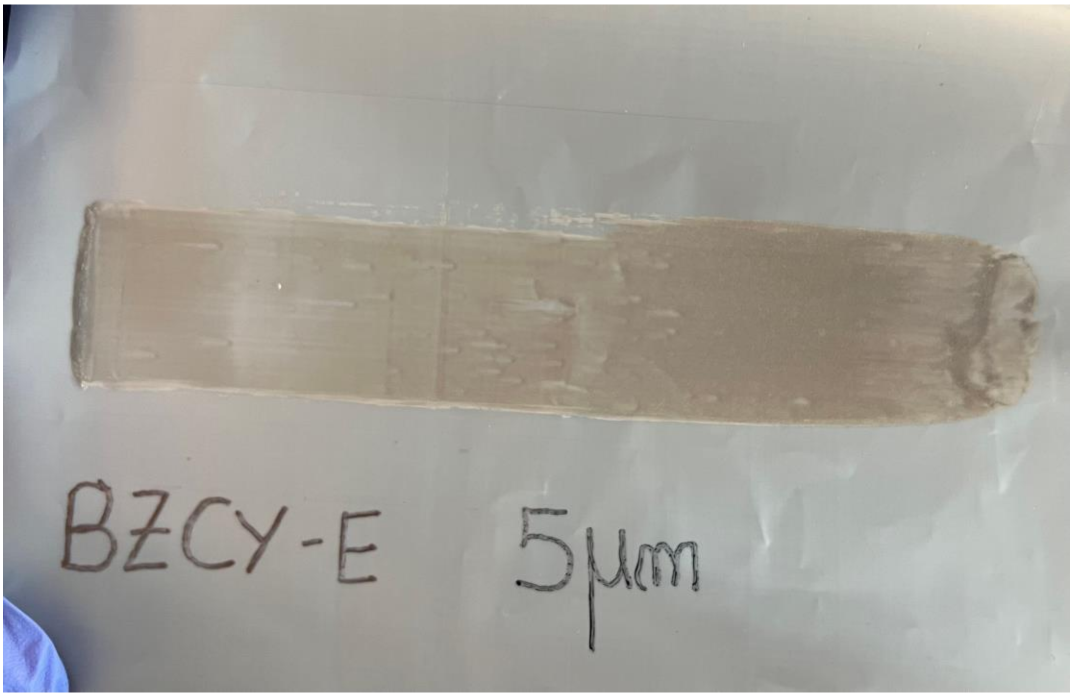

Figure 44. Tape casted and dried BZCY-8 slurry 5 μm

SEM has been performed on the first well performing composition of the BZCY slurry, acquiring images of both an un-sintered sample and a sintered sample. The most interesting images are related to the sintered samples without the presence of sintering aid and with sintering aid, even though the sintering was unsuccessful, as the sample turned black and didn’t densify. These images provide an insight on the surface structural differences between the slurry not containing MnO2 as sintering aid and the one containing it.

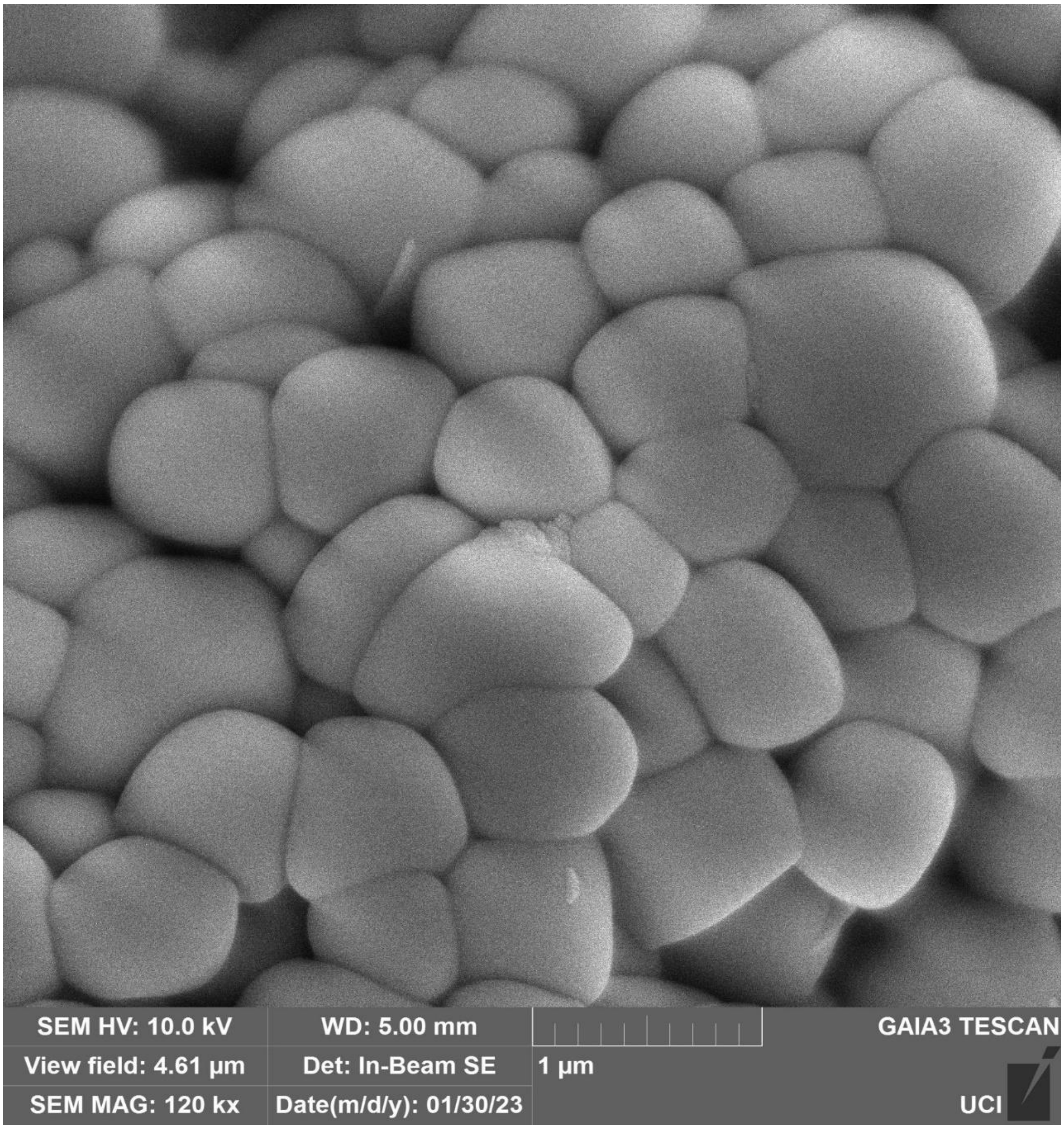

Figure 45. SEM image of unsintered BZCY without sintering aid

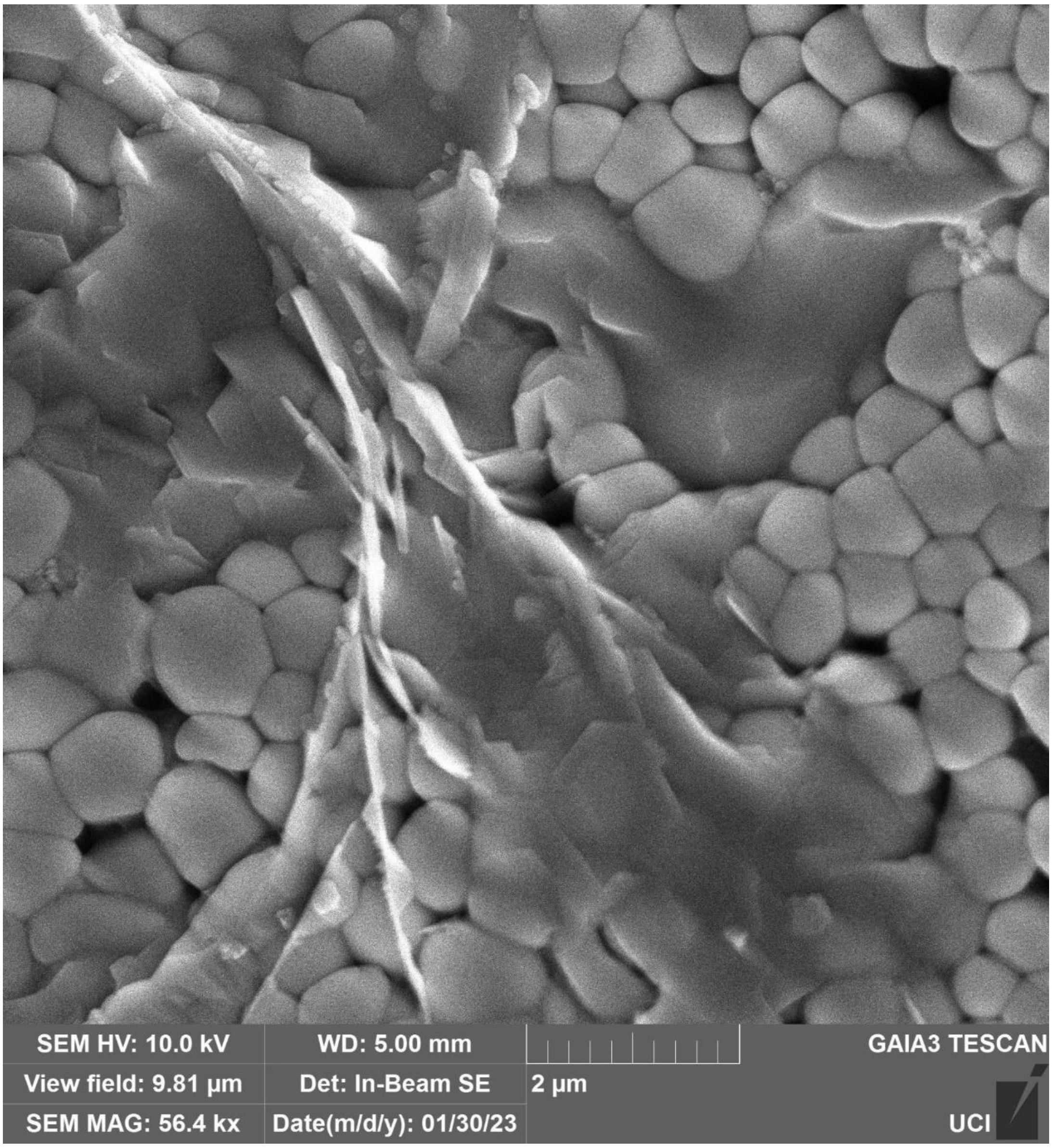

Figure 46. SEM image of unsintered BZCY. Cracks on the surface are visible

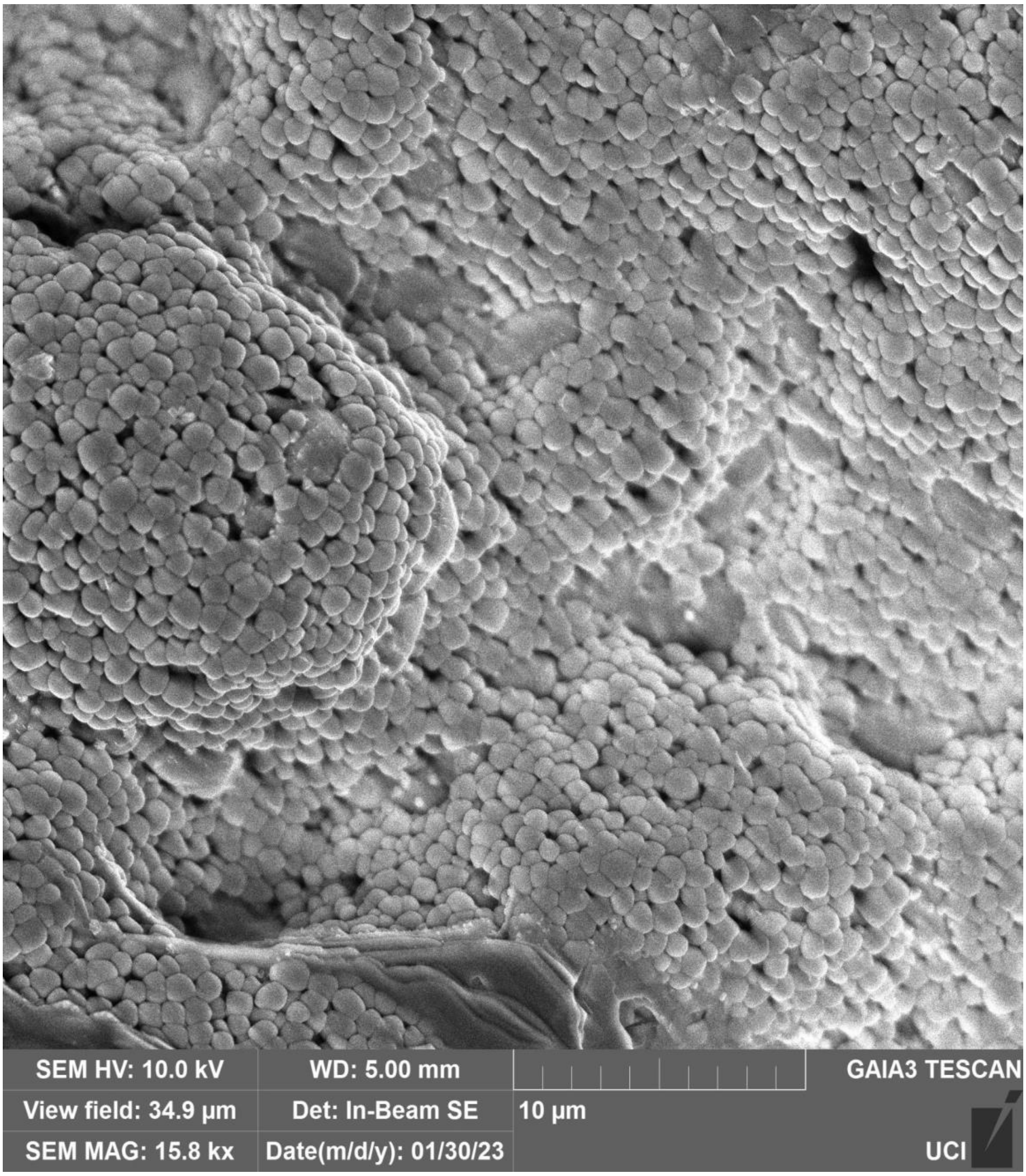

Figure 47. SEM image of unsintered BZCY

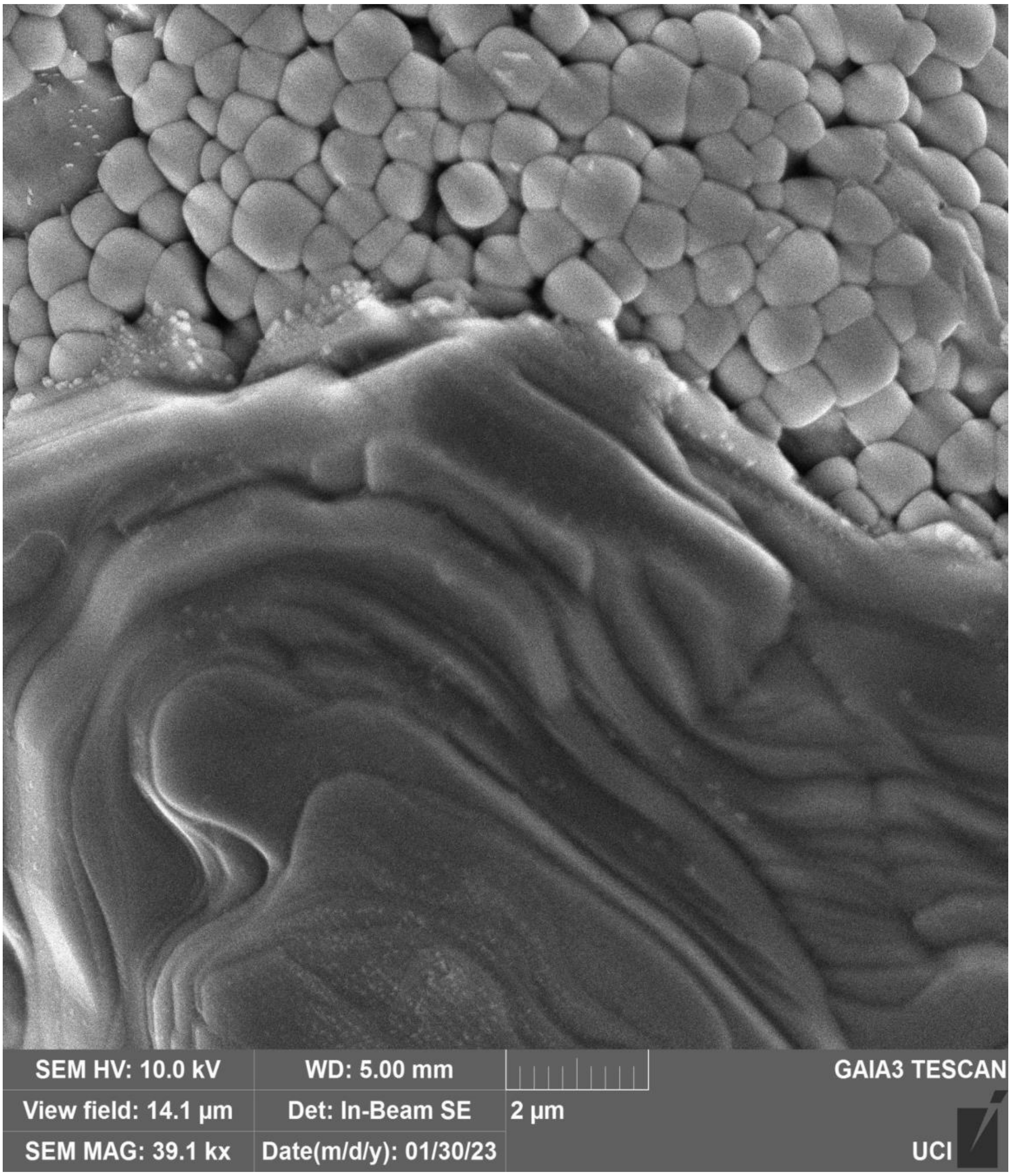

Figure 48. SEM image of unsintered BZCY

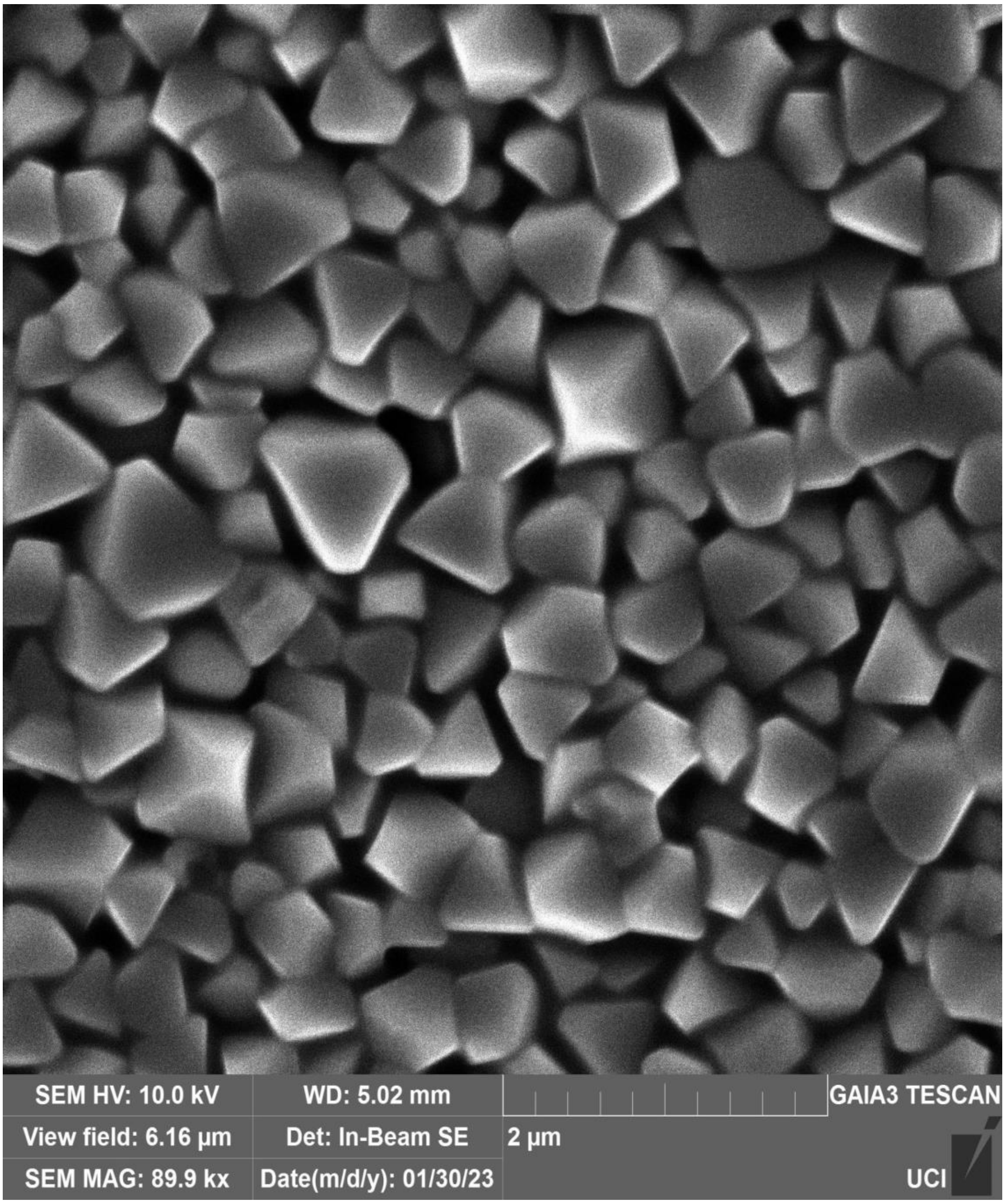

Figure 49. Sintered BZCY with sintering aid

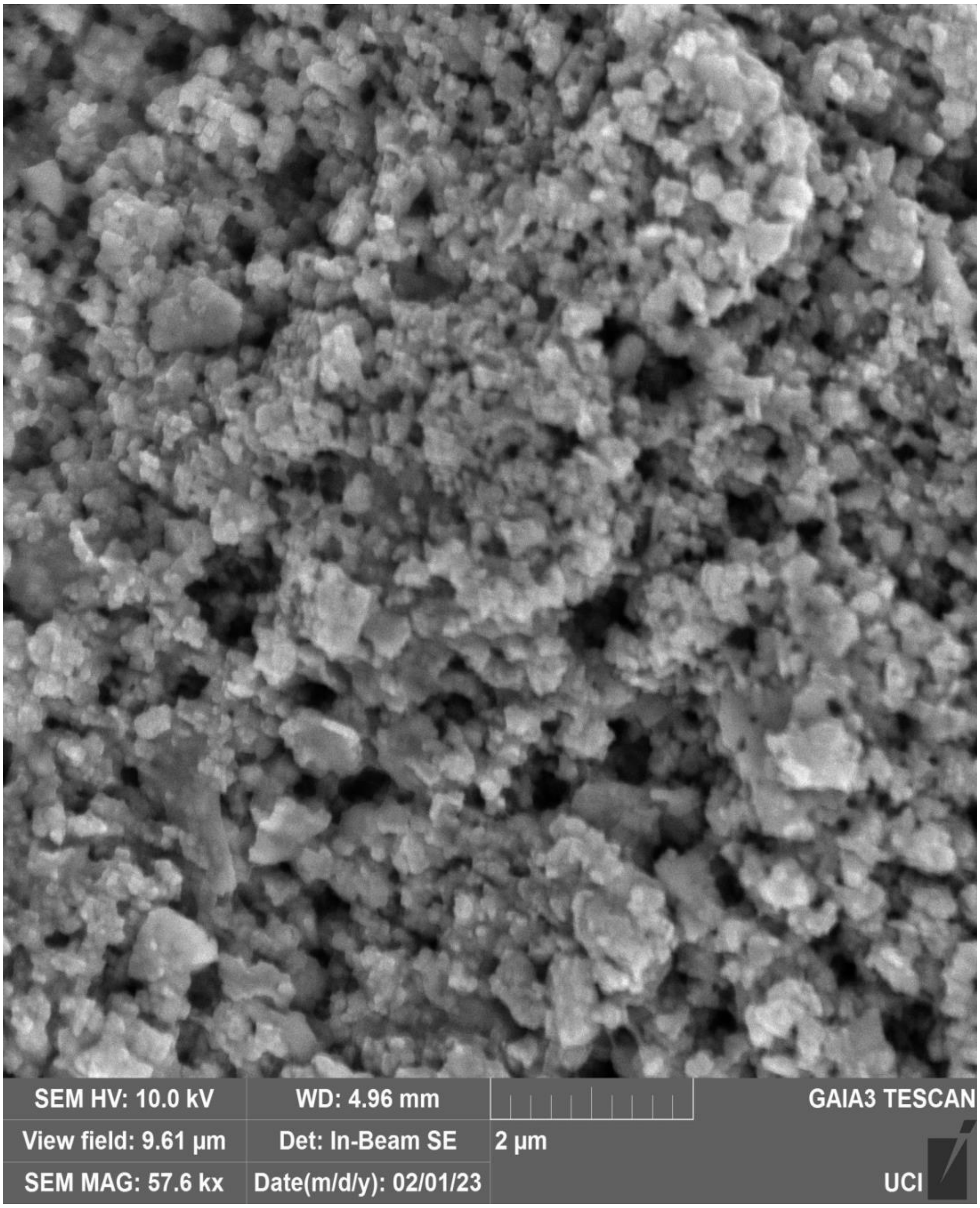

Figure 50. Un-sintered BZCY with sintering aid

It’s possible to notice the change in the structure of the surface particles. MnO_2 shaped the grains turning them into polygons after sintering, defining grain boundaries and creating pores in the structure. The creation of pores is certainly due to the incomplete sintering, which is an issue it’s worth avoiding when trying to sinter and densify the samples properly.

Thermogravimetric analysis and differential scanning calorimetry

The NETZSCH STA 449 F3 Jupiter® simultaneous thermal analyzer (STA) present in the TEMPR facility of UCI allows for simultaneous application of Thermogravimetry (TGA, monitoring mass changes) and Differential Scanning Calorimetry (DSC, testing thermal effects) between 25 °C and 1600 °C with a single sample in a single experiment. This is enabled by a high-performance Heat-Flux DSC, a sub-microgram-resolution thermobalance, and a silicon carbide furnace. The TGA and DSC signals obtained from STA are based on identical test conditions: same atmosphere, gas flow rate, vapor pressure on the sample, heating rate, thermal contact to the sample crucible and sensor, and radiation effect. Furthermore, sample throughput is improved as more information can be gathered from each test run. An integrated auto sampler provides streamlined measurement capabilities with minimal human intervention. Vacuum-tight design enables measurements at a wide variety of defined environments (e.g. vacuum, N2, He, Ar, O2). The STA is also coupled with evolved gas analysis using mass spectrometry (NETZSCH Aeolos QMS 403 D) and FT-IR spectroscopy (Bruker ALPHA) to provide measurements in sync against time.

Logical workflow of the Standard Operation Procedure

1. Pay attention to the Instrument Hazards & Safety Best Practices section.

2. Login to the IMRI Facility management System and enable the instrument.

3. Make sure that all gas pressures read 7.5 psi.

4. Prepare a sample-filled crucible and record sample mass and empty crucible mass.

5. Prepare a reference crucible and record its mass if needed.

6. Place sample and reference in the sample tray.

7. Define STA experimental method for each sample.

8. Configure proper QMS and FT-IR procedures if needed.

9. Run the measurement through STA control software.

10. Data analysis and export.

11. Finish up and sign the logbook.

Here following, both TGA (curve in green) and DSC (curve in blue) have been performed at 800 °C on the BZCY well performing slurry.

Thermogravimetric analysis and differential scanning calorimetry have been performed on the BZCY sample using alumina as crucible. The resulting diagram presents a peak for the TGA curve at around 640 °C, possibly due to a reaction between BZCY and alumina happening at that temperature. This result is certainly conditioned by the presence of this unwanted reaction, therefore it’ll be necessary to change the crucible material.

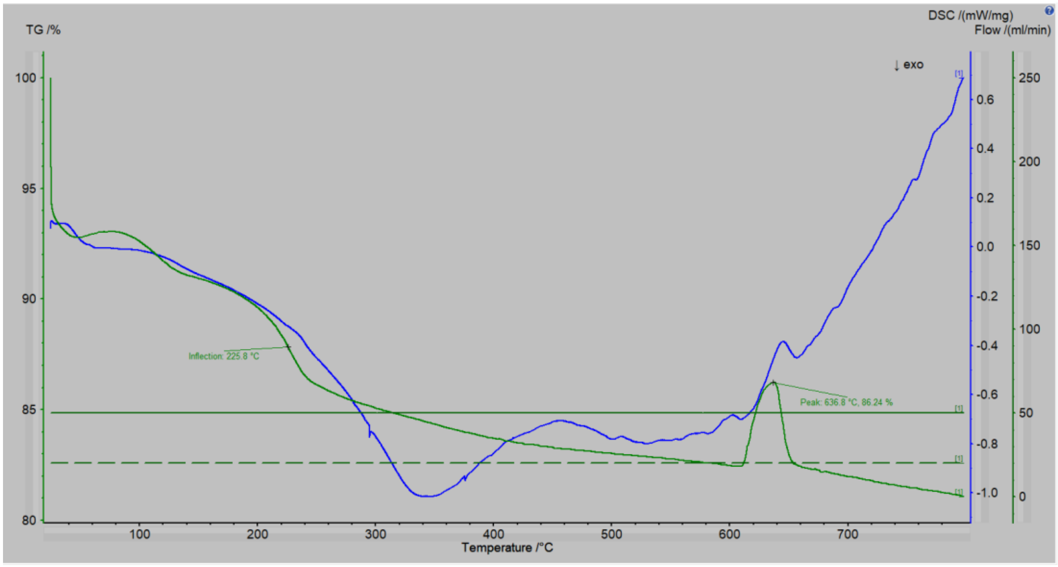

Figure 51. Result of the simultaneous thermal analysis (STA)

8.Anode

Ni-based cermets are state-of-the-art anode materials for hydrogen-fuelled SOFCs because of their sufficient conductivity and electrocatalytic activity for hydrogen oxidation. However, their performance deteriorates quickly because of coke formation over the anode surface if carbon-containing fuels are used as Ni-based cermets are highly active for catalytic fuel cracking reactions. In an attempt to conquer this problem, much attention has been paid to the development of non-nickel anode materials such as Cu-based cermets and perovskite oxides.10–13 However, these non-nickel anodes are associated with problems of low electrocatalytic activity, low chemical stability because of the easy interfacial reactions with other cell components and the high price of synthesis, which impede their further application. Despite these considerable efforts, Ni-based cermets are still the preferred anode material for SOFC design, and there are still some research opportunities to improve these Ni-based anodes with enhanced coking resistance to accommodate these carbon-containing fuels, which is the major concern of this study.

the application of a robust proton-conducting ceramic with a water storage capability and a deep bulk incorporation with Ni will improve the SOFC anode performance to inhibit coke formation. Proton-conducting perovskite oxides such as $BaZr_{0.4}Ce_{0.4}Y_{0.2}O_3$ (BZCY) have been widely investigated because of their potential in the fields of high-temperature electrochemical devices such as sensors, galvanic hydrogen pumps or hydrogen membrane reactors to replace the expensive Pd membranes. These proton-conducting oxides do not have the host constituents to liberate conducting protons, but they can inherently capture the water molecules and take the protons from water dissociation, which helps to mitigate the carbon deposition. [23]

Mixed ionic and electronic conducting materials (MIECs) have been suggested to represent the next generation of solid oxide fuel cell (SOFC) anodes, primarily due to their significantly enhanced active surface area and their tolerance to fuel components. In this thesis, the main focus has been on determining and tuning the physicochemical and electrochemical properties of ceria-based MIECs in the versatile perovskite or fluorite crystal structures. In one direction, BaZr0.1Ce0.7Y0.1 M0.1O3-delta (M = Fe, Ni, Co and Yb) (BZCY-M) perovskites were synthesized using solid-state or wet citric acid combustion methods and the effect of various transition metal dopants on the sintering behavior, crystal structure, chemical stability under CO2 and H 2S, and electrical conductivity, was investigated. BZCY-Ni, synthesized using the wet combustion method, was the best performing anode. [24]

[24] Ceria-Based Anodes for Next Generation Solid Oxide Fuel Cells. Mirfakhraei, Behzad

9.Cathode

Lanthanum strontium cobalt ferrite (LSCF) perovskite is the most popular and representative mixed ionic and electronic conducting (MIEC) electrode material for SOFCs. LSCF-based materials are characterized by high MIEC properties, good structural stability and high electrochemical activity for ORR, and have played a unique role in the development of SOFCs technologies.

Thus materials which are used as the cathodes of SOFC should possess mixed ionic and electronic conductivity (MIEC) in order to extend the reaction sites beyond TPB in addition to high catalytic activity, chemical stability and compatibility with the electrolyte and other cell components. Due to the high activation energy associated with the ORR, the development of high-performance cathode materials is most critical for the development and commercial viability of IT-SOFCs technologies. Lanthanum strontium cobalt ferrite (LSCF) perovskite is the most investigated and representative MIEC cathode for IT-SOFCs. LSCF has a high ionic and electrical conductivity (1×10^{-2} and 10^2 S cm^{-1} at 800 °C, respectively) and high oxygen diffusion properties, e.g., its oxygen self-diffusion coefficient ($D*$) and oxygen surface exchange coefficient (k) is 5×10^{-7} cm^2 S^{-1} and 6×10^{-6} cm S^{-1} at 800 °C, respectively. This is much higher than that of the state-of-the-art LSM materials (e.g., $D^* = 4.0 \times 10^{-15}$ cm^2 S^{-1} and $k = 5.62 \times 10^{-9}$ cm S^{-1} at 800 °C). Though LSCF is not chemically compatible with the most popular YSZ electrolyte of SOFCs due to the formation of resistive strontium zirconate($SrZrO_3$) phase, LSCF is chemically and thermally compatible with doped ceria such as gadolinium-doped ceria (GDC), another popular electrolyte material of SOFCs. The thermal expansion coefficient (TEC) of LSCF is $14–15.2 \times 10^{-6}$ K^{-1}, higher than $11.5–11.9 \times 10^{-6}$ K^{-1} of GDC, but LSCF can be mixed with GDC to modify the thermal expansion properties as well as enhance the electrochemical activity. LSCF is also the most important MIEC oxygen electrode for solid oxide electrolysis cell (SOECs), and one of the most important MIEC membranes used for the separation of oxygen from air in both coal gasification and oxy-fuel power plants.

LSCF belongs to the space group with near-cubic perovskite-type phase of the ABO3 structure with trivalent transition metal ions in the B site and a trivalent rare earth in the A site. Early studies by Teraoka et al. on the oxygen permeation properties of La1-xSrxCo1-yFeyO3-δ (δ in the subscript is used to represent the oxygen non-stoichiometry) found that perovskite-type ABO3 compositions containing more than two types of transition metal ions on the B site are always more reactive than those with only one type of transition metal ion and LSCF with higher Sr and Co contents have a higher oxygen permeability. This occurs because Sr on the A site lattice of LSCF acts as an acceptor, enhancing the oxygen vacancy formation, and Co ions on the B site lattice have a smaller binding energy for oxygen than that with Fe ions, increasing the electronic conductivity. Thus, the activity and electrical properties of LSCF are critically related to the LSCF composition.

The electrical conductivity of LSCF is critically related to the composition as substitution of Fe for Co in the undoped or Sr-doped $LaCo_{1-y}Fe_yO_3$ alters not only the crystal structure but also the orbital configuration of valence electrons.

The major advantages of lanthanum cobalt ferrite-based perovskites over lanthanum manganite-based perovskites are their significantly higher oxygen diffusion and exchange properties. The oxygen self-diffusion coefficient of cobaltite based materials is several orders of magnitude higher than that of the manganite. In comparison to the manganite-based materials, the cobaltite-based perovskites exhibit much lower activation energies. [25]

10.Results

Several trials have been made in the composition of both the YSZ and BZCY slurry. The best results in terms of homogeneity are the following:

Components	Composition
Alpha-Terpineol	0,16 mL
YSZ powder	5 g
Isopropanol	3,3 mL
PVB	2,5 g
Phthalate	0,144 mL

Table 16. YSZ-4 composition

Components	Composition
Alpha-Terpineol	0,16 mL
BZCY powder	5 g
Ethanol	3,8 mL
PVB	1,25 g
Phthalate	0,144 mL
Manganese Oxide	0,2 g

Table 17. BZCY-3 composition

This BZCY composition performed well both in the tape casting process and in sintering for thickness values of 400, 300, 200 and 100 µm, showing a correct densification of the samples after a sintering protocol consisting in four segments or steps: a ramp up from 25 °C to 525 at 100 °C/h, the second segment is another ramp up from 525 to 1350 °C at 100 °C/h, the third segment is a dwell type at 1350°C for two hours, the fourth segment is a ramp from 1350 down to 25 °C at 100 °C/h. Plus, the addition of the manganese oxide sintering aid showed substantial surface structural change while performing SEM. A last BZCY slurry trial revealed the possibility to decrease the thickness up to 5 µm, if a proper amount of solvent is added to the composition in order to decrease the viscosity level, an important factor in determining a successful tape casting process, as seen by performing rheology.

Components	Composition
Alpha-Terpineol	0,16 mL
BZCY powder	5 g
Ethanol	5 mL
PVB	1,25 g
Phthalate	0,144 mL
Manganese Oxide	0,2 g

Table 18. BZCY-8 composition

This sample hasn’t been sintered yet, but, since the thinnest samples are 5 µm thick, they are very promising, as the literature reports densified electrolytes usually not thinner than 10 µm. [26]

Here following, the costs regarding the manufacturing of the electrolyte only are reported, considering that all the equipment needed was already present in the different laboratory facilities and YSZ electrolyte trials have been included in the study to better assess the BZCY composition.

Item	**Vendor name**	**Price [$]**
YSZ powder (150 g)	Fuel cell Materials	135
BZCY powder (150 g)	Fuel cell Materials	690
Setter plates (2) to prevent warping while sintering	Fuel cell Materials	240
GDC barrier layer	Sigma Aldrich	370
MnO2 sintering aid	U.S Research Nanomaterials	65
Teflon foils	Amazon	60
Total		1560

Table 19. Electrolyte manufacturing costs

Assuming the only use of BZCY powder, the cost would have been 1425$, which still makes the technology not cost-effective, despite the good results in the manufacturing process and the possibility to scale-up the different techniques.

Since BZCY powder constitutes the major cost, it’s crucial reducing the quantity used by obtaining an as thin as possible electrolyte layer, which has benefits in terms of overall efficiency as well. Scaling-up the technology would allow the reduction of the costs to take place thanks to economies of scale.

11.Conclusions

In conclusion, the development of proton conducting electrolytes has played a critical role in the advancement of fuel cell technology. These materials have shown great promise in improving the efficiency, performance, and durability of fuel cells, which are important for the widespread adoption of this technology. Through careful design and optimization, researchers have been able to tailor the properties of proton conducting electrolytes to meet the specific requirements of different fuel cell applications. While, as seen in this work, challenges remain, such as the need to improve the stability, reduce the cost of materials, and find scalable manufacturing techniques, the progress made to date demonstrates the potential of proton conducting electrolytes to enable a more sustainable energy future. The effectiveness of the tape casting and sintering techniques in the manufacturing of very thin layers has been demonstrated and it’s indeed a promising indicator of the near-future commercialization. Thanks to the up scaling of the proton conducting technology, spreading it to larger applications, especially in the mobility sector with car, truck, ship and plane transport, as well as in stationary installments, a substantial cost reduction from economies of scale will happen, radically changing energy markets. As such, further research and development efforts in this area are crucial for realizing the full potential of fuel cells as a viable alternative to traditional energy sources and be among the first technologies in line for the energy transition era.

12.References

[1] Hanchen Tian, Zheyu Luo, Yufei Song, Yucun Zhou, Mingyang Gong,

Wenyuan Li, Zongping Shao, Meilin Liu & Xingbo Liu (2022): Protonic ceramic materials for clean and sustainable energy: advantages and challenges, International Materials Reviews, DOI: 10.1080/09506608.2022.2068399

[2] Ceramic tape casting: A review of current methods and trends with emphasis on rheological behavior and flow analysis M. Jabbari a, R. Bulatova b , A.I.Y. Tok c , C.R.H. Bahl b , E. Mitsoulis d , J.H. Hattel a

[3] Sintering. Densification, Grain Growth, and Microstructure Suk-Joong L.Kang

[4] DIRECT LASER SINTERING OF CERAMICS F. Klocke, C. Ader Fraunhofer Institute for Production Technology IPT, Aachen, Germany

[5] Laser sintering of ceramics, Bin Qian, Zhijian Shen

[6] Manière, C., Lee, G. & Olevsky, E.A. All-Materials-Inclusive Flash Spark Plasma Sintering. Sci Rep 7, 15071 (2017).

[7] EM Sample Preparation Coating Technology, April 2013, Leica

[8] Akhtar, K., Khan, S.A., Khan, S.B., Asiri, A.M. (2018). Scanning Electron In: Sharma, S. (eds) Handbook of Materials Characterization. Springer, Cham. https://doi.org/10.1007/978-3-319-92955-2_4

[9] Andrei A. Bunaciu, Elena gabriela Udriştioiu & Hassan Y. Aboul-Enein (2015) X-Ray

Diffraction: Instrumentation and Applications, Critical Reviews in Analytical Chemistry, 45:4, 289-299, DOI: 10.1080/10408347.2014.949616

[10] Raman spectroscopy – Basic principle, instrumentation, and selected applications for the characterization of drugs of abuse - Gurvinder Singh Bumbrah Rakesh Mohan Sharma

[11] https://www.thermofisher.com/it/en/home/materials-science/eds-technology.html#applications

[12] Using Rheology to Characterize Flow and Viscoelastic Properties of Hydrogels, Adhesives and Biopolymers. Tianhong Terri Chen PhD Senior Applications Scientist TA Instruments – Waters LLC

[13] https://www.tainstruments.com/products/rheology/

[14] Thermomechanical and spectroscopic characterization of natural fiber composites, K.R.RajishaB.DeepaL.A.PothanS.Thomas

[15] Chapter 9 - Thermal characterization of materials using differential scanning calorimeter. M. Singh, A. Singh

[16]Titanium Dioxide Nanostructured Based Supercapacitors

Nurul Asma Samsudin, ... Jagadeesh Pasupuleti, in Encyclopedia of Energy Storage, 2022

[17] A review on recent status and challenges of yttria stabilized zirconia modification to lowering the temperature of solid oxide fuel cells operation

Zulfirdaus Zakaria, Saiful Hasmady Abu Hassan, Norazuwana Shaari, Ahmad Zubair Yahaya, Yap Boon Kar

[18] Production and characterization of YSZ tape-cast films using aqueous slurries

November 2011 Conference: 8th International Latin American Conference on Powder TechnologyAt: Florianópolis, Brasil

[19] Fabrication of multi-layered structures for proton

conducting ceramic cells

Wendelin Deibert,*a Mariya E. Ivanova, *a Yuanye Huang,b Rotraut Merkle, b

Joachim Maierb and Wilhelm A. Meulenberg ac

[20] Hanchen Tian, Zheyu Luo, Yufei Song, Yucun Zhou, Mingyang Gong, Wenyuan Li, Zongping Shao, Meilin Liu & Xingbo Liu (2022): Protonic ceramic materials for clean and sustainable energy: advantages and challenges, International Materials Reviews, DOI: 10.1080/09506608.2022.2068399

[21] Approaches for Co-Sintering Metal-Supported Proton-Conducting Solid Oxide Cells with Ba(Zr,Ce,Y,Yb)O3-δ Electrolyte. Ruofan Wang1, Grace Y. Lau1, Dong Ding2, Tianli Zhu3, and Michael C. Tucker1*

[22] The Effect of a CGO Barrier Layer on the Performance of LSM/YSZ SOFC Cathodes. K. Kammer Hansen,*,zM. Menon,*J. Knudsen, N. Bonanos, and M. Mogensen* Fuel Cells and Solid State Chemistry Division, Risø National Laboratory for Sustainable Energy, Technical University of Denmark, DK-4000 Roskilde, Denmar

[23] Nickel-Based Anode with Water Storage Capability to Mitigate Carbon Deposition for Direct Ethanol Solid Oxide Fuel Cells Dr. Wei Wang, Dr. Chao Su, Prof. Ran Ran, Bote Zhao, Prof. Zongping Shao, Prof. Moses O. Tade, Prof. Shaomin Liu

[24] Ceria-Based Anodes for Next Generation Solid Oxide Fuel Cells. Mirfakhraei, Behzad

[25] Development of lanthanum strontium cobalt ferrite perovskite electrodes of solid oxide fuel cells – A review. San Ping Jiang.

[26] Large-area protonic ceramic cells for hydrogen purification

Qingjie Wang a,1, Ting Luo b,1, Yongcheng Tong c, Mingxuan Dai c, Xing-Yuan Miao a, Sandrine Ricote d, Zhongliang Zhan c,*, Ming Chen a,*